PRODUCTION AND EVALUATION OF CONDUCTION MECHANISMS OF THE AU/(RUO_2: PVC)/N-SI (MPS) STRUCTURES IN A WIDE RANGE OF ILLUMINATION AND FREQUENCY USING CURRENT-VOLTAGE AND IMPEDANCE-VOLTAGE MEASUREMENTS

2023
PhD THESIS
ELECTRICAL-ELECTRONICS ENGINEERING

Hasan Meloud M. ELAMEN

Thesis Advisor
Assoc. Prof. Dr. Muhammet Tahir GÜNEŞER

PRODUCTION AND EVALUATION OF CONDUCTION MECHANISMS OF THE AU/(RUO$_2$:PVC)/N-SI (MPS) STRUCTURES IN A WIDE RANGE OF ILLUMINATION AND FREQUENCY USING CURRENT-VOLTAGE AND IMPEDANCE-VOLTAGE MEASUREMENTS

Hasan Meloud M ELAMEN

Thesis Advisor
Assoc. Prof. Dr. Muhammet Tahir GÜNEŞER

T.C.
Karabuk University
Institute of Graduate Programs
Department of Electrical -Electronics Engineering
Prepared as
PhD Thesis

KARABUK
July 2023

I certify that in my opinion the thesis submitted by Hasan Meloud M ELAMEN titled "PRODUCTION AND EVALUATION OF CONDUCTION MECHANISMS OF THE AU/(RUO$_2$:PVC)/N-SI (MPS) STRUCTURES IN A WIDE RANGE OF ILLUMINATION AND FREQUENCY USING CURRENT-VOLTAGE AND IMPEDANCE-VOLTAGE MEASUREMENTS" is fully adequate in scope and in quality as a thesis for the degree of Ph.D.

Assoc. Prof. Dr. Muhammet Tahir GÜNEŞER ....
Thesis Advisor, Department of Electrical -Electronics Engineering

This thesis is accepted by the examining committee with a unanimous vote in the Department of Electrical -Electronics Engineering as a Ph.D thesis. July 12, 2023

Examining Committee Members (Institutions)		Signature
Chairman	: Prof. Dr. Muharrem GÖKÇEN (DU)	....
Member	: Prof. Dr. Şemsettin ALTINDAL (GU)	....
Member	: Prof. Dr. Habibe TECİMER (KBU)	....
Member	: Assoc. Prof. Dr. Muhammet GÜNEŞER (KBU)	....
Member	: Assist. Prof. Dr. Satiye KORKMAZ (KBU)	....

The degree of Ph.D by the thesis submitted is approved by the Administrative Board of the Institute of Graduate Programs, Karabuk University.

Prof. Dr. Müslüm KUZU ....
Director of the Institute of Graduate Programs

“I declare that all the information within this thesis has been gathered and presented in accordance with academic regulations and ethical principles and I have according to the requirements of these regulations and principles cited all those which do not originate in this work as well.”

Hasan Meloud M. ELAMEN

ABSTRACT

Ph.D. Thesis

PRODUCTION AND EVALUATION OF CONDUCTION MECHANISMS OF THE AU/(RUO_2:PVC)/N-SI (MPS) STRUCTURES IN A WIDE RANGE OF ILLUMINATION AND FREQUENCY USING CURRENT-VOLTAGE AND IMPEDANCE-VOLTAGE MEASUREMENTS

Hasan Meloud M. ELAMEN

Karabük University
Institute of Graduate Programs
The Department of Electric and Electronic Engineering

Thesis Advisor:
Assoc. Prof. Dr. Muhammet Tahir GÜNEŞER
July 2023, 107 pages

In this study, the RuO_2-doped PVC composite structures were produced and used as an interfacial layer in the Au/n-Si (MS) Schottky structures to improve their photo response, electric and dielectric performance. The basic photovoltaic, electric, and dielectric factors of the fabricated Au/(RuO_2:PVC)/n-Si (MPS) structure were analyzed from the I-V characteristics under various illumination levels and the impedance spectroscopy method, including capacitance/conductance (C and G/ω) data in wide ranges of voltage and frequency at room temperature in the dark.

The ideality factor (n), zero bias barrier height (Φ_{B0}), inverse saturation current (I_o), and both series and shunt resistances (R_S and R_{Sh}) were evaluated using the I–V data in the dark and definite illumination intensities. Also, the values of n, $\Phi_{B,}$ and R_S were obtained and compared with each other using Cheung and Norde functions. The energy distribution profile of interface states (N_{SS}) were also extracted (N_{SS} vs (E_C - E_{SS})) with considering the voltage-dependent of ideality factor ($n(V)$) and zero barrier height (Φ_{B0} (V)). In addition, the photocurrent (I_{Ph}), photosensitivity (S_{Ph}), and photo-response (R) were calculated under various illumination intensities. The value of photocurrent in the reverse bias (I_{Ph}) increases with illumination intensity due to the creation of hole-electron pairs at the junction and their drifting in opposite directions. Also, the short circuit current (I_{SC}), open circuit voltage (V_{OC}), fill factor *(FF)*, and efficiency (η) of the produced structure were obtained and found to be 6.4μA, 0.118 V, 46%, and 0.088 % at 50mW/cm^2.

In addition, the capacitance/conductance (C-V-f and G/ω-V-f) data at room temperature in the dark were used to analyze the main electric and dielectric parameters. The depletion layer width (W_D), barrier height (Φ_B(C-V)), the fermi energy level (E_F), and the density of donor atoms (N_D) were calculated using the reverse bias of C^{-2}- V plot. Voltage-dependent profiles of the interface states (N_{SS}) were also analyzed from the high-low frequency capacitance techniques (C_{HF}-C_{LF}). Finally, both the real and imaginary elements of the complex permittivity (ε' and ε''), tangent loss (*tan* δ), *ac* electrical conductivity (σ_{ac}), complex electric-modulus (M^*), and complex impedance (Z^*) were obtained by from C- V-f and G/ω-V-f measurements. The obtained higher values of ε' and ε'' at low frequencies wear attributed to the existence of dipole polarizations and N_{SS}.

According to these results, the organic interlayer (RuO$_2$:PVC) has improved the photo response, electric and dielectric performance of the fabricated structures, and the structures are sensitive to illumination, frequency, and voltage. Therefore, the produced device can be used in electronic applications, such as photodiodes and photodetectors, and as a capacitor instead of a conventional MIS type structure.

Key Words: RuO$_2$:PVC, Schottky Barrier Diodes (SBDs), Photocurrent, Photoresponse, Interface States, Electrical and Dielectric Properties, C-V and G/ω-V Characteristics

Science Code : 90517

ÖZET

Doktora Tezi

AU/(RUO2:PVC)/N-SI (MPS) YAPILARIN İLETİM MEKANİZMALARININ GENİŞ AYDINLATMA VE FREKANS ARALIĞINDA AKIM-GERİLİM VE EMPEDANS-GERİLİM ÖLÇÜMLERİ İLE ÜRETİMİ VE DEĞERLENDİRİLMESİ

Hasan Meloud M. ELAMEN

Karabük Üniversitesi
Lisansüstü Eğitim Enstitüsü
Elektrik-Elektronik Mühendisliği Bölümü

Tez Danışmanı:
Doç. Dr. Muhammet Tahir GÜNEŞER
Temmuz 2023, 107 sayfa

Bu çalışmada, RuO_2 katkılı PVC kompozit yapılar üretilmiş ve Au/n-Si (MS) Schottky yapılarında foto tepkiyi, elektrik ve dielektrik performansları iyileştirmek amacıyla arayüz tabakası olarak kullanılmıştır. Üretilen Au/(RuO_2:PVC)/n-Si (MPS) yapısının temel fotovoltaik, elektrik ve dielektrik faktörleri; karanlıkta, oda sıcaklığında, geniş voltaj ve frekans aralıklarında kapasitans/iletkenlik (C ve G/ω) verileri dahil olmak üzere çeşitli aydınlatma seviyeleri ve empedans spektroskopi yöntemi altında I-V karakteristikleri analiz edilmiştir.

İdealite faktörü (n), sıfır bias bariyer yüksekliği (Φ_{B0}), ters doyma akımı (I_o) ve hem seri hem de şönt dirençler (R_S ve R_{Sh}), karanlık ve belirli aydınlatma yoğunluklarında I–V verileri kullanılarak değerlendirildi. Ayrıca n, Φ_B ve R_S değerleri Cheung ve Norde fonksiyonları kullanılarak elde edilmiş ve birbirleri ile karşılaştırılmıştır. Arabirim durumlarının (N_{SS}) enerji dağıtım profili de idealite faktörünün (n(V)) ve sıfır bariyer yüksekliğinin (Φ_{B0} (V)) voltaja bağlı olduğu dikkate alınarak (N_{SS}'ye karşı (E_C - E_{SS})) hesaplanmıştır. Ek olarak, çeşitli aydınlatma yoğunlukları altında fotoakım (I_{Ph}), fotosensitivite (S_{Ph}) ve foto-tepki (R) değerleri de hesaplanmıştır. Ters polarizasyondaki (I_{Ph}) fotoakımın değeri, eklemdeki delik-elektron çiftlerinin oluşması ve bunların zıt yönlerde sürüklenmesi nedeniyle aydınlatma yoğunluğuyla birlikte artmaktadır. Ayrıca üretilen yapının kısa devre akımı (I_{SC}), açık devre gerilimi (V_{OC}), doldurma faktörü (FF) ve verimi (η) elde edilmiş ve 50mW/cm^2'de sırasıyla 6.4µA, 0.118 V, %46 ve %0.088 olarak bulunmuştur.

Ayrıca; karanlıkta ve oda sıcaklığında kapasitans/iletkenlik (C-V-f ve G/ω-V-f) verileri ana elektrik ve dielektrik parametrelerini analiz etmek için kullanılmıştır. Tükenme bölgesi genişliği (W_D), bariyer yüksekliği (Φ_B(C-V)), fermi enerji seviyesi (E_F) ve donör atomların yoğunluğu (N_D), C^{-2}-V grafiğinin ters eğilimi kullanılarak hesaplanmıştır. Arayüz durumlarının (N_{SS}) voltaja bağlı profilleri de yüksek-düşük frekans kapasitans tekniklerinden (C_{HF}-C_{LF}) yararlanarak analiz edilmiştir. Son olarak, karmaşık geçirgenlik (ε' ve ε''), teğet kaybı ($\tan\delta$), ac elektrik iletkenliği (σ_{ac}), karmaşık elektrik modülü (M^*) ve karmaşık empedansın (Z^*) hem gerçek hem de imajiner öğeleri, C-V-f ve G/ω-V-f ölçümlerinden yararlanarak elde edilmiştir. Düşük frekanslarda elde edilen daha yüksek ε' ve ε'' değerleri, dipol polarizasyonlarının ve N_{SS}'nin varlığı ile açıklanmıştır.

Bu sonuçlara göre, çalışmada tasarlanan, üretilen ve kullanılan organik ara katman (RuO_2:PVC); üretilen yarıiletken yapıların foto tepkisini, elektrik ve dielektrik performansını iyileştirmiştir ve üretilen yapıların aydınlatma, frekans ve gerilime duyarlı olmasını sağlamıştır. Bu nedenle üretilen cihaz, geleneksel MIS tipi yapı yerine fotodiyot ve fotodedektör gibi elektronik uygulamalarda ve kondansatör olarak kullanılabileceği sonucuna varılmıştır.

Anahtar Kelimeler : RuO_2:PVC, Schottky Bariyer Diyotları (SBDs), Fotoakım, Fototepki, Arayüz Durumları, Elektriksel ve Dielektrik özellikler, C-V ve G/ω-V özellikleri

Bilim Kodu **:** 90517

ACKNOWLEDGMENT

I would like to express my sincere gratitude to my supervisor, Assoc. Prof. Dr. Muhammet Tahir GUNESER, for his invaluable guidance and support throughout my research project. His expertise and insightful feedback have been instrumental in shaping the direction of my work. I would also like to thank Prof. Dr. Şemsettin ALTINDAL, and Dr. Yosef BADALI at Gazi University for their helpful discussions, valuable assistance, support, and advice, and for making available all required facilities for this study.

My deepest appreciation to the Center for Solar Energy Researches and Studies in Libya, that provides me the chance to complete my studies at one of the international universities in the world.

CONTENTS

LIST OF FIGURES

Page

LIST OF TABLES

SYMBOLS AND ABBREVITIONS INDEX

SYMBOLS

J : current density
I : current
V : voltage
E_C : conduction band
Φ_{Bn} : barrier height of metal-semiconductor
ε : fermi energy level
χ_s : electron affinity of semiconductor
E_V : valance band
V_F : forward bias
V_R : Reverse bias
W_D : Depletion width
Vbi : Built-in potential
ε_r : Static dielectric permittivity
k : Boltzmann's constant
m^* : Effective mass
T : Absolute temperature in kelvin
A^* : Effective Richardson constant
R : Resistance
C : Capacitance
N_{SS} : Surface state
ε' : Dielectric constant
ε'' : Dielectric losses
E : Electric-field
$Tan\ \delta$: Loss tangent
G/ω : Conductance
M' : Electric module

M'' : Electric module losses
σ_{ac} : AC Conductivity
Φ_M : work function of metal
p_{av} : Induced average dipole moment
E_{loc} : Local electric field
I_C : Conduction current
I_P : Polarization current
C_i : Interlayer capacitance
P_{in} : intensity of the illumination
$I_{m,}$: Maximum current according to the maximum Power Point
V_m : Maximum voltage according to the maximum Power Point
α_i : Ionic polarized ability
σ : Density of the surface charge
$q\Phi_o$: Charge neutral level
D : Electric displacement
p : Dipole moment
P_e : Electronic polarization
ξ : Electric field
E_0 : Level of vacuum
E_F : Fermi level
I_{Ph} : Photocurrent
S_{Ph} : Photosensitivity
R : Photo-response
I_{SC} : Short circuit current
V_{OC} : Open circuit voltage
FF : Fill factor
η : Efficiency
W_D : Depletion layer width
N_D : Density of donor atoms
C_{HF} : High frequency capacitance
C_{LF} : Low frequency capacitance

ABBREVITIONS

MIS : Metal/Insulator/Semiconductor
MOS : Metal/Oxide/Semiconductor
MPS : Metal/Polymer/Semiconductor
PVA : Poly-4-Vinylphenolalchol
PVC : Polyvinyl Chloride
LUMO: Lowest Occupied Molecular Orbital
HOMO: Highest Occupied Molecular Orbital
TE : Thermionic Emission
TFE : Thermionic Field Emission
FE : Field Emission
CTM : Conduction Transport Mechanism
BH : Barrier Hight
OFET : Organic Field-Effect Transistor
OLED : Organic Light-Emitting Diode
LED : Light-Emitting Diode
SCLC : Space-Charge-Limited Current
ac : Alternating Signal
TMO : Transition Metal Oxide
RuO$_2$: Ruthenium Dioxide
XRD : X-ray Diffraction
Al : Aluminium
Au : Gold
MIG : Metal-Induced Gap

PART 1

INTRODUCTION

Semiconductor materials such as germanium (*Ge*), gallium arsenide (*GaAs*), and silicon (*Si*) atoms have a unique crystal atomic structure that becomes conductive under the effect of an electric field, optical, thermal, or electromagnetic field. These materials have four valence electrons in their outer orbital that play an essential role in electrical, optical, and thermal excitation. Due to these characteristics, they are commonly used to fabricate electronic devices such as solar cells. Photodiodes, capacitors, and transistors [1, 2]. Generally, if the fifth group atoms (phosphorus (*P*), arsenic (*As*), and antimony (*Sb*)) are doped to silicon, which has four electrons in its final orbit, releases an excess free electron in the crystal structures called donor doping atoms or n-type semiconductor. While when the silicon crystal is doped with the third group of atoms (boron (*B*), indium (*In*), or gallium (*Ga*)), it causes an electron deficiency or excess holes. This structure is called acceptor doping atoms or p-type semiconductors. The p and n-type *Si* crystals are widely used in electronic technology to fabricate traditional p/n junction devices or n/p/n, and p/n/p transistors [1].

In addition, The MS device structures are formed when a metal is contacted with a semiconductor under certain conditions, which are called Walter H. or Schottky barrier diodes (SBD), referring to Schottky. While, when a thin insulator or polymer layer is injected between semiconductor and metal during the fabrication and artificially, it is called MIS or MPS type diodes or SBD structure. However, current conduction in SBDs, is generated by majority carriers (electrons or holes), whereas in p-n junction diodes, current conduction is generally through minority carriers. Therefore, to compare both MS and p-n junction diodes, the MS diodes have a considerably high switching speed than the p-n junction diodes and lower forward bias voltage (V_F), which results in higher switching speeds and better system efficiency. Also, some commercially available p-n-type *Si* diodes are not fast enough at high frequencies.

Despite these advantages, a high reverse leakage current occurs in Schottky diodes due to shunt resistance, interface states, and low barrier height [3]. Therefore, establishing a higher barrier height between semiconductor and metal is extremely important in developing MS structures because the charge carriers in low-barrier Schottky diodes can flow in both directions with a small rectification ratio ($RR=I_F/I_R$).

The dielectric and electrical properties of MS-type Schottky barrier devices generally depend on temperature, frequency, illumination, doping atoms density, interface layer thickness, homogeneity, interface states (N_{SS}), series resistance (R_S), shunt resistance (R_{Sh}), surface cleaning or fabrication conditions, and applied bias voltage [4, 5]. In recent years, many studies have been carried out to modify the barrier and reduce the interfacial states of the Schottky barrier diodes using a composite thin dielectric material (oxide/insulator, or polymer) between metal and semiconductors[6]. This interfacial layer converts MS-type Schottky structures to MIS or MPS-type structures and fills the empty bonds, decreasing the interfacial state density, increasing barrier height, and lower ideality factor values than conventional MS structures. However, conventional SiO_2 and SnO_2 insulating layers have low dielectric constants, expensive/costly, and difficult to grow. Therefore, recently metal insulator semiconductor (MIS) Schottky barrier devices have received much attention for using organic polymers in electronic applications such as transistors, polymer integrated circuits (PICs) photodetectors, and solar cells (SCs) [5, 7]. Another critical factor affecting the performance of MS Schottky diodes with or without an interface layer is the semiconductor substrate used in this structure. Silicon is an abundant semiconductor on Earth and can easily form an oxide/insulating layer (SiO_2) on its surface with high electron mobility. Due to these properties, Si has been widely used in electronic applications as a suitable semiconductor.

Polymers generally have low conductivity, which can be improved by doping appropriate amounts of metals or metal oxides. Thus, it is believed that their electrical and optical properties can be optimized using an organic polymer doped with the appropriate metal or metal oxide material (Ru, ErO_2, RuO_2, In_2O_3) as interfacial layers between semiconductor and metal[8, 9]. However, there are various organic interfacial layers can be sandwiched in between metal and semiconductor, such as polyaniline, polythiophene, polyp indole, polyvinyl pyrrolidone (PVP), Polyvinyl chloride (PVC), and polyvinyl alcohol (PVA)[10, 11]. Among these polymers, Polyvinyl chloride (PVC) is a synthetic polymer made from the monomer vinyl chloride produced by polymerizing vinyl chloride. Depending on the intended use and desired properties, PVC can be fabricated by various processes, including bulk polymerization, emulsion, and suspension. Also, its properties can be modified for different applications, and it can be formulated with a range of additives. Its desirable properties, such as versatility, durability, good dielectric properties, good mechanical features, chemical resistance, and low cost, make it suitable for various applications, such as electrical and electronic applications. PVC is a good polymer as an interface layer because the chlorine atom has a single pair of electrons[12, 13]. However, the passivation behavior and compounds of the polymers can be improved by doping them with metal or metal oxide, which enhances their optoelectrical, dielectric, and electrical characteristics. Organic interlayers can generally inhibit the interdiffusion and reaction at the interface of MS contact, lower leakage current, reduce the density of surface states (N_{SS}) or dislocations, and passivate the unsaturated bonds on the semiconductor surface. The presence of N_{SS} and their impact on measurement results cannot be avoided, regardless of how careful the steps of chemical cleaning and the fabrication processes of the device. Therefore, choosing suitable organic polymer interlayers on the surface of the semiconductor can passivate N_{SS} and reduce their impacts[14–16].

Furthermore, transition metal oxides (TMOs) are frequently used in electronic applications and have good magnetic, optical, and electrical properties. These compounds are in various electrochemical and electrical applications because of their high chemical and thermal stability with low resistance[17, 18]. Among them, Ruthenium dioxide (RuO_2) is a TMOs chemical compound, a dark brown or black solid that is soluble in acids but insoluble in water. It has a good conductor of electricity with a high melting point and has a tetragonal crystal structure, making it useful in electrochemical and electronic applications. RuO_2 is prepared by heating ruthenium (III) oxide or ruthenium metal in the presence of oxygen. It is a semiconductor that has excellent photocatalytic properties with a bandgap of approximately 2.0 eV, making it suitable for manufacturing capacitors, resistors, and some electronic components. It is also used as a photocatalyst material in various chemical reactions [19–21]. Therefore,

RuO_2 has the capability to generate electron and hole ($e^- - h^+$) pairs under the effect of illumination intensity. The nanostructure of RuO_2 is found as a tetragonal crystal phase (110). This element is frequently used in electronic and electrochemical devices due to its chemical and temperature stability [22–25].

The performance of the Schottky structures depends on many factors, such as the barrier inhomogeneity, homogeneity and thickness of the interlayer, the doping level of atoms, and interface trap or states (N_{SS}) levels. Therefore, to produce high-quality SBDs MPS-type structures, their main photoresponse, electrical, and dielectric parameters must be well-known and defined. However, scientists have developed different measurement methods to evaluate these basic parameters, such as interface states (N_{SS}), zero barrier height (Φ_{B0}), series and shunt resistances (R_S, R_{Sh}), and ideality factor, which can be obtained from both the reverse and forward biases of the Current-Voltage (I-V) measurement technique under various illumination intensities. Also, both open circuit voltage and short circuit current (I_{SC}, V_{OC}), fill factor (FF), photosensitivity, and responsivity can be extracted. On the other hand, Fermi energy (E_F), donor doping density (N_D), barrier height (Φ_B (C-V)), maximum electric field (E_m), depletion layer width (W_D), N_{SS} can be evaluated using capacitance and conductance (C, G/ω) characteristics at various frequencies and voltages. Furthermore, the dielectric parameters such as real and imaginary elements of the dielectric permittivity (ε' and ε''), dielectric loss coefficient ($\tan \delta$), ac conductivity (σ_{ac}), and real and imaginary parts of the complex electrical module (M' and M'') can also be evaluated using the same measurements. However, this thesis mainly aims to improve the photoresponse, electric, and dielectric properties of the produced device by using a metal dioxide-doped polymer interface (PVC-doped RuO_2) with high dielectric (MPS) structures instead of the conventional low dielectric insulator/oxide interlayer. Therefore, the basic photoresponse, electric, and dielectric characteristics of RuO_2 doped in a PVC organic polymer were investigated using both the I-V data under various illumination intensities and the impedance spectroscopy method, including capacitance/conductance (C-V-f and G/ω-V-f) characteristics at room temperature in the dark. This interlayer may improve its optoelectronic and electrical performance.

In this thesis, Au/(RuO_2:PVC)/n-Si (MPS) devices were fabricated. First, the effects on the interfacial layer (RuO_2- doped PVC) behaviors were analyzed. For this purpose, X-ray diffraction (XRD), UV-Visible region, and scanning electron microscopy (SEM) were performed. Then the interfacial polymer layer RuO_2:PVC was grown in between the semiconductor and metal contact, and the effect of the polymer interfacial layer on the essential basic photovoltaic, electrical, and dielectric parameters on the produced MPS Schottky devices were investigated. The basic photovoltaic and electrical parameters were extracted from reverse and forward bias current-voltage (*I-V*) at various illumination levels. Also, the electrical and dielectric factors were analyzed at room temperature from capacitance and conductance (C, G/ω) data at a wide range of frequencies and voltages. While *I-V* measurements were done between ±5 V and 50 mW to 300 mW with 50 mW steps, C and G/ω data were obtained between ±4 V and at various frequencies. Some basic electrical and photovoltaic parameters, such as n, Φ_{B0}, R_S, R_{Sh}, V_{OC}, I_{SC}, *FF,* and N_{SS}, were evaluated using the *I-V* measurements. The V_{OC}, I_{SC}, and *FF* results have a regular variation in the light-dependent *I-V* characteristic. Also, the N_{SS} vs. ($E_C - E_{SS}$) profile distribution were evaluated using the forward bias of *I-V* data as voltage-dependent of both n and Φ_{B0} in the dark and at diverse illumination intensities. On the other hand, the other electrical parameters like E_F, $\Phi_B(C\text{-}V)$, N_D, and W_D were evaluated using *C-V-f* and *G/ω-V-f* data. Also, the dielectric factors such as real and imaginary elements of dielectric permittivity (ϵ' and ϵ''), dielectric loss coefficient ($\tan\delta$), *ac* conductivity (σ_{ac}) and real and imaginary parts (M' and M'') of the electrical module were extracted using the same measurement.

1.1. THEORETICAL INFORMATION

1.1.1. Literate Summary of Schottky Structures

Numerous theoretical and experimental studies have been carried out on MS devices, which are usually performed via depositing a metal onto the semiconductor surface in a high-temperature and vacuum environment. Recently, researchers have attempted to improve the performance of MS structures by using substances with various electrical and chemical properties as an interfacial layer, such as oxide, polymer, and insulator, which leads to converting the MS structures into MIS or MPS structures. However, despite these studies, completely reliable and accurate results on the nature of the barrier between the semiconductor and metal of the Schottky devices and their conduction mechanisms have not been obtained. Since Walter Hans Schottky presented the first research on MS structures in 1938, these devices are typically known as Schottky barrier diodes. Schottky described the barrier-creation process and explained various models for evaluating the shape and height of the barrier. Later, Bethe proposed the thermionic emission theory (TE) or model representing the current conduction mechanism in MS structures in 1942. According to this model, current is defined as the transmission of electrons to or from the metal [26].

The MS structure converts into MIS/MOS, MPS, or MFS structures when an oxide/insulator, polymer, or ferroelectric layer forms naturally or artificially at the metal-semiconductor contact. If the interfacial layer is thin enough (≤ 30-40 nm), these structures are called diodes, while when it is thicker, they are used as a capacitor and can store charge or energy. The MIS-type capacitor was first developed by J.L.Moll in 1959. Both values of the dielectric coefficient and the thickness of the interfacial layer are essential effective parameters in the MIS-type capacitor structure. Also, to obtain an ultra-capacitor, there is a limitation in the interfacial layer thickness. However, the capacitance of the capacitor can be significantly increased using high-dielectric materials, and the capacitance of MIS or MPS structures also varies considerably with the applied voltage[3, 27]. The performance and reliability of these devices depend on many factors, especially the dielectric constant/thickness of the interfacial layer, the distribution/homogeneity of the Schottky barrier performed between the M/S, series resistance, and interface states. The first study on the interfacial insulator layer in the Schottky structure was made by Sze and Cowley[28] in 1965. In 1971, Rhoderick and Card [29]obtained the interfacial state density at the M/S interface from the I-V data as a function of energy based on the assumption that the BH and n change with voltage. Then, many researchers investigated the effects of the existence of both interfacial layer and N_{SS} on the performance of Schottky barrier diodes and obtained the energy-dependent distribution of these interfacial state densities located at the M/S contact within the forbidden energy band of the semiconductor, using I-V characteristic [29, 30].

Although the insulator SiO_2 is generally stable and easy to grow, it has a low dielectric constant ($3,8\varepsilon_o$) that causes a high leakage current and cannot passivate the surface states. Therefore, recently, polymer or organic materials are used by scientists instead of low-dielectric insulators. However, the performance of the MPS structures depends on many factors, such as the series resistance, barrier height, and interfacial states between metal and polymer, polymer and semiconductor. Both series resistance and interfacial organic layer are mainly affected parameters on the performance of MPS structures. Because the voltage or electric field applied is shared between the depletion layer interface, series resistance, and the depletion layer. Therefore, many researchers have revealed that these devices' performance and reliability depend highly on the performance of a high-quality interfacial layer, series resistance, interface states, and barrier height. For instance, Campbell et al. (1996) used thin films of organic material to adjust the Schottky barrier height and semiconductor band gap formed between the semiconductor and organic interface layer to control the properties of MS-type electronic devices. They observed that the barrier has increased using this material and successfully described the surface changes potential. Thus, their modified contact barrier height demonstrated the advantage of organic thin-film Schottky diodes over conventional MS Schottky diodes. In addition, this study provided a physical reason to change the relative energy levels between metal and semiconductors [31]. Also, various materials have been added to the polymer matrix in many scientific studies to reduce both the interface states, leakage current and improve its optical, electrical, and dielectric properties.

Yakuphanoglu et al. (2008) studied the effect of the organic interlayer in Al/p-Si/CoPc Schottky structures on their interface properties and electrical parameters. Using the I-V properties, they obtained some parameters such as the *BH* (0.90 eV), n (1.33), and R_S. They also showed that the obtained barrier height for the produced device is significantly larger than that evaluated for the conventional Al/p-Si Diode. This is because the Cobalt Phthalocyanine interlayer produces a physical barrier between p-Si and Al metal. In addition, in this study, it has been illustrated that the density of the interface state varies between 0.69×10^{14} $eV^{-1}cm^{-2}$ and 1.23×10^{14} eV^{-1}/cm^{2} [32].

Vural et al. (2010), in this study, the Al/Rhodamine/n-GaAs MPS structure was examined using the *I-V* characteristics in various ranges of temperature (80-350 K), and it was shown that the ideality factor (*n*) decrement, but the barrier height (*BH*) increased as temperature increases. Such behavior is attributed to the inhomogeneity of the *BH* that has a Gaussian distribution. In addition, in this study, it was determined that the traditional Al/n-GaA barrier height was considerably higher than the barrier height obtained for Al/ Rh101/n-GaAs[33].

H. KANBUR et al. (2011) investigate the effect of illumination on Au/n-CdTe (SBDs) using the current-voltage, conductance-voltage, and capacitance-voltage characteristics in the dark and under different illumination levels. The essential electrical factors such as I_o, n, Φ_{B0}, R_S, and R_{Sh} evaluated from *I-V* data were strong functions of the illumination intensities, and while the I_0 and n values increase Φ_{B0}, R_S, and R_{Sh} reduce as the density of illumination increases. The obtained results show that both capacitance and conductance values are increased with increasing levels of illumination and have peaks at high levels of illumination. Also, both of the forward and reverse currents values are increased as illumination intensity increases [34].

H.G. Çetinkaya et al. (2013) analyzed the performance of the Au/ Bi:PVA /n-Si Schottky structures from (*I-V-T*) data in the dark and at different illumination intensities. Some main parameters were obtained, such as I_o, n, Φ_{B0}, R_S, and R_{Sh} as functions of illumination level and temperature, and all of them are highly functions of temperature and illumination. The fill factor (*FF*) value was found as 0.40 under 50 W at 320 K, which is near a photodiode. As a result, the produced structure can be used in optoelectronic applications[35].

S. Demirezen et al. (2013) have investigated the effect of illumination on the performance of the Au/ Bi:PVA /n-Si Schottky devices using both (*I-V*) and (*C/G/ω - V*) data in the dark and at 250 W illumination power. The obtained R_S and n values were high due to the barrier inhomogeneity, particular distribution of N_{SS} at the interface, form of BH at M/S interface, and fabrication processes. While the values of R_S and R_{Sh} decrease, *C* and *G/ω* increase under illumination due to the induced e^- - h^+ pairs in the depletion region. Also, the fill factor (*FF*) was to be as 28.5% under 250 W illumination level, which is sufficiently high. Therefore, the produced photodiodes are highly sensitive to light and can be candidates as a capacitance sensor or photodiode[36].

Murat Soylu et al. (2014) have investigated the illumination intensity effects of $GaFeO_3$/p-Si heterostructure on its electrical characteristics using current-voltage data in dark and under different illumination intensities. The photocurrent is strongly sensitive to illumination in reverse-biased measurements. Also, both zero-bias barrier height (Φ_{B0}) and ideality factor (n) are dependent strongly on illumination, and while n increases, Φ_{B0} decreases with decreasing illumination. The combination of a thin $GaFeO_3$ layer and p-Si is believed to be used as a photosensor or photodiode [37].

Mekki et al. (2016) produced Schottky photodiodes (Al/p-Si/ GO doped MB /Au). They investigate its illumination effects using the $I–V$ characteristics. The reverse current increases with increased illumination levels. Also, the largest photosensitivity (I_{photo} /I_{dark}) for the diode with the ratio of 8.67 $*10^3$ was obtained at 0.03 for the graphene oxide doped methylene blue ratio under 10 V at 100 mW/cm^2. These findings suggest that the fabricated structure can be used in optoelectronic device applications as a photo-capacitor and a photodiode [38].

Gülçin Ersöz et al. (2017) produced and investigated the Au/PPy/n-Si (MPS) structures using $I–V$ characteristics in the dark and at 100 W/m^2 illumination intensity. The basic electronic parameters were extracted, such as zero-bias barrier height (Φ_{B0}), reverse-saturation current (I_o), ideality factor (n), and both series and shunt resistances (R_{Sh}, R_S). Also, the open-circuit voltage V_{OC} was obtained as 0.36 V at 100 W/m^2 illumination intensity. This indicates that the produced device has a photovoltaic behavior and can be practically used in optoelectronic applications [39].

H E Lapa et al. (2019) studied the effect of the illumination intensities on the produced Au/(P_3DMTFT)/n-GaAs (SBDs) using current–voltage ($I–V$) data in the dark and at different illumination power (50 to 200 W). The values of I_o, n, and Φ_{B0} were extracted as 7.25* 10^{-12} A, 1.34, and 0.91 eV and, in the dark. While these factors were found at 200 W as 5.11* 10^{-10} A 1.85, and 0.80 eV, respectively. Also, Cheung's and modified Norde's techniques were utilized to evaluate the R_S value in the dark and at different illumination levels. Obtained results show that the fabricated devices exhibit photovoltaic characteristics with the values of V_{OC}, I_{SC}, and FF were found as 0.37 V, 1.45 * 10^{-6} A, and 0.65 at 200 W[40].

Sebahaddin Alptekin et al. (2020) fabricated Au/ polymer (PVP)/n-Si structures and investigated their electrical performance from the ($C/G–V–f$) measurements. The evaluated electrical parameters were highly dependent on frequency due to changes in N_{SS} level, polymer interlayer, and dipole / interfacial polarization. The R_S and N_{SS} voltage-dependent profiles were extracted from the Hill-Coleman and Nicollian–Brews / low–high-frequency capacitance. The values of Φ_{B0} and W_D increase almost linearly with increasing frequency. On the other hand, the values of R_S decrease as frequency increases. The obtained results indicate that the produced structures yield a preferable device compared to conventional structures because of some advantages of PVP interlayers, such as easy-grown processes, flexibility, and low-cost/weight[41].

A. Tataroglu et al. (2020) In this study, the PVP-doped In_2O_3 was used as an interfacial layer in the fabricated Au/ (PVP: In_2O_3)/n- structures. The (C-V-f and G/ω-V-f) measurements were analyzed in the wide range of frequency (10 kHz - 1 MHz). The values of both R_S and N_{SS} were extracted from the conductance and Hill-Coleman techniques. Also, some electronic factors such as the *BH*, surface potential, W_D, and diffusion potential were obtained from the C^{-2}-V characteristics. The obtained results indicate that C and G are functions of frequency[42].

Ali Osman Tezcan et al. (2021) fabricated an Au/BOD:Z:EN/n-Si/In Schottky structure to study device applications based on organic compounds from voltage-current data in the dark and at different illumination levels. All main electrical parameters result, such as *BH* and n elements, showed strong dependencies on illumination. The basic photovoltaic elements such as short circuit current and open circuit voltage, were evaluated with various illumination intestines and found as 10μA, 150 mV at 100 mW/cm^2. The obtained results show a photovoltaic behavior, and the device can be used in electrical and photoelectrical applications [43].

Onur Ongun et al. (2021) in this work, the Au/Pyr:BOD/n-Si/In Schottky diodes were produced, and their photovoltaic and electronic properties were studied by current-voltage (I-V) data in the dark and at different illumination levels. The evaluated barrier height and ideality factor in the dark and at 100 mW.cm^{-2} illumination intensities were found to be (0.75 eV, 0.87 eV) and (2.84, 1.55), respectively. Also, both short-circuit current density and open-circuit voltage values were calculated as 0.56 mA/cm^2 and

0.26 V at 100 mW.cm^{-2}. The obtained results suggest that the fabricated device can be used in optoelectronic applications [44].

S¸emsettin Altında et al. (2022). In this study, the illumination effect on the Au/(PVC-Er_2O_3)/n-Si structure was investigated in various illumination levels. The main electrical factors such as the barrier height (Φ_{B0}), ideality factor (n), series and shunt resistances (R_S ,R_{Sh}), energy-dependence of interface states (N_{SS}), photocurrent (I_{Ph}) , and photosensitivity (S) were evaluated using (I–V) measurements. The Φ_{B0} values linearly decrease with increases in both illumination and n. The I_{SC}, V_{OC}, FF, and η values were found to be 0.28 μA, 0.20 V, 29.90%, and 0.2% at 100 mW.cm^{-2}, respectively. The evaluated values indicate that the produced MPS Schottky structures can be used in photovoltaic applications [45].

However, many studies have been carried out in the scientific literature to add various materials to the polymer matrix to improve the interface states between the semiconductor and the polymer and the optical, electrical, and dielectric properties of the Schottky structures. A summary of photovoltaic parameters, such as values of short-circuit current (I_{SC}), open-circuit voltage (V_{OC}), filling factor (FF), and photo-response (I_{photo}/I_{dark}), are stated in Table 1.1. This table shows some discrepancies among these parameters due to the interlayer, doped material in the interfacial layer and its thickness, fabrication processes, surface states, series, and shunt resistances, etc.

Table 1.1. Summary of various photovoltaic parameters for some produced samples.

Samples	**I_{SC} (mA)**	**V_{OC} (V)**	***FF*%**	**I_p/I_d**	**P(mW.cm^{-2})**	**Ref**
This study	6.4*10^{-3}	0.118	46		50	[46]
Au/(Er_2O_3:PVC)/n-Si	0.28*10^{-3}	0.20	29.9	-	100	[47]
Au/Bi:PVA/n-Si	0.170	0.40	28.5	13000	100	[36]
Au/(P_3DMTFT)/n-GaAs	0.5*10^{-3}	0.37	0.65		100	[40]
Al/p-Si/GO:MB/Au	0.193	0.53	-	31500	100	[48]
Al/$GaFeO_3$/p-Si	0.23	0.18	30	-	100	[49]
Al/(PCBM/ZnO:NiO)/p-Si	2.06	0.30	27	1277	100	[50]

1.1.2. Principle of Semiconductor

In solid-state physics, the lowest empty band is called the conduction band (E_C), while the highest full band is known as the valence band (E_V). In an ideal situation, no energy level arises between these two levels (no allowed electron states), which is known as the forbidden band ($Eg=E_C-E_V$) or forbidden energy gap. The semiconductors and insulators are unlike conductors, as shown in Figure 1.1. In conductors, there is no band gap between the E_C and E_V, and these two bands overlap each other. Therefore, electrons can flow inside the partially filled valence band or in two overlapping bands, which generate free electrons that participate in the conduction process. While in both insulators and semiconductors, there is a band gap between both E_C and. The E_V in insulators is completely filled with electrons that cannot move between atoms freely because of their covalent bonds. But in semiconductors, electrons can be exited to the E_C from E_V via optical or thermal excitation. The insulator band gap is higher than 4 eV (≥~ 4 eV), so it is almost impossible to optically or thermally excite electrons from the E_V to the E_C. In contrast, semiconductors have a smaller energy gap compared to insulators. Therefore, even at low temperatures, some electrons can move from the E_V, and thus, the conduction increases with increasing temperature or illumination. However, at absolute temperature (0 K), a semiconductor behaves like an insulator (all electrons in E_V)[3].

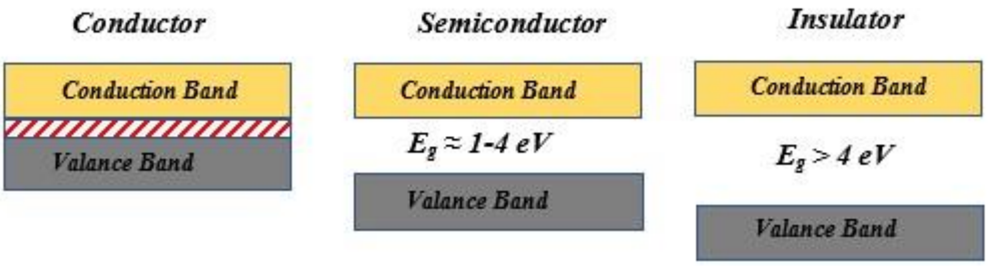

Figure 1.1. Schematic band diagram for conductor, semiconductor, and insulator.

The forbidden energy bands in semiconductors are unequal and take values between 0.1 to 4 eV. The energy gaps of some main semiconductors, such as *Ge*, *Si*, and *GaAs* at room temperature, are approximately 0.66 eV, 1.12 eV, and 1.45 eV, respectively [51]. Also, each electron flows to the E_C from the E_V, producing a positive charge carrier in the valence band (hole) that can be filled by another electron. At a certain temperature, an equilibrium occurs between electrons flowing to the E_C and electrons falling to the E_V. Therefore, conduction in a semiconductor is produced by both holes and electrons. However, holes in the p-type materials are the majority carriers, while electrons are the majority carriers in the n-type. With increasing illumination or temperature, the carriers gain additional energy, and the transmission increases rapidly with increasing both illumination or temperature. Furthermore, semiconductors generally have impedances between 10^{-2} and 10^{9} Ω at room temperature, but they behave like conductors if the number of doping atoms is increased. However, in semiconductor devices, the conduction depends on many factors, such as the density of the doping atoms, the illumination, impurities, lattice defects, or deviation from the chemical composition. However, intrinsic or pure semiconductors have negligible conductivity, with approximately 10^{10} free electrons and holes per cm^{-3} at room temperature. Thus, the semiconductor crystal generally is neutral because of the equal number of negative and positive charges. An additional atom can be added to the semiconductor atom (doped semiconductor) to increase its conductivity. Doping atoms in semiconductors increase or adjust the number of free holes or electrons. In the doping process, when fifth group atoms (5 electrons in their outer orbit) such as Phosphorus (*P*), Antimony (*Sb*), Arsenic (*As*), or Bismuth (*Bi*) are added to the *Si* or *Ge* semiconductor that has four electrons in its outer orbital (valence electrons), an excess of electrons occurs. These structures are called n-type semiconductors, and doping atoms are called donor or donor doping atoms. In contrast, when Boron (*B*), Gallium (*Ga*), Indium (*In*), or Aluminum (*Al*) atoms in the third group (3 electrons in their outer orbit) are doped to these crystals, electron deficiency or an excess of empty space occurs. These semiconductors types are called p-type, and the doping atoms are called acceptors. As seen in Figure 2.2, electrons are the majority carriers in the n-type, and holes in the p-type materials are the majority carriers [1, 51].

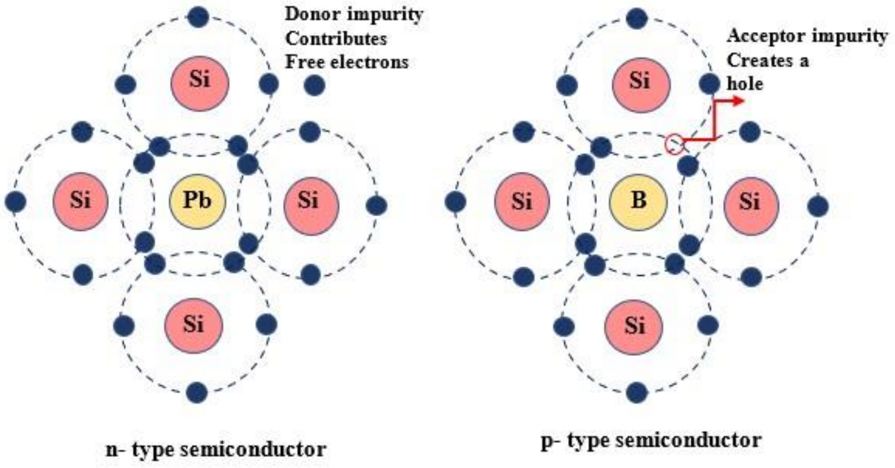

Figure 1.1. Formation of p-type and n-type semiconductors

Semiconductors exist as single elements or compounds. Germanium (*Ge*) and Silicon (*Si*) are the most common single-element semiconductors used in electronic applications with a diamond lattice crystalline structure. In this structure, each atom is located at the center and has four nearest neighbors at the corners of a regular tetrahedron. In contrast, compound semiconductors such as *GaSb, InAs, InSb, GaP, GaAs, SiC, GaN, AlGaNi*, and *InGaP* include various alloys bonding with each other and have special properties that meet specific requirements.

1.1.3. Organic Semiconductor

Electrical conductivity in organic compounds became a new and interesting study subject. Organic semiconductor substances have excellent chemical and physical properties and can be produced by easy formation processes such as electrochemical deposition, electrostatic spraying, sol-gel, hydrothermal growth, super-critical fluid, and spin coating [52]. In addition, using organic compounds in electronic applications has some difficulties, such as operation in ambient conditions (oxygen, moisture, ultra violet light) or stability during manufacturing [53]. However, the characteristics, specifications, and improvement of semiconductors, metals, and polymer materials are essential in the future of nanotechnologies and nanoscience. Semiconducting polymers are conjugated polymers formed with alternating single and double bonds between the polymer's carbon atoms. However, both the edge band of the valance band, which is called to Highest Occupied Molecular Orbital, and the band edge of the conduction band, referred to as the Lowest Unoccupied Molecular Orbital (HOMO, LUMO) levels, exist in organic semiconductors (conjugated polymers), and their energy gap is within the visible photon range. Therefore, when an incident photon with energy more than the energy gap is absorbed, an electron gets enough energy to jump to the level of LUMO, leaving a hole behind in the HOMO[54]. Recently, organic semiconductors have been widely investigated for their potential applications in electronic technologies such as photovoltaics, photodetectors, organic light-emitting diodes (OLEDs), FET's and organic memory devices [55, 56].

1.1.4. Structure of Metal-Polymer-Semiconductor

Braun (1874) is the first scientist to describe the rectifying characteristics of asymmetrical electronic conduction for metal-semiconductor junctions. He discovered that this behavior is due to the high electrical resistance of a thin interlayer. Then Schottky and Mott (1940, 1938) proposed a barrier heights model for metal-semiconductor devices. They proposed that both the semiconductor and metal bands are in contact control to align semiconductor and metal vacuum levels in coincidence. In (1939) Schweikert determined the *BH* and discovered that the barrier height increments nearly linearly as metal work function decreases in metal-selenium rectifiers. In (1954) the first organic semiconductor was discovered by a Japanese chemist. In 1962-63 MOS diodes were employed to investigate a thermally oxidized surface of silicon [3, 57] The research on semiconductor devices increased during the early nineteenth century. Since 1960s several significant investigations and improvements have been performed in Schottky barrier diodes. These investigations were developed in 1970s in two ways. First, the knowledge gained from the previous studies was used in the development of Schottky barrier devices in industrial applications. Secondly, several studies were made in order to get a complete understanding of MS structures [27]. Furthermore, in 1970s, the development of innovative nanoparticles was a result of theoretical and experimental information in the fields of materials science, chemistry, and physics. The physical and chemical properties of a nanoparticle have led to the development of several devices in electronic technologies. Also, several studies have been made on organic semiconductors, which leads to increased interest in organic electronics technology. In 1977 A. J. Heeger, Alan G. MacDiarmid, and H. Shirakawa, have been explored chemically doped polyacetylene with a high-conducting polymer, which suggests that polymers can be used as a good active electrical substance [58] In -1970s, the first polyacetylene conducting polymers were produced as a novel organic material creation that had the same optical and electrical characteristics as inorganic semiconductors and metals. This invention has received significant attention from both engineering communities and researchers. H. Shirakawa, Alan G. Diarmid, and A. J. Heeger discovered and developed the electrically conductive polymer in 2000 and were awarded a Chemistry Nobel Prize. This incredible development opened up a new organic electronics technology in the field of semiconducting organic materials [59] Therefore, according to good specifications of conducting organic polymer when compared with conventional semiconductors, such as low production cost, and flexible electronics, it is important to investigate the mechanical, optical, electric, dielectric, and thermal characteristics of metal polymer semiconductor and metal/polymer: metal dioxide /semiconductor structures with various illumination, voltage, frequency, and temperature conditions.

Generally, electronic devices based on organic semiconductors are referred to as organic electronics devices, particularly conjugated polymers, which is used in the following main technology, solar cells, organic photovoltaic, organic thin film transistors (OFET), and organic light-emitting devices (OLEDs). The π-orbitals exist in organic substances are responsible for semiconducting properties and carrier movement. The OFETs have shown a good performance compared to amorphous silicon thin film transistors [60] . However, significant issues have to be studied to understand the advantages of organic electronics fully. These challenges include some difficulty of polymer solvent-selectivity and dissolution especially encountered in the fabrication process as well as the fabricating stability.

In MS contact structures, an organic interlayer is sandwiched between metal and semiconductor, which can play an essential role in their electrical performance and convert them to MPS structures. There are various types of polymeric interlayers, such as polyaniline, polyvinyl alcohol (PVA), Polyvinyl chloride (PVC), poly (3-

hexylthiophene), poly (alkylthiophene) polypyrrole, and polythiophene. However, the current transport and conduction mechanism (CCM or CTM) and the barrier height formation between semiconductor and metal mainly depend on the interlayer and its homogeneity, surface preparation process, the doping atoms concentration in the semiconductor, the series resistance and surface states located between the semiconductor and interfacial layer. Recently, studying the electric, dielectric, and optical properties of MPS structures is essential in electronics technology. The presence of interfacial interaction at the interface of the semiconductor and metal creates deleterious silicide in traditional MS devices, causing a shift of interface into the bulk region of the semiconductor. In general, the barrier height is linearly dependent on the heat of silicide formation, where the silicide properties will control the formation of the *BH* and affect the evaluation of an accurate BH.

In the MPS structures, enough thin-film polymeric insulator layer is used as an interfacial layer on the surface of the semiconductor. With this interlayer, a significant number of electrons can tunnel through it, reducing both the intrinsic surface state density and the dangling bonds. Also, a thin polymer layer doped with some metals can be penetrated and interact with the semiconductor and produce silicide. However, the polymer layer thicknesses can possibly be controlled by the range of angstroms, but the thickness of polymer layers tends to increase over time which leads to reduce the tunneling current through it.

PART 2

METAL-SEMICONDUCTOR STRUCTURES AND THEIR CONDUCTION MECHANISMS

2.1. METAL-SEMICONDUCTOR (MS) CONTACTS (SCHOTTKY MOTT THEORY)

Metal-semiconductor (MS) structures are essential scientific and technology attractive due to their interesting properties and potential applications in optoelectronic and electronic devices. In solid-state physics, a contact of metal-semiconductor (MS) is an electrical connection type where a metal is directly contacted with a semiconductor. These structures are preferred to be used in many semiconductor devices due to their simplicity of the fabrication process, high rectification rate, and better than the p-n in high-frequency applications.

The metal-semiconductor structures operate as both an ohmic contact (non-rectifying contact) or a Schottky contact (rectifying contact), depending on the distinction between the work functions of metal and semiconductor. The work function of the metal (Φ_M) is the required energy for an electron to move to the vacuum level from the metal Fermi energy level. For instance, the typical value of Φ_M for Aluminium (Al) is from 4.1 to 4.3 eV and from 4.8 to 5.1 eV for Gold (Au). The non-rectifying contact exhibits a linear I-V behavior for both polarities of the applied voltage. This characteristic implies a small interfacial resistance that permits the same current to flow in both directions easily. In contrast, the Schottky contact has a nonlinear I-V behavior where the current can flow easily only in the forward bias while preventing it from flowing in the reverse bias direction. Rectifier contacts are used in MS field-effect transistors, Schottky transistors, and Schottky diodes. When the n-type semiconductor and the metal are brought into contact, electrons in the semiconductor's conduction band can move into the metal until the Fermi levels of the two materials are equalized. This process is known as Fermi level pinning and results in the formation of a potential barrier at the interface, which can inhibit the flow of charge carriers. [3, 27]. A schematic diagram for a metal semiconductor structure is illustrated in Figure 2.1.

According to the Schottky-Mott theory, the potential barrier generated from the direct contact of the semiconductor and metal is caused by the difference between their work functions. When an n-type semiconductor is brought into contact with the metal, the electrons in the conduction band can flow easily from the semiconductor to the metal until an equilibrium state occurs (equalized of two Fermi levels), which leads to a decrease in the concentration of free electron near the boundary region. These electrons leave positive ionized charges (donors), causing the depletion of mobile electrons (depletion region). Also, they produce a thin sheet of negatively charged on the metal side of the interface within the screen distance (0.5 Å), causing an electric field at the junction. Mott assumed that an uncharged thin semiconductor layer is sandwiched between a uniform doped semiconductor and the metal. The electric field strength is fixed, and the potential linearly increases in the narrow layer region, and the resulting barrier is referred to as the Mott barrier.

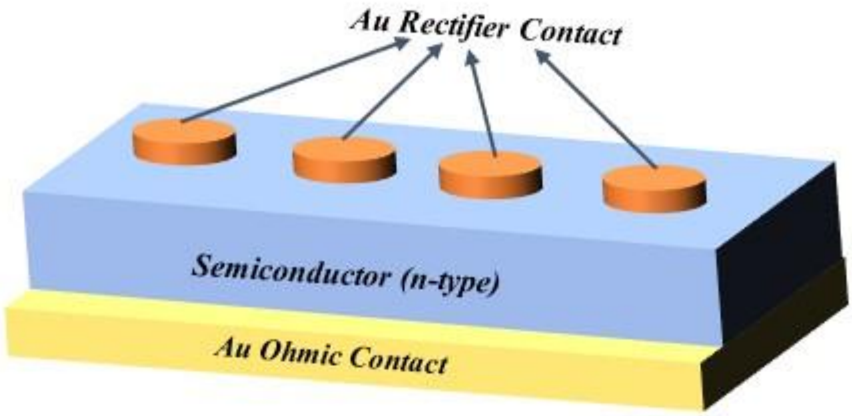

Figure 2.1. Schematic diagram of MS structure.

This chapter discusses the essential physics of MS devices, including both mechanism of barrier formation and current transportation, as well as some of the important parameters that affect them, such as the image force lowering, ideality factor, and interface states[27].

2.1.1. Ideal Rectifier (Schottky) Contacts

Based on the Schottky-Mott model, the energy band diagram for an MS structure for an n-type semiconductor without contact is illustrated in Figure 2.2, where the work function of the metal is higher than the work function of the semiconductor ($\Phi_M > \Phi_S$). Here, Φ_M and Φ_S are the energy required for an electron to liberate from the metal surface and semiconductor Fermi level (E_F) to the level of vacuum (E_0). The energy differences between E_o and the lower edge of the conduction band (E_C) level is defined as the electron affinity of the semiconductor (χ_s). Also, the density distribution of electrons for both semiconductor and metal is illustrated in the same figure. This figure shows that the electron energy of the metal is lower than the electron energy of the semiconductor due to the distinction in their Fermi levels. As the semiconductor and metal are connected, the electrons start flowing to the metal from the semiconductor until the thermal equilibrium is achieved and Fermi levels of both semiconductor and metal are aligned. As displayed in Figure 2.3, the flow of electrons to the metal produces a depleted layer in the semiconductor. While due to the high electron density in the metal, the space charge region width in the metal is relatively small and can be negligible compared to the semiconductor [27].

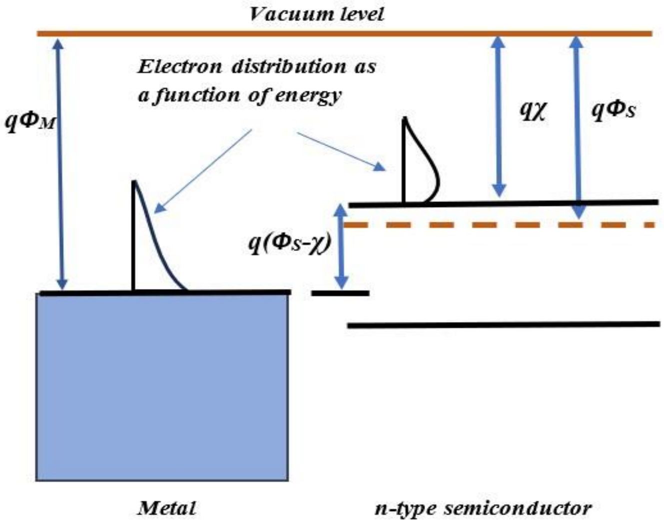

Figure 2.2. Energy band diagram of MS before contact (n-type semiconductor).

At thermal equilibrium, the potential barrier difference between the metal and semiconductor is equal.

$$\Phi_B = \Phi_M - \chi_S \tag{2.1}$$

Here (Φ_B) is the Schottky barrier height. However, electrons flowing to a metal from a semiconductor face a built-in barrier potential (V_{bi}). This barrier is defined as the distinction between both metal/semiconductor work functions, as illustrated in the following equation.

$$V_{bi} = \Phi_M - \Phi_S \tag{2.2}$$

The next Figure 2.3, shows the barrier formation process using energy-band diagrams representations. The Φ_S has a similar Φ_M expression, but its quantity is variable according to the fermi level changes due to the semiconductor doping density (N_D). In an ideal MS contact, the barrier and interface states are not considered. In general, the BH is greater than the thermal voltage (q/kT), and the semiconductor depletion layer (high resistivity area) is depleted from charge carriers. Schottky assumed a uniform doped semiconductor in his analysis. Therefore, the density of charge is uniformly distributed at the depletion region, and the electrical field strength linearly increases with increasing distance in the space-charge region.

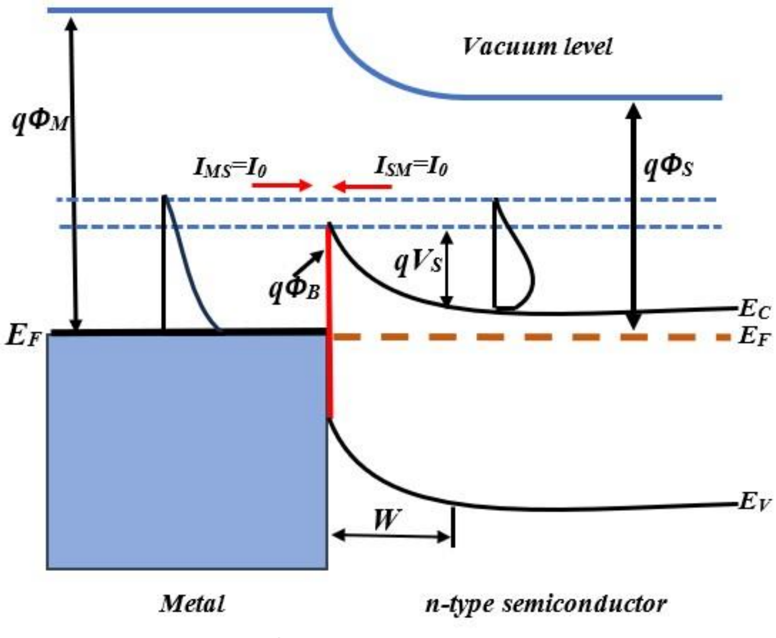

Figure 2.3. Energy band diagram for MS (n-type semiconductor) at equilibrium state ($\Phi_M > \Phi_S$).

2.1.2. Rectifier (Schottky) Contacts

In the ideal case, when a metal and an n-type semiconductor are directly contacted, electrons have larger energy in the semiconductor conduction band flowing to the metal until both Fermi levels align. As the electrons flow to the metal, the free electron concentration decreases and leaves behind a positive charge (ionized donors), as well as generating a depleted free electrons region. However, when the semiconductor work function is lower than the work function of the metal ($\Phi_S < \Phi_M$), this means that the Fermi level of the metal is lower than that of the semiconductor. Furthermore, as shown in Figure 2.3, a bending of the energy bands occurs in the depletion region due to the generated internal electric field (ξ) in the same region, creating a potential barrier between the metal and the semiconductor (qV_0 or qV_{bi}). Where qV_{bi} is the energy required for electrons in the E_C to overcome and move to the metal side.

$$qV_0 = q(\Phi_m - \Phi_S) \tag{2.3}$$

However, the potential barrier height that must be overcome for electrons to move to the conduction band of the semiconductor from the metal is.

$$q\Phi_B = q(\Phi_M - \chi_S) \tag{2.4}$$

Here, χ_s is the energy difference between the level of the vacuum and the semiconductor E_C and is defined as electron affinity [27, 61].

2.1.3. Forward and Reverse Bias

At thermal equilibrium, the electrons flowing to the semiconductor from the metal (I_{MS}) are equal to the electrons traveling to the metal from the semiconductor. Thus, the net flowing current through the junction is zero.

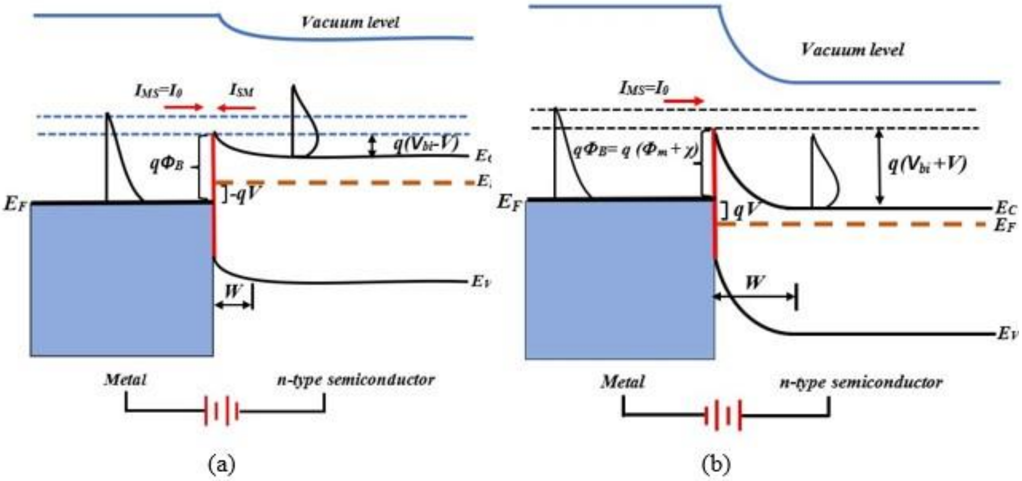

Figure 2.4. Energy band diagrams of an MS Schottky structure (n-type semiconductor). (a) forward bias, (b) reverse bias.

The forward bias of the MS contact occurs when a negative voltage (−*V*) is applied to the semiconductor (n-type). As illustrated in Figure 2-4 (a), both the built-in potential value and depletion layer width (W_D) are decreased. Therefore, the built-in potential value reduces to $q(V_{bi}-V)$, and many electrons can easily move to the metal, leading to an exponential increase in the current (I_{MS}), as illustrated in the next equation.

$$I_{SM} = I_0 \exp\left(V/V_T\right) \tag{2.5a}$$

$$V_T = kT/q \tag{2.5b}$$

Where (V_T) is the thermal voltage. In this situation, both values of the barrier height (Φ_B) and the I_{MS} current remain fixed with the applied voltage as their thermal equilibrium values (I_o, Φ_B). Thus, the following formula can express the forward bias net current flowing through the structure [27].

$$I = I_{SM} - I_{MS} = I_0 \exp\left(V/V_T\right) - I_0 = I_0\left[\exp\left(V/V_T\right) - 1\right] \tag{2.6}$$

$$I = I_0\left[\exp\left(\frac{q(V-IR_S)}{kT}\right) - 1\right] \tag{2.7}$$

Where T is the temperature in Kelvin, I_o is the reverse saturation current, q is the electronic charge, and k is the Boltzmann constant. However, according to the pure *TE* theory (ideal case), the ideality factor (n) is assumed as one in Equation 2.4. If the ideality factor exceeds the value of one and the diode has a series resistance (R_S), Eq.2.8 turns into Equation 2.9, and the (-1) value is too small compared to the exponential expression, especially at room and above temperatures and can be neglected.

$$I = I_0\left[\exp\left(\frac{q(V - IR_S)}{kT}\right) - 1\right] \tag{2.8}$$

The saturation current (metal-to-semiconductor) is not affected by the supply voltage, while it depends on the *BH* height and can be expressed as.

$$I_0 = AA^*T^2 \exp\left(-q\Phi_{B0} / kT\right) \tag{2.9}$$

Where, A is the active area of the Schottky/rectifier structure, and A^* is the effective Richardson constant. The diode equation can be used for both *p* and n-types semiconductors, and the charge carrier of the Schottky barrier diode can easily flow in Forward bias (V_F) and almost zero current in reverse bias (V_R) conditions, with a ratio of $\geq 10^9$ in the ideal case. In Section 2.2, a detailed explanation of the current flow mechanisms will be given.

On the other hand, as illustrated in Figure 2.4 (b), under a reverse bias, the n-type semiconductor is subjected to the positive voltage (V). At this condition, both the value of the built-in potential and the W_D increases. Therefore, the built-in potential increments to $q(V_{bi}\text{-}V)$, and the *BH* will prevent the flow of electrons to the metal. Also, in reverse bias conditions, a small *mV* is enough to prevent electrons from flowing to the metal as the electron density distribution is less than the *BH*, and the net current (I_{SM}) becomes zero. However, as the Φ_B stays fixed, the I_{MS} current is equal to the same value of I_o. As a result, the MS contact exhibits rectifying behavior which almost blocks the current under reverse bias, while under forward bias, it conducts a large current.

2.1.4. Ohmic Contacts

In many electronic applications, an ohmic metal-semiconductor structure with a linear *I*-*V* characteristic in both the forward and backward direction is required. This occurs, when the semiconductor work function is higher than the work function of the metal ($\Phi_S > \Phi_M$). Once the MS contact is established, electrons start flowing into the semiconductor from the metal until both Fermi levels are aligned (thermal equilibrium condition). This flow of electrons creates a positive charge on the surface of the metal and accumulates the electrons on the semiconductor side. As displayed in Figure 2.5 (b), there is no W_D formed in the semiconductor, and no potential barrier is produced to prevent electrons from flowing towards the metal from the semiconductor or in the opposite way with the largest structure resistivity in the bulk region of the semiconductor. Therefore, a little conduction band is bending enough to accommodate more electrons, and, in the forward bias condition, the electrons can move easily into the metal from the semiconductor. In contrast, in the reverse bias condition, electrons can overcome the small barrier and flow to the semiconductor from the metal with any small applied voltage. [13]. Figure 2.5 (c, d) shows the forward and backward biases energy band diagrams, where the electron concentration is increased near the interface, and all the externally applied voltage appears across this bulk region. This MS contact is referred to as an ohmic contact and is almost linearity conducting in both directions. Moreover, using, Ohmic contact can be produced with the same Schottky structure condition ($\Phi_M > \Phi_S$) with a heavily doped semiconductor. The heavily doped semiconductor decreases the width of W_D and increases the tunneling current across the barrier. This is known as the transparent Schottky, and the tunneling mechanism current dominate through the barrier rather than the thermionic emission current [27, 61].

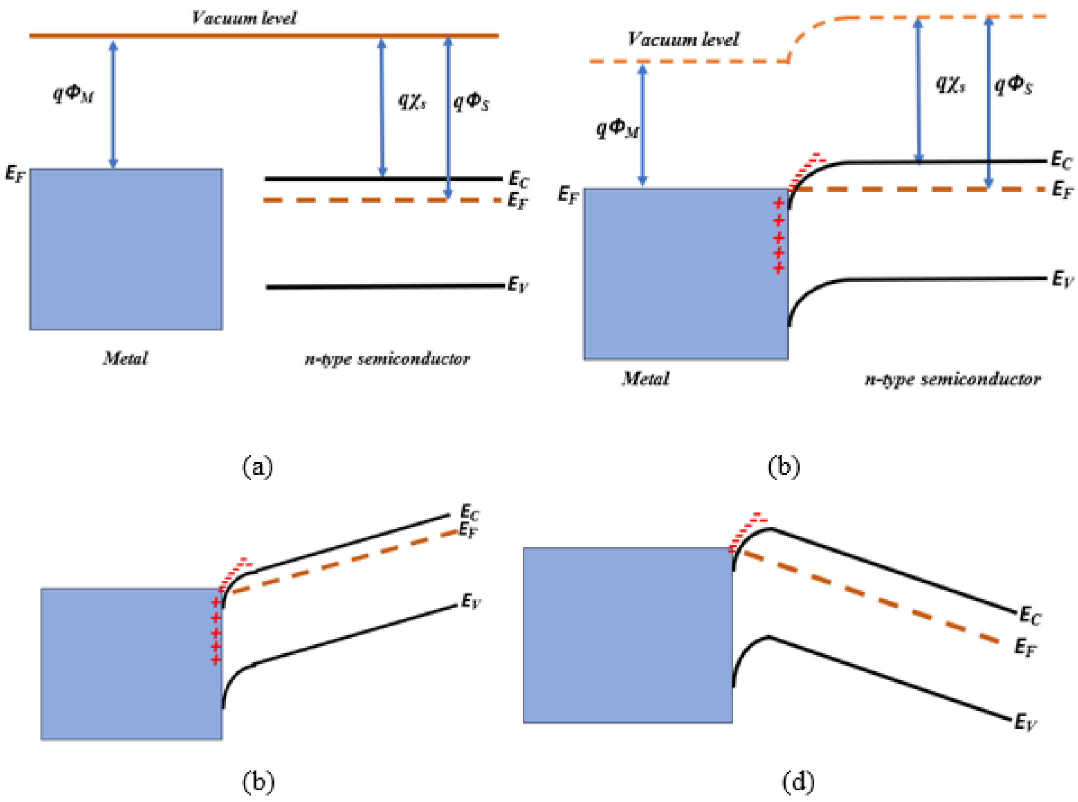

(a) (b)

(b) (d)

Figure 2.5. Energy band diagrams for an ohmic contact ($\Phi_M < \Phi_S$) n-type semiconductor. (a) without contact, (b) with contact, (c) forward bias, and (d) reverse bias.

2.2. CURRENT CONDUCTION MECHANISM OF SCHOTTKY STRUCTURES

Generally, Schottky-type diodes have four main current transport mechanisms (in forward bias condition), as indicated in Figure 2.6, which are thermionic emission (TE), quantum-mechanical tunneling across the barrier, the depletion region carrier recombination, and electron-hole diffusion or hole injection into the semiconductor from the metal /carrier recombination in the semiconductor neutral region. The flow of higher energy electrons to the metal over the potential barrier from the semiconductor is known as the TE mechanism. Only thermionic emission current is assumed to be in an ideal Schottky diode situation because the other current mechanisms cause a deviation from ideal characteristics. On the other hand, the most significant current source for highly doped material and ohmic contacts is quantum-mechanical tunneling, where electrons that do not have enough energy to pass over the barrier can pass through the barrier, as shown in Figure 2.6. Furthermore, for moderately doped semiconductors, the TE current is the dominant current mechanism at room temperature. In contrast, at low temperatures, the dominant one is the quantum mechanical tunneling current in both moderate and heavily-doped semiconductors. The third and fourth important current mechanisms are both recombination in the space-charge region and hole injection into the semiconductor from the metal. Additional currents originate from interface currents from traps and edge leakage currents in the MS contact [27, 61].

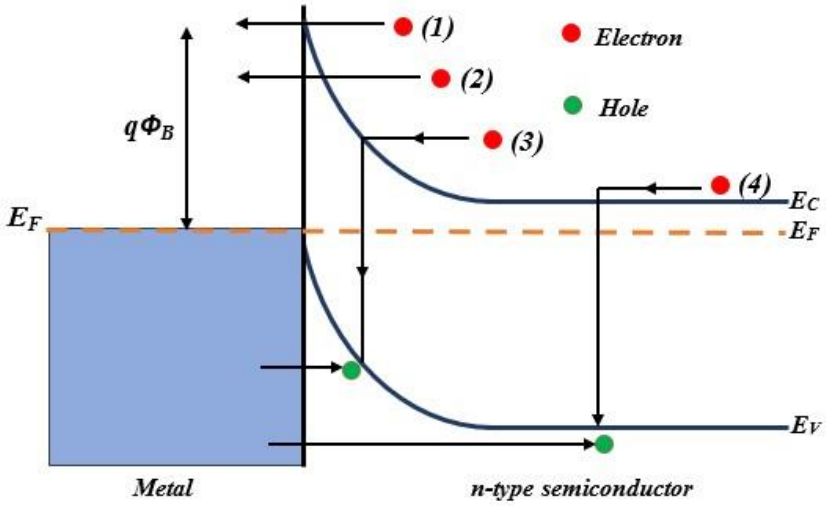

Figure 2.6. Four basic current conduction mechanisms in Schottky structures. 1)Thermionic emission, 2) Tunneling, 3) recombination in the space-charge region, 4) hole injection into the semiconductor.

2.2.1. Thermionic-Emission (TE) Theory

Bethe developed the TE theory based only on the thermionic emission (TE) current that is assumed to be the dominant one through the Schottky structure for moderate-doped semiconductors. The TE theory is a typical model for evaluating the barrier height in Schottky structures. Also, in this model, it was assumed the barrier height is large in comparison to *kT*, and the effect of both diffusion and drift in the depletion region is neglected. According to this theory, the current density is evaluated for electrons only having sufficient energy to pass over the barrier. Therefore. The *I-V* characteristics of an ideal Schottky contact can be described using the following relation.

$$I = I_0\left(\exp^{\left(\frac{qV}{kT}\right)} - 1\right) \tag{2.10a}$$

Here, (I_o) is the device saturation current.

$$I_0 = AA^{**}T^2 \exp^{\left(\frac{-\Phi_B}{kT}\right)} \tag{2.10b}$$

Here $A^{**}$is the Richardson constant that is equal to the following relation.

$$A^{**} = \frac{4\pi qT^2}{h^3}\frac{m_n^*}{m_0} \tag{2.10c}$$

The value of A^{**} can be obtained using the known constant values.

A^{**}=120m^* A/cm^{2}K^2

Here, A^{**} is dependent on the semiconductor material, which is a function of the ratio of both the effective electron mass (m_n^*) and the electron mass in vacuum (m_o). According to TE model (ideal *I-V* characteristics), the diode current increases exponentially in the forward bias as voltage increases. In contrast, in the reverse bias region, the I_o occurs at nearly four times the thermal ($V>4q/kT$). Also, in forward bias region, the semi-log *I-V* graph should have a straight line with a unity slope for an ideal diode situation[3, 27].

2.2.2. Tunneling or Field Emission (FE) Mechanism

The quantum mechanical tunneling current happens with heavily doped semiconductors where the Fermi level lies over the bottom of the conduction band, and the potential barrier is extremely thin. Therefore, the Electrons having energies lower than the Φ_B can move across the barrier. This mechanism occurs in reverse and forward bias directions. The forward bias current at low temperatures is due to electrons tunneling at the E_F

level, referred to as field emission (FE). Also, if the temperature increases, the thermionic field emission (TFE) current occurs, where many electrons get energy above the E_F to produce the TFE current. However, due to the thickness of the barrier decrease and the rapid decreases in the density of electrons above the E_F, the probability of tunneling current increases as temperature increases till it reaches a maximum energy value (E_m). With increased temperature, the TFE is gradual decreases and neglected, whereas the TE current dominates due to the increase of thermally excited electrons. Also, in the moderately doped semiconductors, the tunneling mechanism is expected only the TFE current in reverse bias at the top of the barrier as the barrier's width becomes thinner with the voltage applied [27].

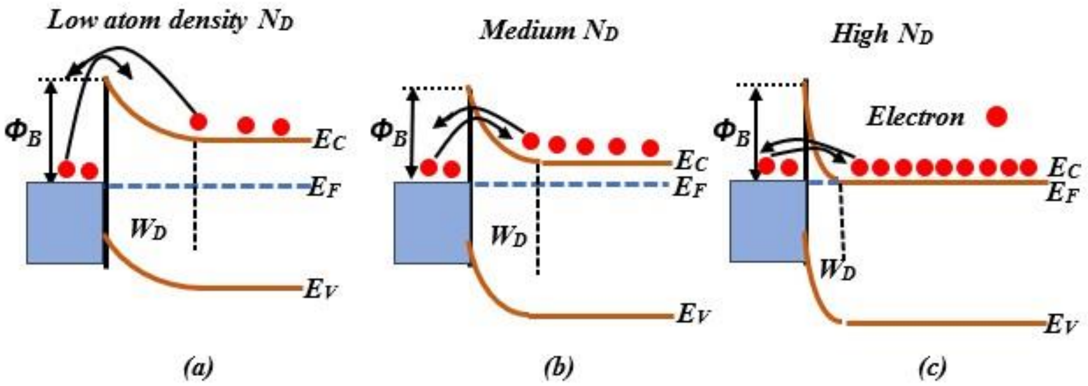

Figure 2.7. Demonstration of current conduction mechanisms. a) Thermionic emission. b) Thermionic field emission. c) Field emission.

Crowell and Rideout have derived the mathematical equations of the current tunneling mechanism. They modified the TE model for I-V characteristics and represented the tunneling current using the next relation.

$$I = I_0 \exp\left(\frac{qV}{E_0}\right) \tag{2.11}$$

Where E_0 is the tunneling probability and given by.

$$E_0 \equiv E_{00} \coth\left(\frac{E_{00}}{kT}\right) \tag{2.12}$$

Here, E_{00} is the tunneling parameter (energy constant) dependent on the material and evaluated using the following equation.

$$E_{00} \equiv \frac{qh}{4\pi}\sqrt{\frac{N_D}{\varepsilon_s m^*}} \tag{2.13}$$

Where ϵ_S is the semiconductor permittivity, h is Planck's constant, and N_D is a concentration of the donor atoms.

2.2.3. Generation and Recombination Mechanisms

The rate of the electron-hole (e^--h^+) generated at thermal equilibrium is equal to the rate of the recombination where the generated values of e^--h^+ pairs are equal to ($\mathrm{n_i^2}$) and the net current is zero. The net recombination or generation current is produced depending on the direction of the bias. When the Schottky structure is reverse-biased (n-type semiconductor), the e^--h^+ pairs generation rate in the depletion region increases, and the generated carrier will flow through the barrier to produce the reverse generation current component. While in the forward bias condition, the electrons move to the depletion region from the neutral bulk of the semiconductor, and holes move from the metal to the semiconductor. Due to the electron accumulation in the depletion region, the recombination process will occur and produce the recombination forward current component. The relation formula of generation and recombination current (Irg) is given as follows.

$$I_{rg} = I_{ro}\left[\exp\left(\frac{qV}{2kT}\right) - 1\right] \tag{2.14a}$$

Here,

$$I_{ro} = \frac{qn_iW}{2\tau_0} \tag{2.14b}$$

Where τ_o is the carrier lifetime for minority carriers, W is related to the depletion layer thickness. Thus, the total Schottky structure current is given by.

$$I = I_{TE} + I_{rg} = I_o\left[\exp\left(\frac{qV}{kT}\right) - 1\right] + I_{ro}\left[\exp\left(\frac{qV}{2kT}\right) - 1\right] \quad (2.15)$$

The recombination current in the forward bias region causes the non-ideality in some Schottky devices. In contrast, the generation current is the main source of unsaturation current in reverse bias. However, the ratio of both saturation currents (I_{r0}/I_0) is defined by.

$$\frac{I_{rg}}{I_o} = \frac{qn_i}{A^* T^2}\left(\frac{W}{2\tau_0}\right)\exp\left(\frac{\Phi_B}{kT}\right) \quad (2.16)$$

This indicates that the generation-recombination current significantly affects the structure, especially on lightly doped semiconductors and at low temperatures where its activation energy is lower than the TE activation energy [27].

2.2.4. Minority-Carrier Injection

The other current mechanism is the injection of minority carriers (holes) into the semiconductor (recombination in the neutral region). Thus, the minority carrier current to total current ratio is known as the injection rate [3, 27].

$$\gamma \equiv \frac{J_P}{J_P + J_n} \quad (2.17)$$

Here, J_n and J_P are electron and hole current densities. The density equations for the majority and minority (electron and hole) carriers are as follows.

$$J_n = q\mu_n N_D E \quad (2.18)$$

$$J_P = q\mu_P N_A E - qD_P \frac{\partial N_A}{\partial x} \tag{2.19}$$

Where μ_P and μ_n are the hole and electron mobility. E is the electric field at the interface, N_A is the hole density in the semiconductor, and D_P is the diffusion of the minority carrier. In J_P equation, the first part is the attracted component, and the second is the diffusion component of the minority carrier. At low-bias conditions, the diffusion of the minority carrier part dominates. Assuming this situation and that the depletion region is less than the diffusion length of the holes, the current density of the hole can be given as [41].

$$J_P = \frac{qD_P}{W} N_A \left[\exp\left(\frac{qV}{kT} \right) - 1 \right] = \frac{qD_P}{W} \frac{n_i^2}{n_e} \left[\exp\left(\frac{qV}{kT} \right) - 1 \right] \tag{2.20}$$

Here, n_i is the carrier concentration of the pure semiconductor. Therefore, Equation 2.17, can be written as;

$$\gamma \cong \frac{J_P}{J_n} = \frac{qD_P n_i^2}{n_e L_P A^{**} T^2 \exp\left(-q\Phi_B / kT\right)} \tag{2.21}$$

At larger forward bias, γ increases because the attracted current component increases compared to diffusion.

2.3. NON-IDEAL CHARACTERISTICS OF SCHOTTKY STRUCTURES

Usually, the *I-V* characteristics in both forward and reverse-bias measurements of Schottky diodes deviate from their ideal situation (TE model). Therefore, the ideal Schottky diode equation has been modified to fit the measurement data by adding the ideality factor (n) into its exponential term, as shown in the next equation.

$$I = I_o \left[\exp\left(\frac{qV}{nkT} \right) - 1 \right] \tag{2.22}$$

For an ideal contact of MS structure, the current is assumed to be only a thermionic emission current where the ideality factor (*n*) equals one. Many factors can increase the value of *n* above unity, such as generation recombination and tunneling currents, image-force effect, and barrier height. The variation of the *I-V* characteristics in the forward bias with increasing ideality factor is shown in Figure 2.8. It is obvious that the ideality factor increases as the current density reduce.

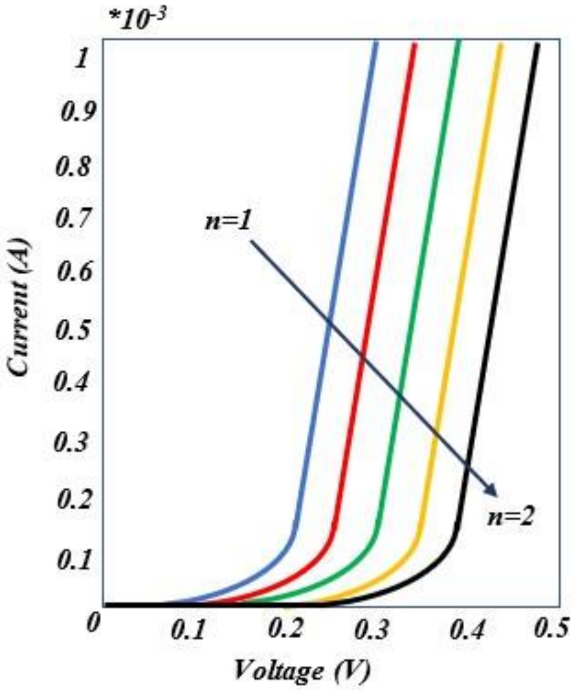

Figure 2.8. The I-V characteristics (forward bias region) at different ideality factor values.

Some other parameters can also cause non-ideality in the reverse bias, where the current keeps increasing and is unsaturated at I_o. The two main effective factors are the lowering of the barrier and both FE and TFE currents which lead to an increase in the leakage current as the voltage applied increases. Also, the potential barrier becomes sufficiently thin at moderate reverse bias, and electrons can move across the barrier to the semiconductor. Both contributions of tunneling current and barrier lowering can extremely increase the reverse bias current [27, 62].

2.4. MODIFICATIONS TO THE BARRIER HEIGHT

The Schottky barrier height (Φ_B) was assumed to be unchanged with any applied voltage. However, it is found that the Φ_B dependent on both forward and reverse applied voltages. But the influence of the *BH* with the reverse bias voltage is more significant than in the forward bias, where the reverse current keeps increasing till it reaches the breakdown voltage.

The bias-dependent of the Φ_B can be the result of three main factors. These parameters are interfacial layer, image-force lowering, and metal-induced gap (MIG) states. These parameters suggest that the Φ_B should decrease as the strength of the electrical field (ξ) at the interface increases.

2.4.1. Interfacial Layers

Most Schottky structure devices have an oxide interfacial layer sandwiched between the semiconductor and the metal with a 10 to 30 Å thickness. The oxide layer performed between the MS contact is often attributed to air exposure or humidity and acts as an insulator layer that significantly affects the structure's performance. Figure 2.9 illustrates the energy band diagram of MS structure with the existence of an interlayer. Also, the interfacial layer significantly affects both the *n* and *BH* due to the voltage drop across it. The barrier height with the existence of an insulator layer is given as [27].

$$\Phi_B = \Phi_M - x - V_i \tag{2.23}$$

The reduction in barrier height due to the effect of the maximum electric field (ξ_{max}) in the semiconductor is given by.

$$\Phi_B = \Phi_{B0} - \alpha\xi_{\max} \tag{2.24}$$

Here, (Φ_{B0}) is the zero bias BH, and α can be written as.

$$\alpha = \frac{\delta \varepsilon_S}{\varepsilon_i + q\delta N_{ss}} \tag{2.25}$$

It is obvious that the reduction in *BH* is a function of the maximum electric field (ξ_{max}), and this relation is valid when the N_{SS} are fixed within the entire energy. Also, a low dielectric constant (ϵ_i) of the insulator layers gives a higher barrier reduction.

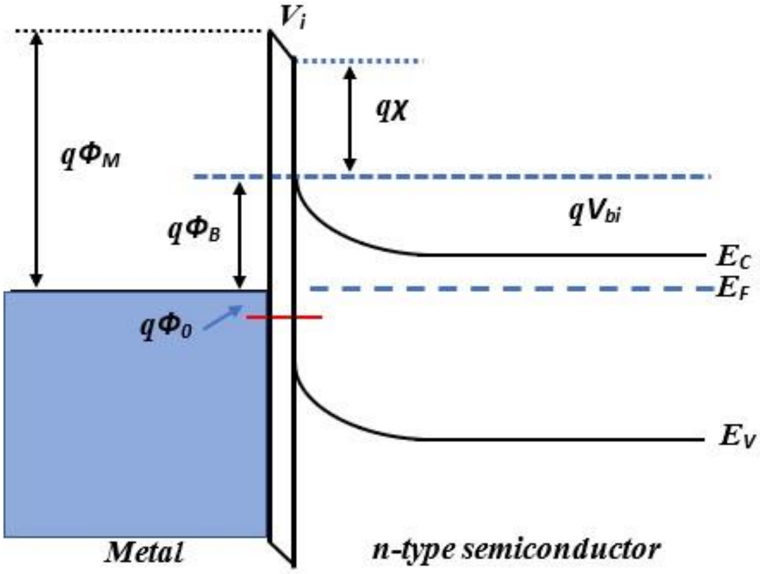

Figure 2.9. Energy band diagram of Schottky contact in forward bias with a very thin insulator layer

Experimental results show that the increases in oxide thickness led to an increase in the values of *n*. Usually, a 20 Å insulator layer thickness increases the value of n by about 1.3 to 1.5. in the forward bias. Also, both the depletion region and electric field across the interfacial layer decrease, leading to a change in the Φ_B with the applied voltage. These variations can be expressed as a function of the ideality factor.

$$n^{-1} = \left(1 - \frac{\partial \Phi_B}{q\partial V}\right) \tag{2.26}$$

Therefore, the value of *n* becomes bias independent only when the energy states at the semiconductor-oxide interface are distributed uniformly. Also, the *BH* reduction with the existence of an interfacial layer in the reverse bias condition leads to an unsaturation current situation [3, 27].

2.4.2. Image-Force Lowering

In the MS structure, when electrons are injected into the semiconductor from the metal, they induce an equal image of positive charges within the metal. These charges tend to attract the electrons to the metal using the following Coulomb attraction force relation.

$$q^2/4\pi\varepsilon_S(2x)^2 = q^2/16\pi\varepsilon_S x^2 \tag{2.27}$$

Where x is the distance between the surface and the electron.

Due to the attraction force, the equivalent electrical field of both particles can be expressed using this relation.

$$\xi_{IF}(x) = -\frac{F_{(x)}}{q} = -\frac{q}{16\pi\varepsilon_S x^2} \tag{2.28}$$

Here, ε_S is the permittivity of the semiconductor. The corresponding potential energy of the electric field is given by.

$$V_{IF}(x) = -\int_x^\infty \xi_{IF}(x)dx = -\frac{q}{16\pi\varepsilon_S x} \tag{2.29}$$

The potential energy of the Schottky barrier (inside the depletion region) has to be joined with the produced image potential energy. However, it is assumed that the potential energy near the surface is constant with a maximum value (ξ_{max}).

$$\xi_{\max} = \sqrt{\frac{2qN_D(\Phi_B - E_{CF} + V_a)}{\varepsilon_S}} \tag{2.30}$$

Also, due to the existence of the uniform external electrical field (ξ_{max}), the MS interface electrostatic potential $\Phi(x)$ at any point (x) is evaluated by.

$$\Phi(x) = -q\xi_{\max} - \frac{q^2}{16\pi\varepsilon_S x} \tag{2.31}$$

Figure 2.10 illustrates the distance (x_m) where the electrostatic field of the depletion region and the image charge force cancel each other, Which indicates the maximum barrier height point, which is described by.

$$\frac{q^2}{16\pi\varepsilon_S x_m^2} = \xi_{\max} \tag{2.32}$$

Therefore, the reduction in the maximum potential barrier is given by

$$\Delta\Phi_B = x_m\xi_{\max} + \frac{q^2}{16\pi\varepsilon_S x_m^2} = 2x_m\xi_{\max} \tag{2.33}$$

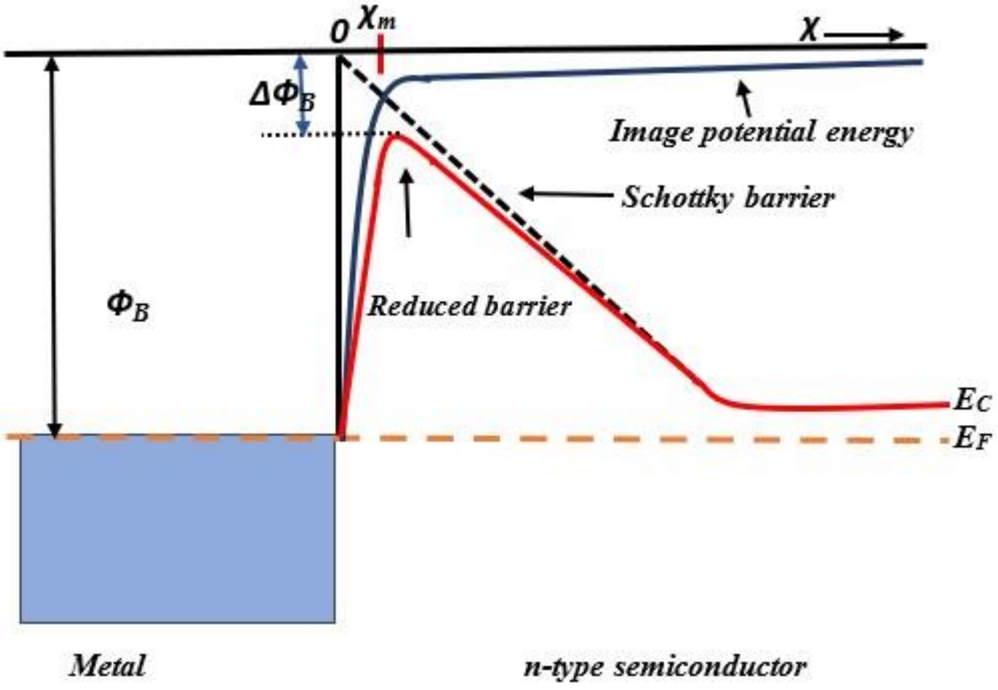

Figure 2.10. Energy band diagram illustrating the effect of the image force on the Schottky structure

It is obvious that from the previous Equations 2.31 and 2.34, the barrier potential reduction is dependent on the dielectric constant of the semiconductor, applied voltage, the semiconductor doping concentration (N_D), and the difference between the edge of the conduction band and the Fermi level of the semiconductor [3, 27].

2.4.3. Surface States

The surface states (N_{SS}) generate from dangling bonds at the semiconductor's surface due to the disturbance of periodic crystals. The N_{SS} can be empty or occupied according to their location at the Fermi level (E_F). Furthermore, as illustrated in Figure 2.11 the N_{SS} is defined by a charge neutral level ($q\Phi_o$) which is evaluated from the edge of the valence band.

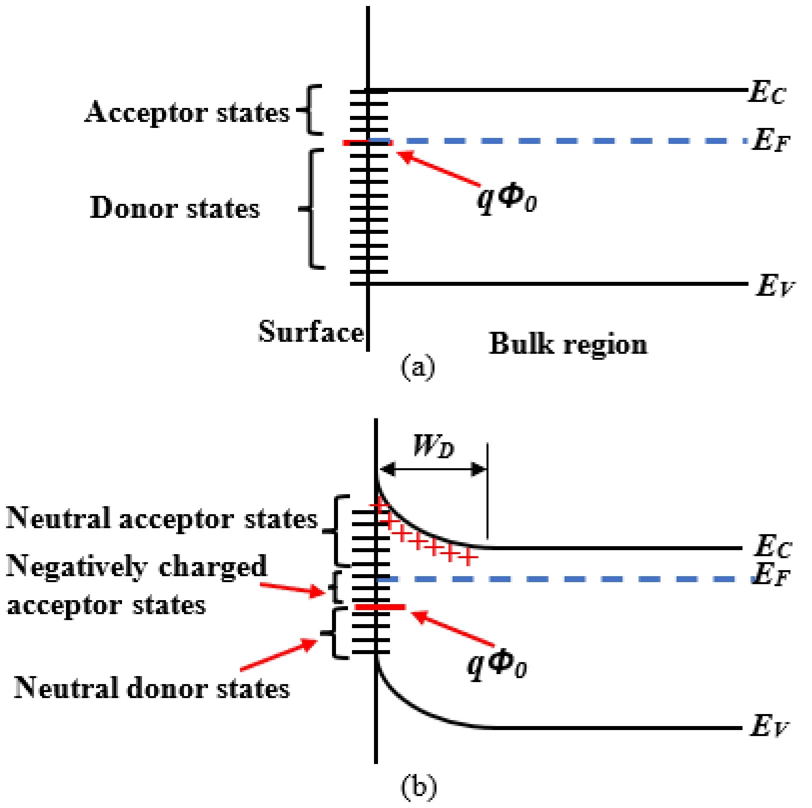

Figure 2.11. Energy band diagram illustrating the distribution of NSS within the band gap at the surface of semiconductor (a) both Fermi and the neutral levels are identical. (b) The Fermi level is over the neutral level

When the N_{SS} are occupied to the level of energy under $q\Phi_o$, they would be positively charged and behave as donors. While, if the N_{SS} are occupied to the level of energy over $q\Phi_o$ they would be negatively charged and behave as acceptors. Also, the BH will be decreased or increased according to the position of $q\Phi_o$ with respect to the E_F. Also, if the position of $q\Phi_o$ is over the E_F, the energy states act as acceptors as the downward band bending reduces. While when the position of $q\Phi_o$ is less than the E_F, the energy states act as donors and the downward band bending increases. Therefore, the energy states around the $q\Phi_o$ pinned the E_F at the surface, and thus, the ideal Schottky-Mott model for the BH can be modified as in the following relation [27].

$$q\Phi_B = E_g - q\Phi_0 \tag{2.34}$$

2.4.4. Ideality Factor

According to the thermionic emission theory, the ideality factor (n) equals unity, as stated in the simple I-V model. However, many parameters can affect the diode performance, which increases the value of n above unity (unideal situation), such as image force effect, interfacial layer, quantum mechanical tunneling (FE and TFE), illumination, and temperature. In general, the I-V measurements of a Schottky structure at various illumination or temperatures can be used to observe the variation of n with respect to both of them and thus, the values of n can be obtained at every individual temperature or illumination [3, 27].

2.5. SERIES AND SHUNT RESISTORS

Both series and shunt resistors significantly affect the main I-V characteristic of the MS or MIS/MPS Schottky devices. The shunt resistance (R_{Sh}) should be much higher than the series resistance (R_S) and ideally greater than 1 GΩ but not infinite. The low shunt resistance produces an opposite-direction current and leads to an increase in the leakage currents. Also, the R_{Sh} is generally caused by defects, disturbances, and oxides at the contact boundary. In contrast, the value of series resistance (R_S) depends on various factors such as the N_{SS}, the resistivity of the semiconductor material, the interface insulator layer, the back ohmic contact, and the resistance of the contact wires. Also, the deviation of the *I-V* characteristic from the ideal situation is caused by the voltage reduction across R_S. Furthermore, As seen in Figure 2.12 (a), in the *I-V* characteristic, the effect of R_S in the forward region is higher. Therefore, the value of R_S is responsible for the curve bending in the forward bias region of the *I-V* characteristics. On the other hand, the current value in the backward bias is affected by R_{Sh}. However, both R_S and R_{Sh} are basically evaluated from Ohm's law ($Ri = \delta V_i/\delta I_i$) using forward and reverse bias measurements. According to this expression, the resistance value obtained from the reverse bias voltage and current is R_{Sh}. In contrast, the resistance value obtained from the forward bias voltage and current is R_S.

Figure 2.12 (b) displays the equivalent circuit diagram of a Schottky diode, where R_{Sh} is connected in parallel and R_S in series with the diode. Here, the currents flowing through R_{Sh} and diode are I_{Sh} and I_D, respectively. As illustrated in this figure, when a diode has low R_S and high R_{Sh}, the majority of the current will flow across the diode, while almost zero current will move through the R_{Sh}, and the diode will have its maximum power rating. For an ideal diode, the R_S value is approximately zero, and the value of R_{Sh} is higher than $10^9\Omega$ [3, 27].

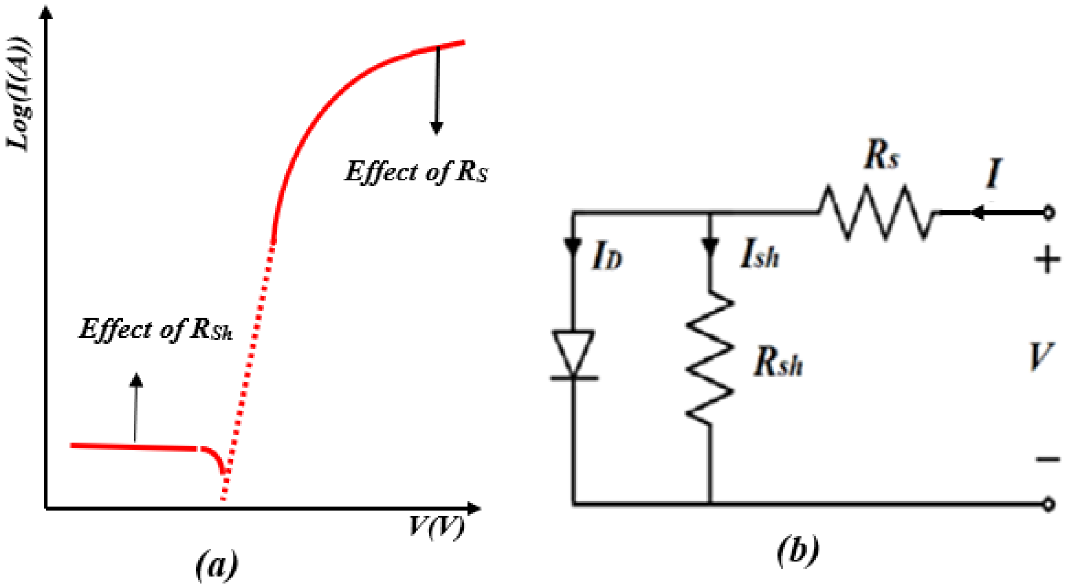

Figure 2.12. a) I-V characteristic curve of an MS/MIS type Schottky diode, b) Equivalent circuit of an MS/MIS type Schottky diode with resistors R_S and R_{Sh}.

Both series and shunt resistors significantly affect the performance of the Schottky devices as well as the solar cell. Increasing the series resistance (R_S) can significantly reduce the contact voltage of the solar cell and decrease the terminal voltage (V)of the I-V curve with a slight decrease in the short-circuit current (I_{SC}). Therefore, it reduces the performance of solar cells. In contrast, the low shunt resistance (R_{Sh}) implies power losses in the device, which decreases both the voltage and current of the device.

PART 3

PHOTOVOLTAIC, ELECTRIC AND DIELECTRIC PROPERTIES

3.1. PHOTODIODE AND SOLAR CELL SCHOTTKY BARRIER STRUCTURES

3.1.1. Solar Radiation

Solar radiation intensity outside the earth's atmosphere is based on the mean orbital distance around the sun, known as the solar constant (equal to 1367 W/m^2). Generally, the sunlight on the earth is attenuated from the absorption of the scattering atmosphere. This attenuation mostly depends on both the air mass or the atmosphere and the path light length through the atmosphere. The air mass is known as l/cos(θ), and θ (zenith angle) is the angle between the position of the sun and the vertical path. Figure 3.1 shows two plots for solar spectral irradiance. However, the higher plot represents the spectrum of solar outside the atmosphere (zero air mass condition (AM_0)). The AM_0 spectrum is essential for space vehicle and satellite applications. While, the spectrum of *AM1.5* (the air mass 1.5) is relevant for the performance of terrestrial solar-cell. This spectrum indicates the sunlight at the surface of the Earth when the angle between the sun and the vertical is 48, and the power incident is about 963 W/m2 [27].

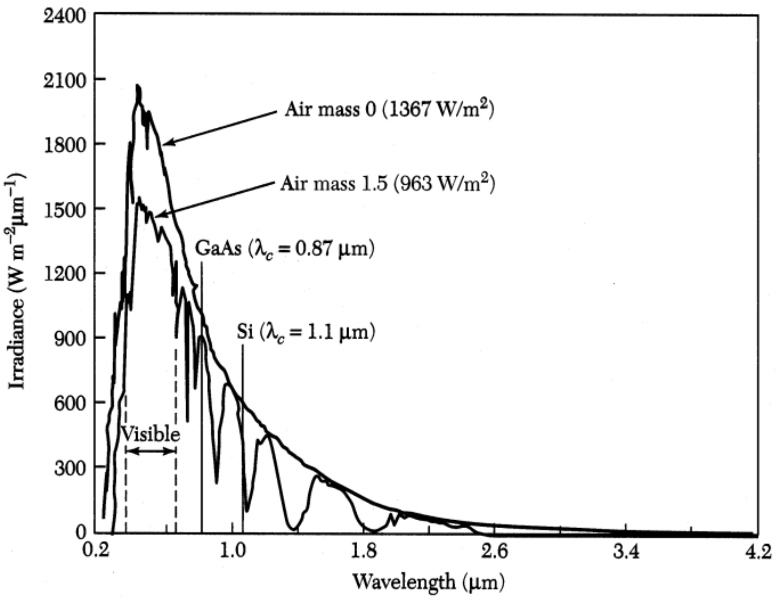

Figure 3.1. Air mass 0 and air mass 1.5 of the Solar spectral irradiance.

3.1.2. Schottky Barrier Photodiodes Structures

The Schottky structure can be used as a photodiode, which is an electronic device that converts illumination to electrical current. When light strikes the photodiode Schottky structure, it produces e -h pairs. In the reverse bias, the electrons are flowed to the metal and leave holes behind in the semiconductor due to the effect of the junction's electric field. This flow of electrons to the metal from the semiconductor produces an electrical current. However, the carriers generated in the depletion zone flow out and create a photocurrent. While the carriers generated in the bulk region (near the barrier region) can diffuse to the depletion layer and sweep out.

Schottky photodiodes exhibit many advantages over *p-n* traditional diodes, including their lower dark current, faster time response, and less sensitivity to variations in temperature. Also, they are widely used in many applications, including imaging, optical communications, and sensing, where their low noise, high-speed response, and ability to detect light at low intensities and high frequencies make them a good choice[27].

3.1.3. Schottky-Barrier- Photovoltaic Structures

The MS Schottky barrier photovoltaic devices operate within the fourth region of the *I-V* characteristics, and the generated current under the effect of the light intensity can be expressed as.

$$I = I_{light}(V,P) - I_{dark}(V,P) \tag{3.1}$$

Generally, Photovoltaic devices are used explicitly as solar cells (produce power) or detectors. However, to improve the structure performance, one must decrease I_{dark} and increase I_{ljght} as much as possible. To increase I_{ljght}, the depletion layer width W_D or both the depletion layer width and diffusion length ($W_D + Ln,p$) have to roughly match the light absorption depth. In the previous cases, the photocurrent is dependent only on the drift in the barrier zone, or it is dependent on diffusion into the depletion region. In reality, it is more complex than this due to the effect of back contact, which may absorb the carriers. Therefore, both the back contact and base width properties must also be considered and optimized[3, 27].

3.1.3.1. Solar Cells

Solar cells are a significant alternative terrestrial energy source because they can directly convert sunlight to electricity with a good conversion rate, non-polluting, and provide nearly continuous energy with low operating costs. However, to obtain a high open-circuit voltage in Schottky barrier MIS-type solar cells, a high internal field at the interface must be generated. Also, the thickness of the oxide or interfacial layer should not be higher than $20A^0$. Otherwise, both the fill factor *FF* and the short circuit current I_{SC} would be reduced.

In general, when the solar cell is subjected to solar radiation, only photons with energy higher than E_g ($hc/q\lambda \geq E_g$) can quickly create a large number of e^--h^+ pairs at the junction, and the extra higher energy is dissipated as heat. These electric charges are swept immediately from the polymer or insulator interlayer to create the photocurrent I_{ph} due to the effect of the internal electric fields.

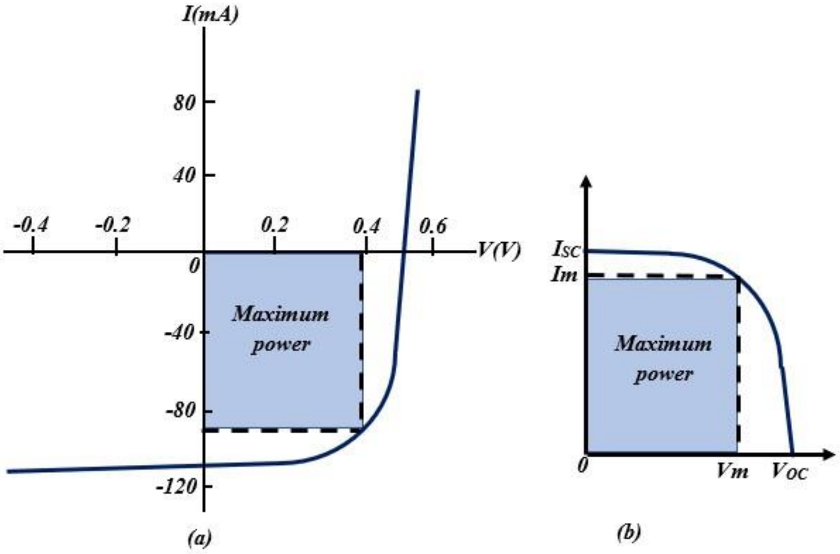

Figure 3.2. (a) Current-voltage characteristics under the illumination of a solar cell. (b) the reverse of (a) around the voltage axis

The *I-V* characteristics of the solar cell is represented by Figure 3.2 (b), which is reversed around the voltage axis of Figure 3.2 (a). With selecting a suitable load, nearly 80% of the power from a product of V_{OC} and I_{SC} can be obtained. Also, the maximum power of the cell is demonstrated by the rectangle area in the plot, which is equal to the product of both V_{max} and I_{max} that correspond to the maximum power output ($P_{max}= I_{max} x V_{max}$) of the cell.

Also, power conversion efficiency can be obtained using this relation.

$$\eta = (FF.V_{OC}.I_{SC}) / (P_{in}.A) \tag{3.2}$$

Where *A* is the effective contact area of the structure, P_{in} is the power incident, and *FF* is the fill factor defined as the ratio between the maximum power P_{max} and the product of the (I_{SC} x V_{OC}).

$$FF = (V_m.I_m) / (V_{OC}.I_{SC}) \tag{3.3}$$

Furthermore, photoconductive performance can be investigated using $I_{ph}=AP^m$ relation. Where m is the slope value can be evaluated using the double-logarithmic I_{ph}-

P plot at different illumination levels. Also, the photosensitivity ratio can be analyzed using I_{photo}/I_{dark} relation. These values indication for the photoconduction behavior of the fabricated structures[3, 27, 63, 64]. In general, Schottky-barrier photodiode devices are operated in the third I-V quadrant, while Schottky-barrier photovoltaic devices are designed to operate in the fourth *I-V* quadrant. As a photovoltaic structure, a Schottky barrier device can be developed as a photodetector or a solar cell device. These structures are highly convenient because they use only one semiconductor for junction formation (single conductivity) and can be produced with low-temperature processing that reduces the degradation of material properties.

3.2. METAL-INSULATOR-SEMICONDUCTOR (MIS) SCHOTTKY STRUCTURES

The oxide layer in MS contact can be performed automatically, while in Metal-Insulator/ Oxide / Polymer -Semiconductor (MIS/ MOS / MPS) structures can be obtained using interfacial layer materials. The existence of this insulator/polymer/oxide layer is used to isolate metal and semiconductors and control the charge flowing between them. Figure 3.3 shows an MIS structure. Here δ is the insulating layer thickness, and the applied voltage is *V*. In this section, it will be assumed that the voltage *V* is positive when the metal has a positive charge compared to the semiconductor.

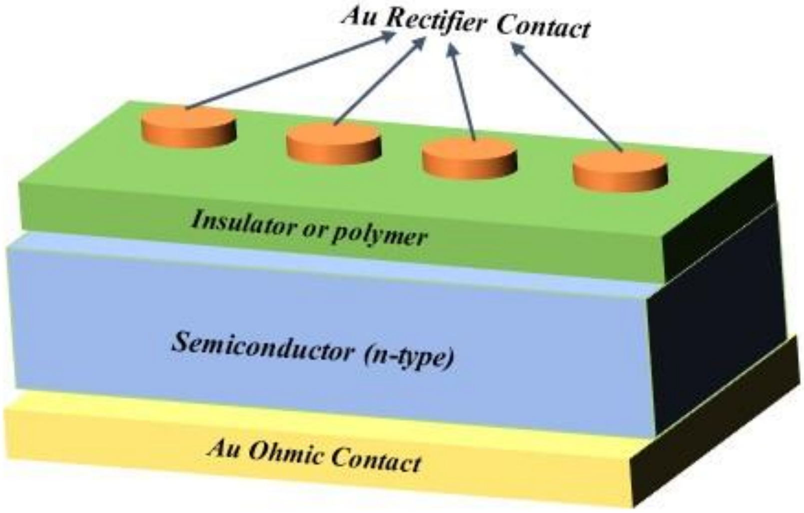

Figure 3.3. Metal-insulator-semiconductor (MIS) structure

3.2.1. Ideal Metal Insulator Semiconductor (MIS) Structures

The energy band diagram of an ideal MIS device at zero bias ($V=0$) is illustrated in Figure 3.4. In an ideal MIS structure, both interface traps and oxide charges are zero. In this structure, no charge carriers can flow through the insulating layer when a *DC* voltage is applied to the structure. In addition, when both Fermi levels are aligned in thermal equilibrium with zero bias, the distinction between semiconductor and metal work functions will be zero ($\Phi_{MS} = \Phi_M - \Phi_S = 0$).

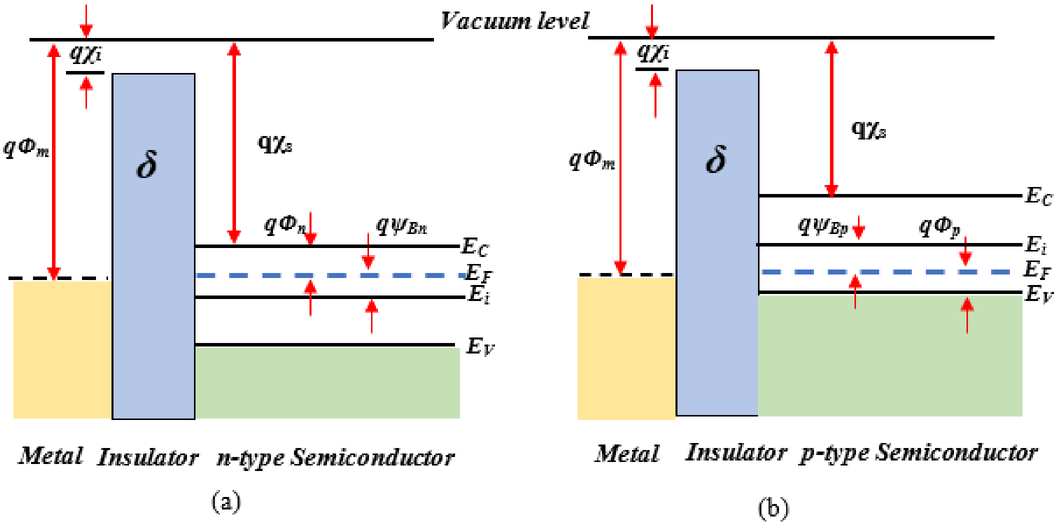

Figure 3.4. Equilibrium energy band diagram of ideal MIS/MPS structures (a) n-type semiconductor, (b) p-type semiconductor

Considering Figure 3.4, the above situations are for an n and p types semiconductor, and Φ_{MS} can be expressed as follows [3].

$$\Phi_{MS} = \Phi_M - \left(x_s + \frac{E_g}{2q} - \Psi_{Bn} \right) = \Phi_M - \left(x_S + \Phi_n \right) = 0 \tag{3.4}$$

$$\phi_{ms} = \phi_m - \left(x_s + \frac{E_g}{2q} - \Psi_{Bp} \right) = \phi_m - \left(x_S + \frac{E_g}{q} - \phi_p \right) = 0 \tag{3.5}$$

Here χ_i and χ_s are electron affinities for insulator and semiconductor, respectively, and $q\Psi_B$ (for *p* or *n*-type) is the energy difference between intrinsic and Fermi energy levels

(E_i, E_F). However, basically, three different cases can occur on ideal MIS structures when a negative or positive voltage is applied to them.

1) Accumulation: when a negative voltage ($V<0$) is applied to the metal layer for a p-type semiconductor in MIS structure, charges flow into the interfacial region of the semiconductor, and the valence band in this zone approaches E_F, as shown in Figure 3.5 (a). Also, since it is an ideal MIS structure, there is no current flow in the structure. Therefore, the Fermi level in the semiconductor does not change ($dE_F/dx=0$), and the band bending occurs because the majority of carriers accumulated (p-type holes) near the semiconductor. The accumulation of majority carriers at the interface region of the semiconductor is called accumulation.
2) Depletion: for a p-type semiconductor, when the metal layer is subjected to a small positive voltage ($V> 0$), producing an electric field in the interfacial layer. This field will remove positive charges from the semiconductor interface, while acceptor ions will attract negative charges. In this situation, the density of holes on the surface of the semiconductor is lower than the internal hole density. Also, as shown in Figure 3.5 (b), most carriers are depleted in the interfacial region of the semiconductor and the bands bend downward. Thus, this region is called the "depletion region" or depletion.
3) Inversion: for a p-type semiconductor, when the metal layer is subjected to a higher positive voltage ($V >> 0$), the bands bend downward further, and at the surface of the semiconductor, the intrinsic energy level (E_i) falls under the Fermi level (E_F), as in Figure 3.5 (c). In this situation, the values of minority carriers (electrons) on the surface become higher than the holes, and the p-type semiconductor behaves like an n-type. Therefore, this area is inverted and is referred to as an inversion region. However, the same results can be extracted for the n-type semiconductor, and the applied voltage must be in the opposite direction for the n-type semiconductor [3].

3.2.2. Ideal MIS Capacitor

Figure 3.6 illustrates a more detailed energy band diagram for an ideal MIS capacitor with the p-type semiconductor. Here, $\Psi p(x)$ is the potential and is measured according to the intrinsic energy level ($\Psi p(x)=E_i(x)/q$), and Ψs represents the surface potential. The densities of electron and hole at any x position as a function of Ψp are provided in the next equations.

$$n(x) = n_0 \exp\left(q\Psi p / kT\right) \tag{3.6}$$

$$p(x) = p_0 \exp\left(-q\Psi p / kT\right) \tag{3.7}$$

At equilibrium, p_0 and n_0 are the density of holes and electrons in the semiconductor bulk zone, respectively, and can be evaluated as [3].

$$n(0) = n_0 \exp\left(q\Psi s / kT\right) \tag{3.8}$$

$$p(0) = p_0 \exp\left(-q\Psi_S / kT\right) \tag{3.9}$$

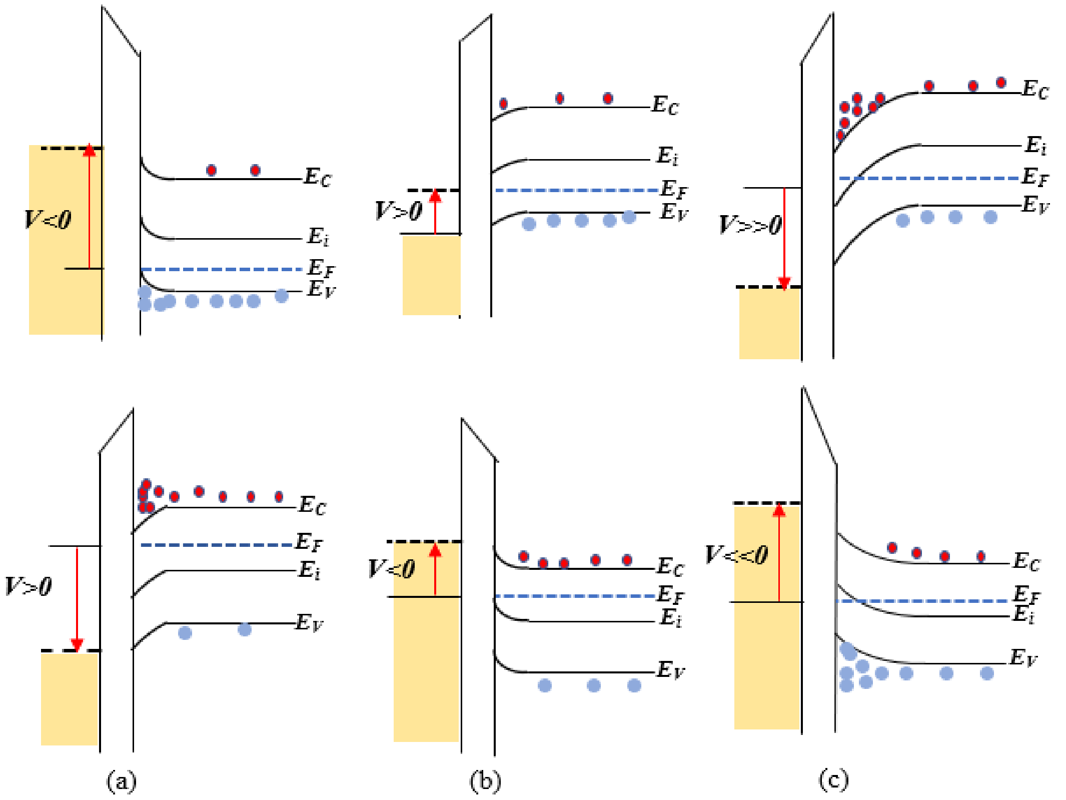

Figure 3.5. Energy band diagrams for an ideal MIS structure with various applied voltage: (a) Accumulation, (b) Depletion, and (c) Reversal

Since the bands are bent downwards, as shown in Figure 2.14, the surface potential, Ψ_S, must be positive.

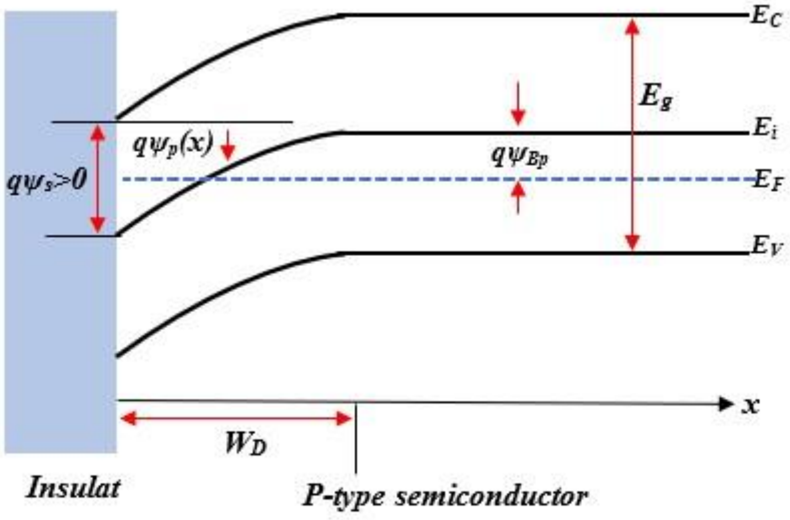

Figure 3.6. P-type semiconductor energy band diagram with an insulating layer.

For example, when $\Psi_S < 0$, the bands bend upwards and at $\Psi_S = 0$ indicates flat band status. When $\Psi_B > \Psi_S > 0$, the depletion condition occurs, and there is a small downward bend in the bands. Also, when $2\Psi_B > \Psi_S > \Psi_B$, the number of electrons increases, indicating the weak inversion state. If $\Psi_S > 2\Psi_B$, the bending increases and indicates a strong inversion state, where the E_i value on the bulk is higher than the E_F value, while the E_i value on the surface remains under the E_F. Figure 3.7 (a) shows the energy band diagram of an ideal MIS device at strong inversion ($V \gg 0$). Figure 3.7 (b) shows the charge distribution, which can be expressed using the following equation.

$$Q_m = -\left(Q_n + qN_A W_D\right) = -Q_S \tag{3.10}$$

Here, Q_m is the charge per unit area of the metal, qN_AW_D is the ionized acceptors per unit area of the depletion layer, Q_n is the electrons near the surface in the inversion region per unit area, and Q_S is the total semiconductor charge per unit area. The following equation can express the voltage applied to the structure (V).

$$V = V_i + \Psi_S \tag{3.11}$$

Here, V_i is the voltage across the insulator.

$$V_i = Ed = \frac{|Q_S|\, d}{\varepsilon_i} = \frac{|Q_S|}{C_i} \tag{3.12}$$

Where ε_i is the permeability of the insulator, and C_i is the insulator capacitance per unit surface. The depletion layer (W_D) is obtained as a function of Ψ_S by.

$$W_D = \left[\frac{2\varepsilon_S \Psi_S}{qN_A}\right]^{0.5} \tag{3.13}$$

This depletion layer increases with increasing applied voltage until it reaches an inversion state. After that, an increase in voltage strengthens the inversion rather than expanding the depletion layer. The maximum value of the depletion region can reach is expressed as follows.

$$W_m = \left[\frac{2\varepsilon_S \Psi_S (inversion)}{qN_A}\right]^{0.5} = 2\left[\frac{\varepsilon_S kT \ln\left(N_A/n_i\right)}{q^2 N_A}\right]^{0.5} \tag{3.14}$$

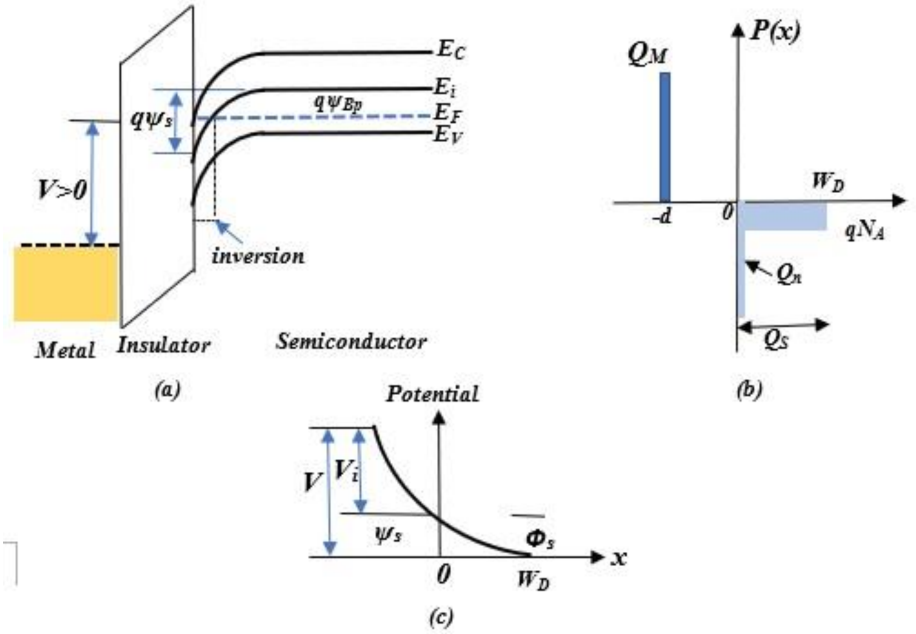

Figure 3.7. (a) energy band diagram of an MIS structure (ideal condition) under a strong inversion. (b) distribution of the charge. (c) Potential distribution

The depletion region charge per unit area (Q_d) in the strong inversion is given by,

$$Q_d = -qN_A W_m = -2\left(\varepsilon_S N_A \Psi_B\right)^{0.5} \tag{3.15}$$

Also, the applied voltage must be large enough to generate both surface potential and depletion charge. The threshold voltage (V_T) for strong inversion is given by.

$$V_T = -\frac{Q_d}{C_i} + \Psi_B \tag{3.16}$$

The V_T represents the lowest voltage value required to get strong inversion. Also, the capacitance of the MIS device is voltage-dependent, and the semiconductor capacitance is expressed by.

$$C_S = \frac{dQ}{dV} = \frac{dQ_S}{d\Psi_S} \tag{3.17}$$

According to the equivalent electrical circuit of an MIS device, the total equivalent capacitance is the series combination of a voltage-dependent semiconductor capacitance and a voltage-independent fixed insulator capacitance. Thus, the total MIS capacitance becomes voltage-dependent. Therefore, the total capacitance of the MIS structure (C) is equivalent to the series coupling capacitance of the semiconductor (C_D) and the insulator capacitance (C_i).

$$C = \frac{C_i C_D}{C_i + C_D} \tag{3.18}$$

The value of C_i for a given insulator thickness d_i ($C_i = \varepsilon_i A/d_i$) is fixed and corresponds to the device's maximum capacitance. However, the capacitance of the semiconductor C_D is not only a function of the applied source (or Ψ_S) but is also dependent on the measurement frequency. Therefore, C-V graphs are measured at various frequencies, and the obtained results exhibit different properties. This difference occurs mainly in the region of inversion, especially in strong inversion [3].

3.2.3. Dielectric Property

A dielectric is an electrical insulator that an applied electric field can polarize. The term insulator represents low electrical conductivity, while the term dielectric typically refers to highly polarizable materials and is used to indicate the capacity to store energy through polarization. With the effect of an electric field, the electric charges cannot move across the dielectric substance but only slightly deviate from their average equilibrium position and causes dielectric polarization. Thus, the negative charges shift in opposite direction of the applied field, and the positive charges displace in the same direction. This produces an internal electric field which reduces the total electric field. However, studying dielectric properties is concerned with the diffusion and storage of magnetic and electric energy in materials. Dielectrics are essential to explain various events in solid-state physics, optics, and electronics.

The classical dielectric model involves the separation of negative and positive charges at the molecular or atomic level to produce an electric dipole structure. There are two types of dielectric materials. The first is called a polar dielectric with a permanent electric dipole moment, and the polar molecule's orientation is randomly distributed without an applied electric field (E). but with the effect of an external electric field, the dipoles can be aligned toward the direction of the electric field. The second type is non-polar dielectric materials. These types do not possess a permanent electric dipole moment, and each atom has a positive center charge surrounded by electrons with a cloud of negative charge. The positive and negative charges are displaced when an electric field is applied, and the atoms return to their original state within the specific time τ (relaxation time) when the electric field is removed[3, 65].

The dielectric constant (ε) represents the material permittivity and refers to the ability of a material to become polarized in response to an applied electric field. Traditionally, dielectric materials are made from inorganic materials such as SiO_2, and TiO_2. However, polymers have been widely used as dielectric substances due to their unique properties, such as flexibility, the ability to be produced specifically for specific uses, and chemical resistance. Polymers have been used as dielectric materials in capacitors since the 1960s. The polymer dielectric constant is generally greater than 2.0 and can be affected by frequency, temperature and illumination. Table 3.1 shows the dielectric constants of a few polymers in comparison with a few inorganic materials.

Table 3.1. The dielectric constant of various polymers and inorganic materials

Polymer Material	Dielectric Constant	Inorganic Material	Dielectric Constant
PVP	~3,80	Alümina (Al_2O_3)	8,5-10
PVDF	~9,12	HfO2	22-25
PVC	~ 4.60	barium titanat	100-300
PVA	~7,80	Silikon (Si)	11.8-12.1
Polyethylene (PE)	~2.40	S_iO_2	3.5-4.5
Teflon	~2.10	T_iO_2	80-100

3.2.4. Parallel Plate Capacitor

A capacitor is an electronic component that stores electric charge as a form of an electrostatic field and is made of two conductors (usually plates) isolated by a dielectric material. The dielectric material can be ceramic, glass, mica, plastic film, air, and paper. Capacitors are used in many electrical devices as a part of electrical circuits. As shown in Figure 3.8, due to the potential difference between the plates, one plate attracts a negative charge (-Q), and the other attracts a positive charge (+Q). Also, σ represents the density of the surface charge, and the electric field between the plates is given by[3, 62].

$$E = \frac{\sigma}{\varepsilon_0} \tag{3.19}$$

Here, ε_o (=8.85x10-12 Fm^{-1}) is the free space permittivity and is referred to the ratio of the total electric charge inside a certain closed surface in empty space to the electric flux passing through this surface. The potential difference between the two plates can be written as.

$$E = V = \frac{\sigma d}{\varepsilon_0} \tag{3.20}$$

Also, the capacitor's capacitance (C) is defined as the electric charge (Q) divided by the voltage (V) and expressed in farads (F).

$$C = \frac{Q}{V} \tag{3.21}$$

Here Q is the electrical charge stored in the capacitor expressed in coulombs (C), and V is the voltage applied (V) between two plates. Also, the capacitance of a capacitor with a space d between its two plates is.

$$C = \varepsilon_0 \frac{A}{d} \tag{3.22}$$

The surface charge density σ can be considered a source of electrical displacement in the region between the plates. Accordingly, electric displacement can be obtained by [92].

$$D = \sigma = \varepsilon_0 E \tag{3.23}$$

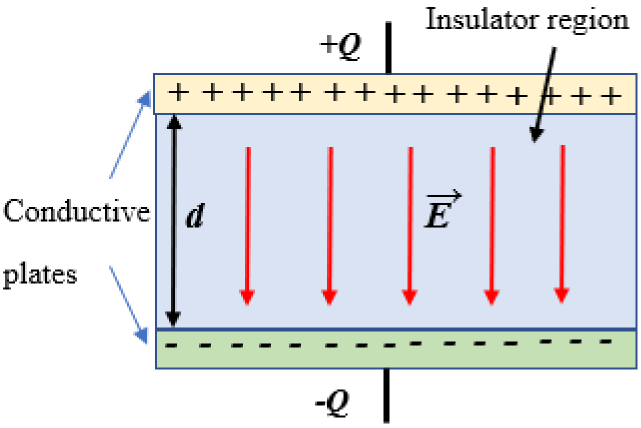

Figure 3.8. The parallel conductive plate capacitor structure

If a dielectric material is placed in the capacitor and fills the entire space between two parallel conductive plates, the value of the capacitance is experimentally expressed as follows.

$$C = \varepsilon \frac{A}{d} = \varepsilon_0 \varepsilon_r \frac{A}{d} \tag{3.24}$$

Here, ε is called the absolute permittivity of the dielectric substance, and the dimensionless $\varepsilon_r = \varepsilon/\varepsilon_o$ is the dielectric constant or dielectric relative permittivity [3, 62].

3.2.5. Dielectric Polarization

Polarization is a field vector that expresses induced or permanent electric dipole moments in a dielectric material. The electric polarization of the dielectric substance is the induced electric dipole moment per unit volume. Also, Polarization density indicates how the response of the material to an applied electric field. The dielectric polarization for a capacitor using dielectric material placed between two conductive parallel plates is shown in Figure 3.9. With the effect of the external applied field, negative charges are concentrated on the left, and positive charges are concentrated on the right surface of the material. At the same time, negative charges are formed on the conductive plate facing the positively charged surface, and positive charges are formed on the conductive plate facing the negatively charged surface. Also, the number of charges on the left and right surfaces are equal (neutral dielectric material). The polarization density is represented by the vector *P* with Coulombs per square meter (C/m^2) SI unit.

$$p = \chi \varepsilon_0 E \tag{3.25}$$

Here, $\chi = \varepsilon_r - 1$ is the electrical susceptibility of the material. Since the vacuum has no material to polarize, $\chi = 0$.

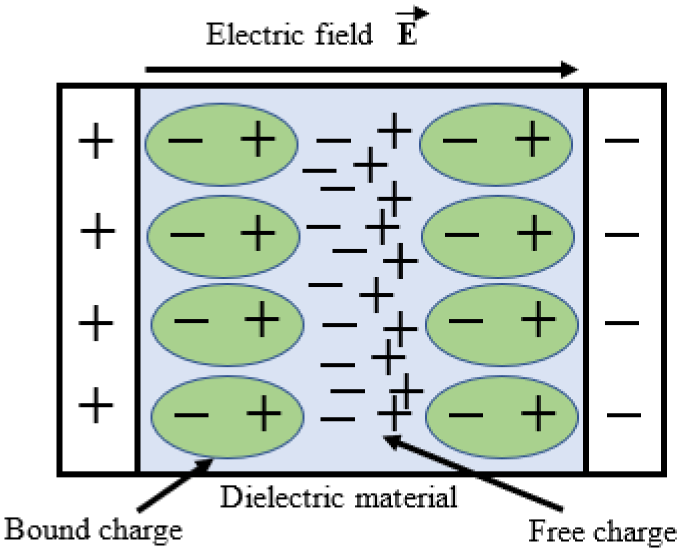

Figure 3.9. Dielectric polarization in a parallel plate capacitor

It is possible to describe the dielectric constant or relative permittivity using a capacitor model which is equivalent to the capacitance ratio of the measured and tested capacitors. Also, this is equal to the absolute permeability of the material divided by the vacuum permeability [62, 66, 67].

$$\varepsilon_r = \frac{Q}{Q_0} = \frac{C}{C_0} = \frac{\varepsilon}{\varepsilon_0} \tag{3.26}$$

For polarized dielectrics, the electric displacement *D* or the density of electric flux is proportional to the field *E* inside the dielectric and is expressed as [3, 62].

$$D = \varepsilon_0 E + P = \varepsilon_0 E\left(1+\chi\right) = \varepsilon_r \varepsilon_0 E \tag{3.27}$$

3.2.6. Polarization Mechanisms of Dielectric Materials

Various electrical polarization mechanisms in dielectric materials can be classified as electronic, ionic, directional (dipole), and interface (space charge) polarization. The polarization mechanisms depend on the applied frequency, as displayed in Figure 3.10. This Figure shows the Polarization mechanisms of a dielectric material. The total dielectric polarization in a material is the combination of ionic, interfacial, directional polarization, and electronic.

3.2.6.1. Electronic Polarization

When a dielectric material is subjected to an electric field, a slight shift of the negatively charged cloud electron relative to the nuclei in the atom produces the dielectric molecule, and it causes an induced dipole moment in the molecule, as displayed in Figure 3.10 (d). Electronic polarization occurs at ultraviolet and visible frequencies (~10^{15} Hz) in a short time (around 10^{-14} s). The displacement of the electrons produces a dipole moment *p*, which is defined as the product of both displacement distance and electric charge (*p*=*qd*). The dipole moment is also directly proportional to the strength of the electric field *E*[62, 66].

$$p = \alpha_e E \tag{3.28}$$

Where electronic polarization constant α_e is a microscopic polarization phenomenon that happens in all materials. However, the material's polarization must be evaluated to explain how the dielectric constant relates to the electronic polarization (P_e) and is described via the total dipole moment per unit volume, as presented in the following equation.

$$P_e = N_e p \tag{3.29}$$

Here. N_e is the density of molecules. Therefore,

$$P_e = N_e \alpha_e E = \chi_e \varepsilon_0 E \tag{3.30}$$

Also, this polarization is independent of temperature. Therefore, the relative permittivity and electronic polarization equation can be given using the next relation.

$$\varepsilon_r = 1 + \frac{N_e \alpha_e}{\varepsilon_0} \tag{3.31}$$

3.2.6.2. Ionic Polarization

Ionic polarization is usually observed in ionic crystal components (LiBr, NaCl, KCl) that contribute to the relative permeability of the substances. In general, inside these materials, there is no net polarization without the effect of the applied field because both dipole moments of positive and negative ions are canceled by each other. However, with the effect of an external field, the ions are displaced, and polarization occurs inside the material, as displayed in Figure 3.10 (a). The next relation explains the effect of this polarization.

$$p_{av} = \alpha_i E_{loc} \tag{3.32}$$

Where p_{av} is the induced average dipole moment per ion pair, E_{loc} is the local electric field, and α_i is the ionic polarized ability. However, the ionic polarization capability is up to 10 times greater than the electronic polarization capability. Therefore, ionic components generally have high dielectric constants.

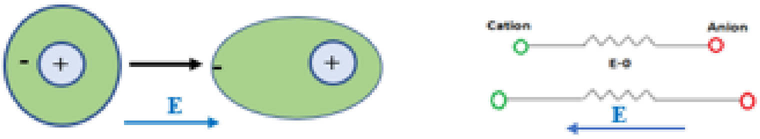

(a) Electronic polarization (b) Ionic polarization

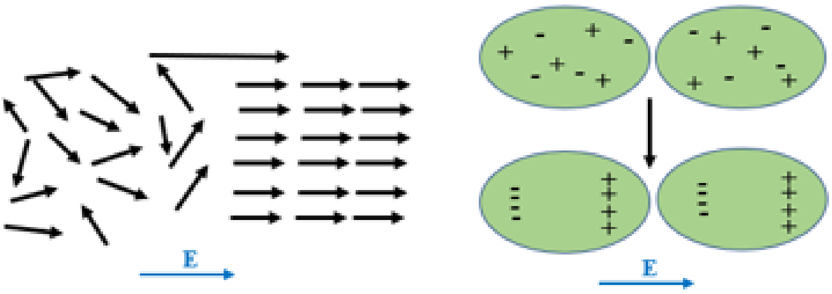

(c) Dipole polarization (d) Interface polarization

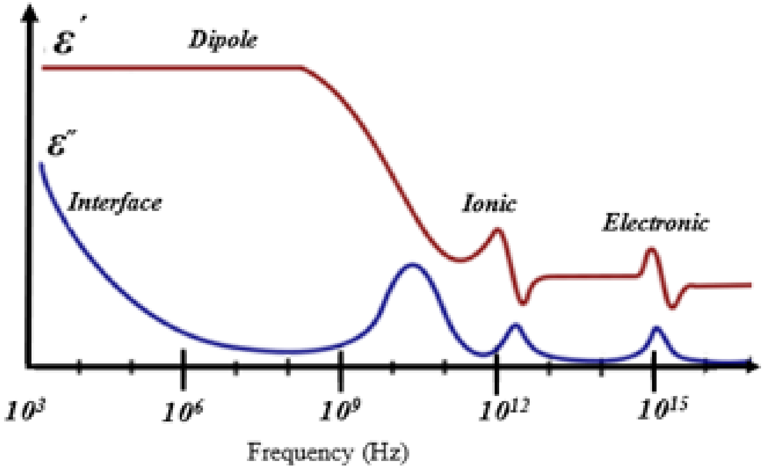

(d)

Figure 3.10. Polarization mechanisms of a dielectric material; a) Ionic, b) Oriented, c) Interface polarization, d) Electronic, e) Polarization mechanism depending on the applied frequency.

When an external electric field is applied to the material, the dipoles tend to align with the field direction, leading to a net polarization of the material. The strength of this polarization depends on various factors such as the strength and frequency of the applied field, the temperature of the material, and the nature of the dielectric material itself [62, 66].

3.2.6.3. Directional (Dipole) Polarization

Directional, dipolar, or Orientational polarization is typically observed in polar dielectrics with permanent dipoles, such as dipolar ceramics and polymeric materials. In polar dielectric materials, the dipoles are randomly oriented without external field effect due to their thermal energy, and the net dipole moment is zero. While with the applied external field, the dipoles start to rotate to align with the field resulting in polarization and non-zero net dipole moment, as shown in Figure 3.10 (b)[66].

3.2.6.4. Interface Polarization

Space charge polarization or interface polarization observes when the charges are performed at the interface between two regions within a material or two materials by the effect of an external electric field (Figure 3.10 (c)). Such polarization can occur when two electrodes are connected to a dielectric material or a dielectric compound. Unlike directional and ionic polarization, this polarization affects free charges at the interface rather than ionic and covalently bonded electrical charges and is usually observed in polycrystalline or amorphous solids. Interfacial polarization is observed at lower frequencies, otherwise referred to as space-charge polarization or Maxwell Wagner.

Usually, more than one polarization process happens in a dielectric medium. Therefore, the typical dipole moment induced per molecule is the total of contributed polarization.

3.2.7. Dielectric Loss

The ε_r is the static dielectric permittivity constant of the polarization under *DC* conditions. In *ac* electric field, two currents flow through a capacitor known as the conduction current (I_C) and polarization current (I_P). In this situation, the dielectric constant is given as a complex quantity.

$$\varepsilon^* = \varepsilon_r^{'} - j\varepsilon_r^{''} \tag{3.33}$$

Here, both ε' and ε'' are the real (dielectric constant) and the imaginary parts of the complex dielectric constant. When an applied periodic electric field ($E = E_0 e^{i\omega t}$) with angular frequency ($\omega=2\pi f$) to a dielectric substance. The current I_P flowing through the capacitor stores energy, while the current I_C (consumes energy) passes through the resistor, as shown in its equivalent circuit shown in Figure 3.11. The polarization and conduction currents are expressed as follows.

$$I_p = j\omega\varepsilon_0\varepsilon_r^{'} A E_0 e^{i\omega t} \tag{3.34}$$

$$I_C = j\omega\varepsilon_0\varepsilon_r^{''} A E_0 e^{i\omega t} \tag{3.35}$$

This indicates that the conduction current remains in phase with the applied field, while the polarizing current is 90° before the applied field phase. Also, the ratio between two currents represented the dielectric distribution or dielectric loss (tangential loss) [62, 66, 68].

$$\tan\delta = \frac{I_C}{I_p} = \frac{\varepsilon_r^{''}}{\varepsilon_r^{'}} = \frac{1}{\omega RC} \tag{3.36}$$

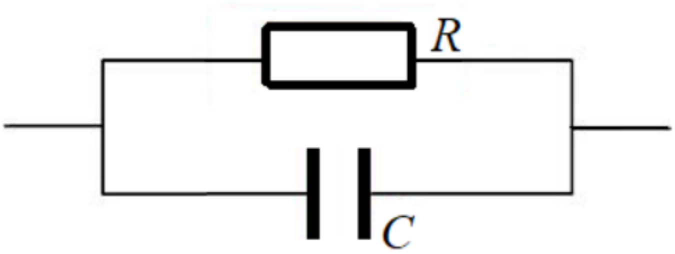

Figure 3.11. Equivalent circuit for dielectric capacitor

3.2.8. Dielectric Relaxation

The time response to an external periodic electric field is one of the main problems with dielectrics. Dielectric relaxation occurs when the polarization is delayed relative to an external periodic electric field. Dielectric relaxation can occur at a specific time (τ) for a given polarization. Thus, the specific polarization mechanism can be recognized. Dielectric relaxation has been studied using dielectric spectroscopy technology in the frequency domain according to the inverse relationship ($f = 1/t$). To explain a relaxation mechanism, various electrical factors can be investigated, such as the complex dielectric constant $\varepsilon^* = \varepsilon' - j\varepsilon''$, complex admittance $Y^* = Y' - jY''$, complex impedance $Z^* = Z' - jZ''$, and complex electrical modulus $M^* = M' - jM''$. The M^* is the inverse of the ε^* ($M^* = 1/\varepsilon^*$) [92], which corresponds to the electric field relaxation when the electrical displacement stays constant in a material.

Debye relaxation; To describe the relaxation phenomenon, the Debye relaxation relation is the simplest and most elegant mathematical relation used.

$$\varepsilon_r = \varepsilon_\infty + \frac{\varepsilon_S - \varepsilon_\infty}{1 + j\omega t} \tag{3.37}$$

Here, ε_∞ and ε_S are the higher frequency and static dielectric permittivity, and t is the characteristic relaxation time. Physicist Peter Debye describes this relaxation for non-interacting dipoles in an external *ac* electric field (Debye model). **Relaxation of Maxwell-Wagner**; occurs in electrically inhomogeneous materials, such as dielectric and electrode interfaces, grain boundaries, etc. It is commonly demonstrated using a two-layer equivalent capacitor circuit, as illustrated in the next graph.

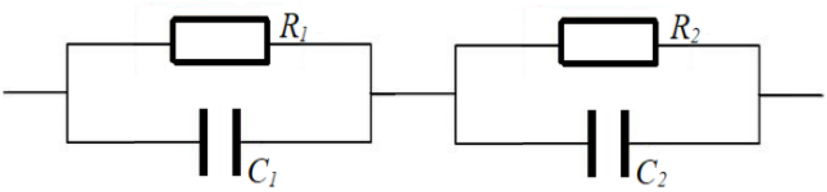

Figure 3.12. Equivalent bilayer circuit of Maxwell-Wagner relaxation

Also, the Debye relaxation mode can express the permittivity of the dielectric for Maxwell-Wagner relaxation.

$$\varepsilon_r = \varepsilon_\infty + \frac{\varepsilon_S - \varepsilon_\infty}{1 + j\omega t} - j\frac{\sigma}{\omega} \tag{3.38}$$

It is clear that when there is a considerable distinction between the two resistances, the relaxation can be observed. Also, each *RC* circuit corresponds to a component in the investigated dielectrics, the electrode-dielectric interface, or grain boundaries, as shown in Figure 3.12, both electrical modulus and impedance are investigated.

To separate the two relaxation components, both the impedance and electrical modulus are investigated. The impedance of the substances can be evaluated in a wide range of frequencies, to obtain information on the various relaxation processes in the component. Also, the electrical modulus illustrates the behavior of the dielectric material as a function of frequency and is used to obtain information on the relaxation times distribution related to the various components in the device[62, 66].

$$Z' = \frac{R_1}{1+\left(\omega R_1 C_1\right)^2} + \frac{R_2}{1+\left(\omega R_2 C_2\right)^2} \tag{3.39}$$

$$Z'' = R_1 \frac{\omega R_1 C_1}{1+\left(\omega R_1 C_1\right)^2} + R_2 \frac{\omega R_2 C_2}{1+\left(\omega R_2 C_2\right)^2} \tag{3.40}$$

and the electrical module of the circuit is.

$$M' = \frac{C_0}{C_1} \frac{\left(\omega R_1 C_1\right)^2}{1+\left(\omega R_1 C_1\right)^2} + \frac{C_0}{C_1} \frac{\left(\omega R_2 C_2\right)^2}{1+\left(\omega R_2 C_2\right)^2} \tag{3.41}$$

$$M'' = \frac{C_0}{C_1} \frac{\omega R_1 C_1}{1+\left(\omega R_1 C_1\right)^2} + \frac{C_0}{C_1} \frac{\omega R_2 C_2}{1+\left(\omega R_2 C_2\right)^2} \tag{3.42}$$

However, the electric equivalent circuit can change, and a more complex circuit model can be applied to modify the dielectric behavior of Maxwell-Wagner relaxation. This is the simplest case involving only two dielectric materials.

PART 4

EXPERIMENTAL PART

4.1. PRODUCTION PROCESS OF THE Au/(RuO$_2$:PVC)/n-Si SCHOTTKY STRUCTURES

To fabricate the diodes, firstly, in order to produce RuO$_2$, both ruthenium chlorate (RuCl$_3$) and sodium hydroxide (NaOH) components have been obtained from Sigma-Aldrich. Then 0.83 grams of RuCl$_3$ were dissolved in ionized water (20cc) to produce a solution of 0.2 M. Also, 0.24 gram of the NaOH were diluted in 20cc of ionized water and produced a solution of 0.3 M. After that, the NaOH solution was gradually added to the RuCl$_3$ solution for 15 minutes with continuous stirring. The obtained compound was dried in an autoclave at 180^{o}C for 24 hours. Then washed and dried at room temperature four times in ethanol. The resulting nanopowder was calcined for 1 hour at 700 C^0 in a furnace. The n-type silicon substrate with 100> oriented and 1-10 Ω.cm resistance was cleaned by a chemical cleaning technique (RCA) to fabricate the Au/ RuO$_2$:PVC /n-Si SBD. Moreover, to perform the ohmic contact, the substrate's back surface was thermally coated. With 0.999 purity of gold at 10^{-6} Torr and about 300 nm width. At 3000 rpm, the thin layer of the RuO$_2$:PVC was spin-coated for 1 minute. Then an Au with high purity (0.999) was used to perform Schottky contact and was formed on the RuO$_2$:PVC with 1 mm diameter of a circular dot. Using a profilometer, the thickness of the interfacial layer was obtained and shown to be 50 nm. The schematic of the obtained structure is shown in Fig.4.1.

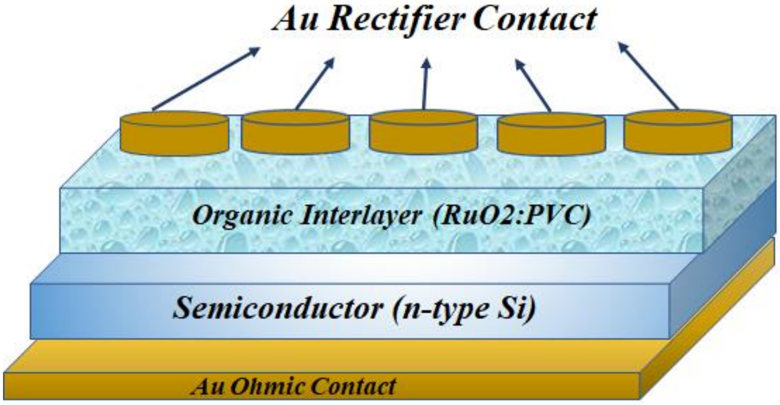

Figure 4.1. The Au/ RuO_2:PVC /n-Si structures Schematic diagram

4.2. SCANNING ELECTRON MICROSCOPY (SEM) IMAGES

Images of scanning electron microscopy at 100 kx and 10 kx magnifications of the ruthenium oxide nanostructures (RuO_2) (FESEM, Czech Republic, TeScan-Mira III) are illustrated in Figure 4.2 (a and b). These figures show that the nanostructures of RuO_2 consisted of clusters of micron-sized and circular nanoparticles having an average size below 50 nm. Both images of SEM for the polymer layer (PVC) and PVC: RuO_2 are illustrated in Figure 4.2 (c and d), respectively. The stoichiometry and purity of the produced nanostructures of the RuO_2 and PVC layer were analyzed using the energy dispersion spectroscopy technique. Figure 4.2 (e) illustrates that only atoms of ruthenium and oxygen exist in the structure of ruthenium dioxide, and it has not any additional imperfections in the structure. Also, Figure 4.2 (f) shows the chlorine and carbon components of the polymer (PVC). The hydrogen atoms are absent in this profile because of their lightness. The remaining elements are also related to the elements of the sub-layer. As shown in Figure 4.2 (e), the percentages of oxygen and ruthenium elements in the nanostructure of RuO_2 are 10% and 90%. Also, Figure 4.2 (f) shows that the percentage of chlorine and carbon atoms in PVC composition are 11.3% and 44.4%, respectively.

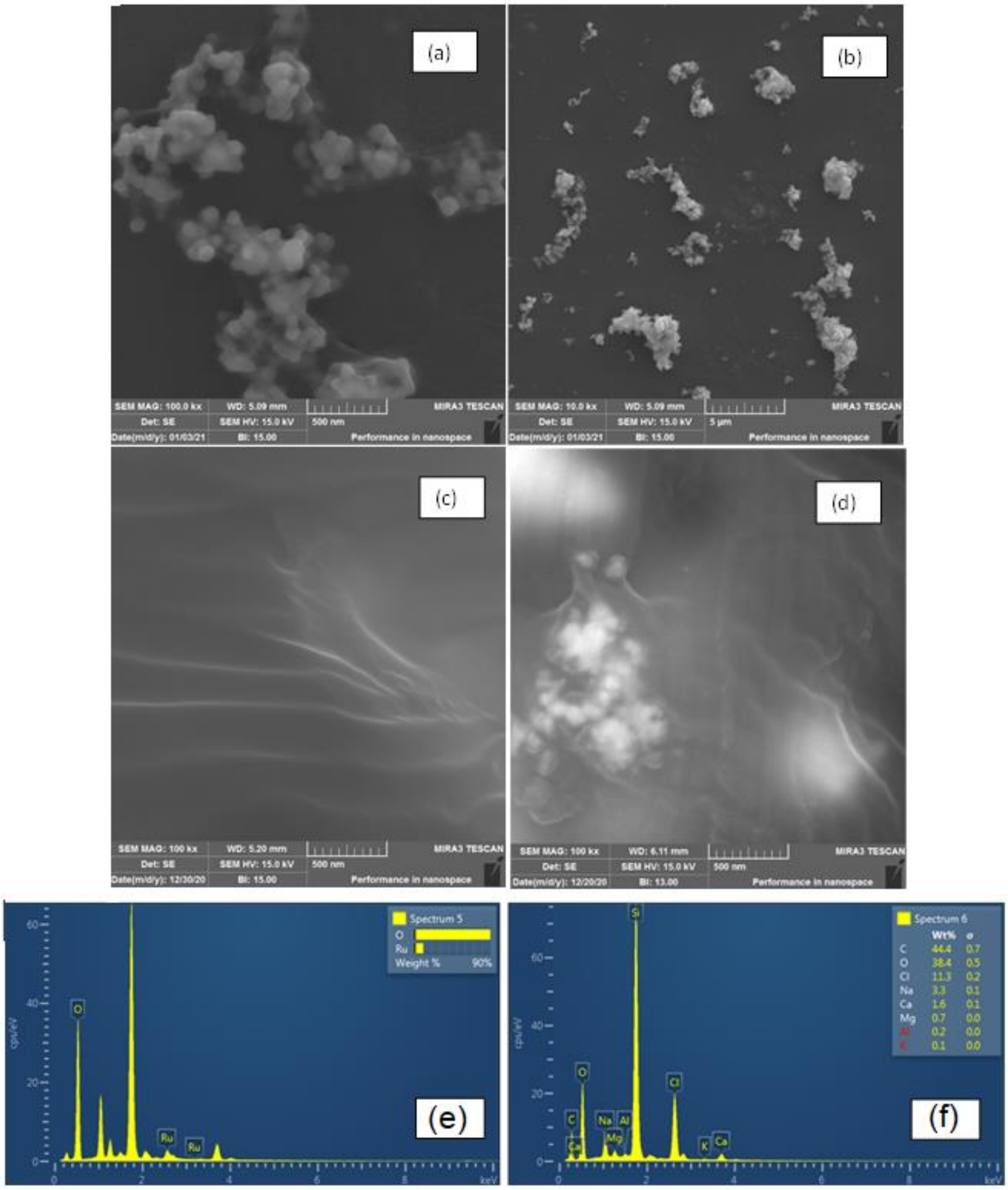

Figure 4.2. Scanning electron microscopy (SEM) images a) nanostructures of RuO2 at 100 kx , b) magnifications at 100 kx, c) PVC, d): RuO2 : PVC. e) EDX of RuO2. f) EDX of PVC

4.3.THE *X*-RAY DIFFRACTION (XRD)

Figure 4.3 displays the pattern of *X*-ray diffraction for the nanostructure's component of RuO_2. The peaks of diffraction according to the crystal plates (110), (101), (200), (210), (211), (220), (002), (310), (112), (301), and (202) at position 2θ = 28.1°, 35.2°, 40.3°, 45.1°, 54.5°, 58.1°, 59.6°, 65.8°, 67.2°, 69.8° and 74.3° of the RuO_2

nanostructures were also displayed. This pattern of diffraction is a spatial group exhibiting a tetragonal phase (P42/mnm) that matches ICDD Standard measurements (00-040-1290). The RuO_2 nanocrystal's average size was evaluated from the relation of Scherer as illustrated in equation [69].

$$D = k\lambda / (\beta \cos(\theta)) \tag{4.1}$$

where k, λ, θ, and β are a constant quantity (~0.94), the wavelength of X-ray, an angle of diffraction, and a maximum half-width (5414.1 Å). The evaluated average size was 24 nm for the RuO_2 nanocrystals.

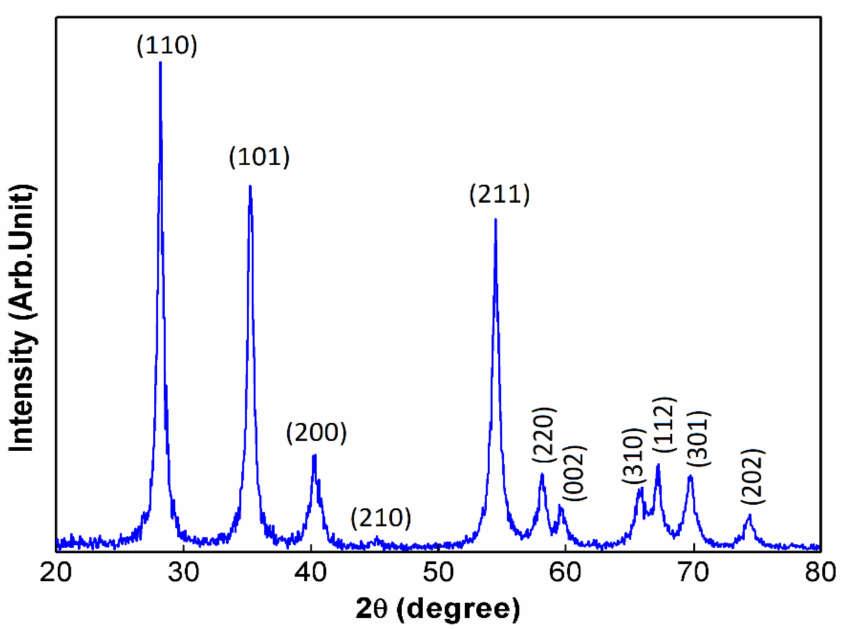

Figure 4.3. The pattern of XRD for the ruthenium dioxide powder nanostructures

Furthermore, the optical properties of the RuO_2 nanostructures have been analyzed through the visible-ultraviolet transmission and absorption spectrum were between 200-800 nm wavelength range of the produced sample, as illustrated in Figure 4.3 (a). Also, the sample UV-V spectrum has been used to evaluate the nanostructure's energy gap by the next equation.

$$\alpha hv = B(hv - E_g)^n \tag{4.2}$$

Here, $h\nu$ is the photon energy, α is the optical absorption coefficient, B is the proportionality constant, and the value of n is equal to 2 or 0.5 for indirect or direct transitions, respectively. Also, α was calculated from the spectral data using $\alpha = \left(-1/d\right)\times\ln\left(Tr\right)$ relation. Where Tr is the measured transmittance and d represents the length of optical passage (d =7 mm). Figure 4.4 (b) displays the sample diagram $(\alpha h\nu)^2$ with respect to the energy $h\nu$. The E_g of the ruthenium dioxide nanostructures is evaluated using the distance from the origin of the linear portion in Figure.4.4 (b). The obtained value is 1.77 eV for direct transition.

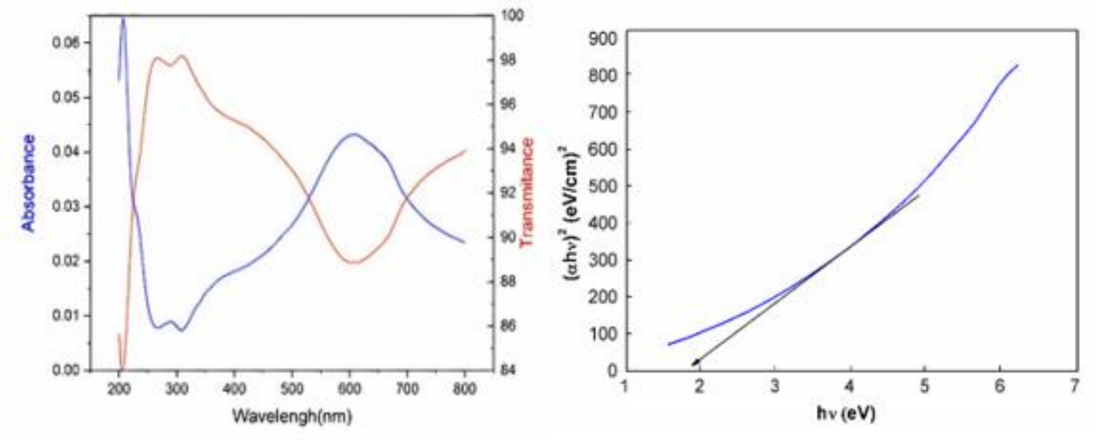

(a) (b)

Figure 4.4. (a) The UV-V spectrum (b) the tauc of the produced RuO_2

4.4. RESULTS AND DISCUSSIONS

4.4.1. Electric Characteristics of The Au/(RuO_2:PVC)/n-Si Devices

The *I-V* measurements of the Au/(RuO_2:PVC)/n-Si SBD, were executed under various illumination-intensity using *I–V* source meter (Keithley 2400) and the source light arc lamp (The solar simulator, Newport Oriel Ins, Version 76,011.) was used for controlling the intensity of the light. The AM1.5 filters have been used to pass the various intensities of photons to reach the device surface.

The Au/(RuO_2:PVC)/n-Si structures were examined in the dark and under different illumination intensities at room temperature using the *I-V* measurements as illustrated in Figure 4.5. As shown in this graph, all curves exhibited good rectification performance, and rectifier-ratio ($RR=I_{for.}/I_{rev}$ at ±5V) gradually decreases based on increases the levels of illumination. The plots of ln(I)-V exhibit a straight line behavior in the range of 0.3 to 0.61 V, but they deviated from the linearity at adequately high forward biases due to the series resistance R_S and doped-organic interlayer (RuO_2:PVC). Moreover, the reverse current values increase in both reverse and forward bias, indicating that the valance band's electrons get sufficient energy ($hc/q\lambda \geq E_g$) to move to the conduction band and generate electron-hole pairs under the illumination effect. Therefore, the produced device exhibits solar cell and photodiode characteristics [63, 64].

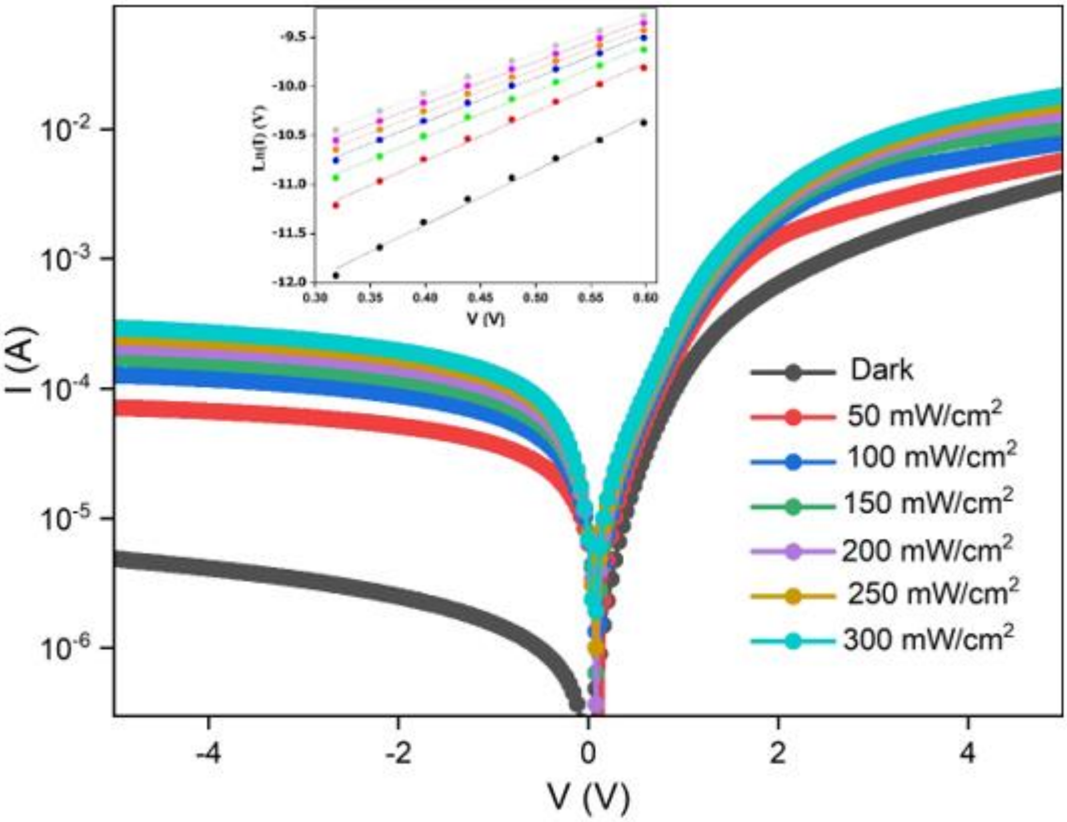

Figure 4.5. The I-V plots of the structure with the linear region of the Ln(I)- V plot at definite illumination intensity.

According to the Thermionic emotion model, the voltage and current relation for the intermediate forward bias region ($V \geq 3kT/q$) is given as [27, 61].

$$I = I_0\left[\exp\left(\frac{q\left(V-IR_s\right)}{nkT}\right)-1\right] \tag{4.3a}$$

Here, IR_S is the device voltage drop, and I_o is the backward-saturation current. The I_o value was evaluated from the linear part intersection point of the Ln(I)- V figure using the next relation.

$$I_0 = AA^{*}T^{2}\exp\left(\frac{-q\Phi_{B0}}{kT}\right) \tag{4.3b}$$

In this equation, A^* is the Richardson constant, with a value of 112 A/cm^{2}K^2 for n-Si, and A is a rectifier contact area. Also, the value of Φ_{B0} can be evaluated using the evaluated I_o value with neglecting the voltage drop (IR_S) using the following equation.

$$\Phi_{B0} = \frac{kT}{q}\ln\left(\frac{AA^{*}T^{2}}{I_0}\right) \tag{4.4a}$$

Furthermore, the n value can be calculated using the slope of the forward Ln(I)-V graphs linear region by the following formula.

$$n = \frac{q}{kT}\frac{d\left(V-IR_s\right)}{d\left(\ln I\right)} \tag{4.4b}$$

All the previous evaluated parameters (I_o, Φ_{B0}, and n) values were shown in Figure 4.6 (a, b) and summarized in Table 4.1. The obtained values varied from 1.2 μA, 0.640 eV, and 7.0 under dark conditions to 8.0 μA, 0.595 eV, and 9.3 at 300 mW/cm^2 illumination, respectively. The quantity of n for an ideal case is closer to unity (n=1), but this situation is extremely different in applications because of the influence of many factors such as the dielectric properties, interfacial layer thickness (d_i), depletion-layer width (W_D), doping concentration atoms, and surface states [70, 71]. Also, as displayed in Fig.4,6 (a, b), while the Φ_{B0} values decrease almost as exponentially, the n values linearly increase with increasing illumination level.

Coworkers and Monch used the theoretical approach of Tung, and they found a linear relation between n and Φ_{B0} which indicates a lateral inhomogeneity of the BHs at the interface of MS. Also, they found that the homogeneous of BH should be given in the case of n=1 in the Φ_{B0} vs n plot[72, 73]. However, there is a linear relation between n and Φ_{B0} as the Φ_{B0} = (- 202*10^{-4}n + 0.7818) eV. Thus, for an ideal case ($n=1$), the value of Φ_{B0} was evaluated as 0.7616eV. This behavior may be caused by the increases in the illumination intensities, shrinking of the depletion zone width, the generation of e^{-}-h^{+} pairs and their recombination under the effect of illumination, and the N_{SS} effects [74].

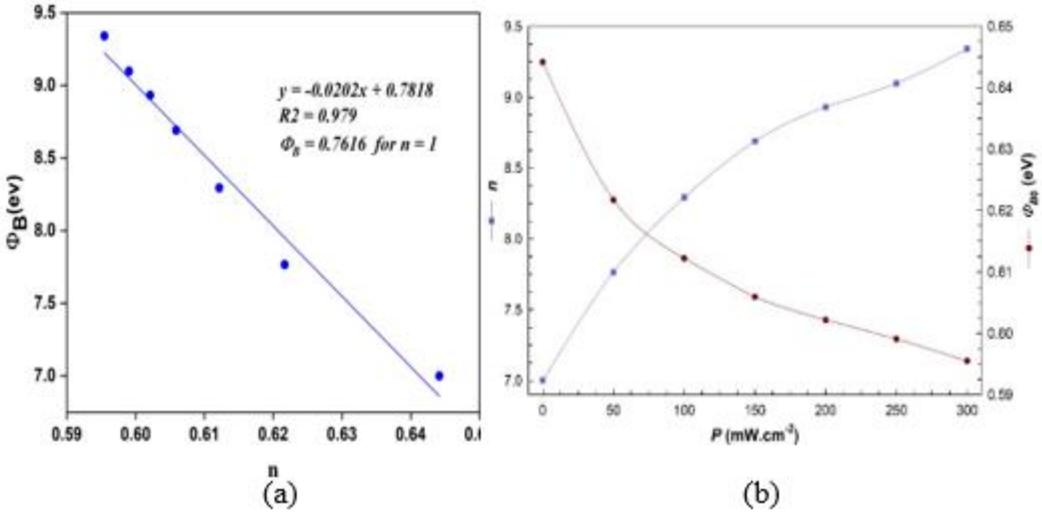

(a) (b)

Figure 4.6. (a) The Φ_{B0} vs. n and (b) Φ_{B0}, n vs. P graphs of the device

Table 4.1. Basic electrical parameters obtained using *TE* and Cheung function

P (mW/cm²)	***n***	***I*₀ (μA)**	**Φ_{B0} (eV)**	**R_{Sh} (k Ω)**	**R_S (Ω)**	**(*dV*/*d*ln(*I*))-*I***		**H(*I*) - *I***	
						R_S (k Ω)	n	Φ_B (eV)	R_s (Ω)
0	7.0	1.20	0.64	1021	1270	1115	5.9	0.88	1653
50	7.7	2.90	0.62	70	823	933	7.0	0.75	735
100	8.2	4.20	0.61	39	632	300	8.3	0.65	394
150	8.6	5.30	0.605	29	475	235	8.7	0.64	310
200	8.9	6.10	0.602	23	377	200	8.9	0.632	294
250	9.0	6.90	0.599	19	317	177	9.0	0.631	220
300	9.3	8.00	0.595	17	274	161	9.7	0.62	196

The applied voltage to the structure is divided among the depletion zone, R_s, and interface structure. Accordingly, both quantities of R_S and R_{Sh} of the device can be calculated by using various methods from the I-V data. These methods are Ohm's law

($Ri = dV_i / dI_i$), Norde, and Cheung. In Ohm's law process, the values of R_S and R_{Sh} were evaluated from sufficient high forward and reverse voltages. As shown in Fig. 4.8 and Table 4.1, the R_S and R_{Sh} values are strongly dependent on illumination intensity (decrease with increasing illumination intensity) and applied voltage. Their decreases are due to an increment in conductivity with illumination levels. Because numerous electrons in the valance band (E_V) and interface states can increase their conductivity ($\rho=q\mu N$) under the illumination effect and are easily excited to the conductance band (E_C) [3]. As a result, many electrons in both the traps and E_V levels can pass through the traps to other traps or E_C to produce a photocurrent (I_{ph}).

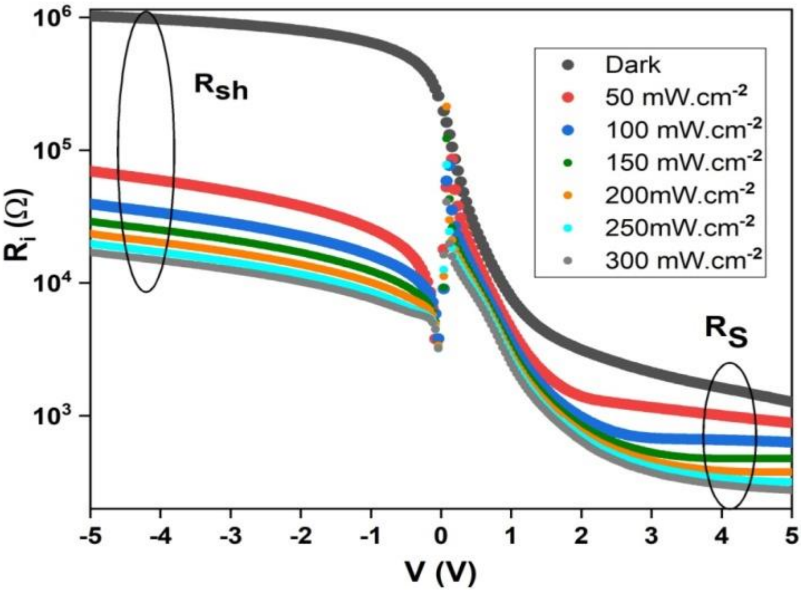

Figure 4.7. Changes of Ri under definite illumination levels

Furthermore, there are considerable deviations from the linearity ln(I) vs V graphs at high enough biasing voltage zones. Also, in the intermediate biasing region, there are not enough large linear regions. Therefore, Norde and Cheung [75, 76] proposed new alternative methods to obtain the main device elements at different temperatures or illumination levels. The Norde technique was proposed for the intermediate bias zones, while the Cheung approach was proposed at the bending zone of the I–V characteristics. However, both the barrier height (Φ_B) and R_S values were obtained from the Cheung technique using the next equations.

$$\frac{dV}{d(\ln I)} = \left(\frac{nkT}{q}\right) + IR_S \tag{4.5a}$$

$$H(I) = V - \left(\frac{nkT}{q}\right)\ln\left(\frac{I}{AA^{*}T^{2}}\right) = n\Phi_B + R_s I \tag{4.5b}$$

The previous relations were used to extract both *H(I)* and *dV/d(Ln(I))* as a function of *I* characteristics at ordinary room temperature in the dark and at different illumination intensities. These graphs exhibit good linear behavior over a wide current and voltage range. The value of R_S can be obtained directly for each illumination level from the slopes of the above equations, and the *n* values can be evaluated using an intercept point in Equation 4.5 (a). Also, the value of Φ_B can be obtained using Equation 4.5 (b) from the evaluated values of *n*. As shown in Table 4.1, the evaluated values of R_S and BH are almost identical compared to TE theory, and both decrease with increased illumination levels.

Also, the values of Φ_B and R_S for the Au/(RuO$_2$:PVC)/n-Si SBDs were extracted from the modified Norde technique using the next presented relations[77].

$$F(V) = \frac{V}{\gamma} - \frac{kT}{q}\ln\left(\frac{I(V)}{AA^{*}T^{2}}\right) \tag{4.6}$$

$$\Phi_B = F(V_{\min}) + \frac{V_{\min}}{\gamma} - \frac{kT}{q} \tag{4.7a}$$

$$R_S = \frac{kT(\gamma - n)}{qI_{\min}} \tag{4.7b}$$

Here, *F*(V_m) is referred to as the lowest value for the *F*(*V*) - *V* graph. I_m is the minimum value of current according to *F*(V_m), V_m is the minimum voltage applied that is equivalent to *F*(V_m), and γ is referred to as the first integer quantity greater than *n*[76]. Figure 4.9 displays *F(V) –V* plots at specified illumination intensities. These graphs were analyzed to evaluate the I_m , V_m, and $F(V_m)$ values to obtain both quantities of Φ_B and R_S using equations. 4.7(a) and (b) as displayed in Table 4.2.

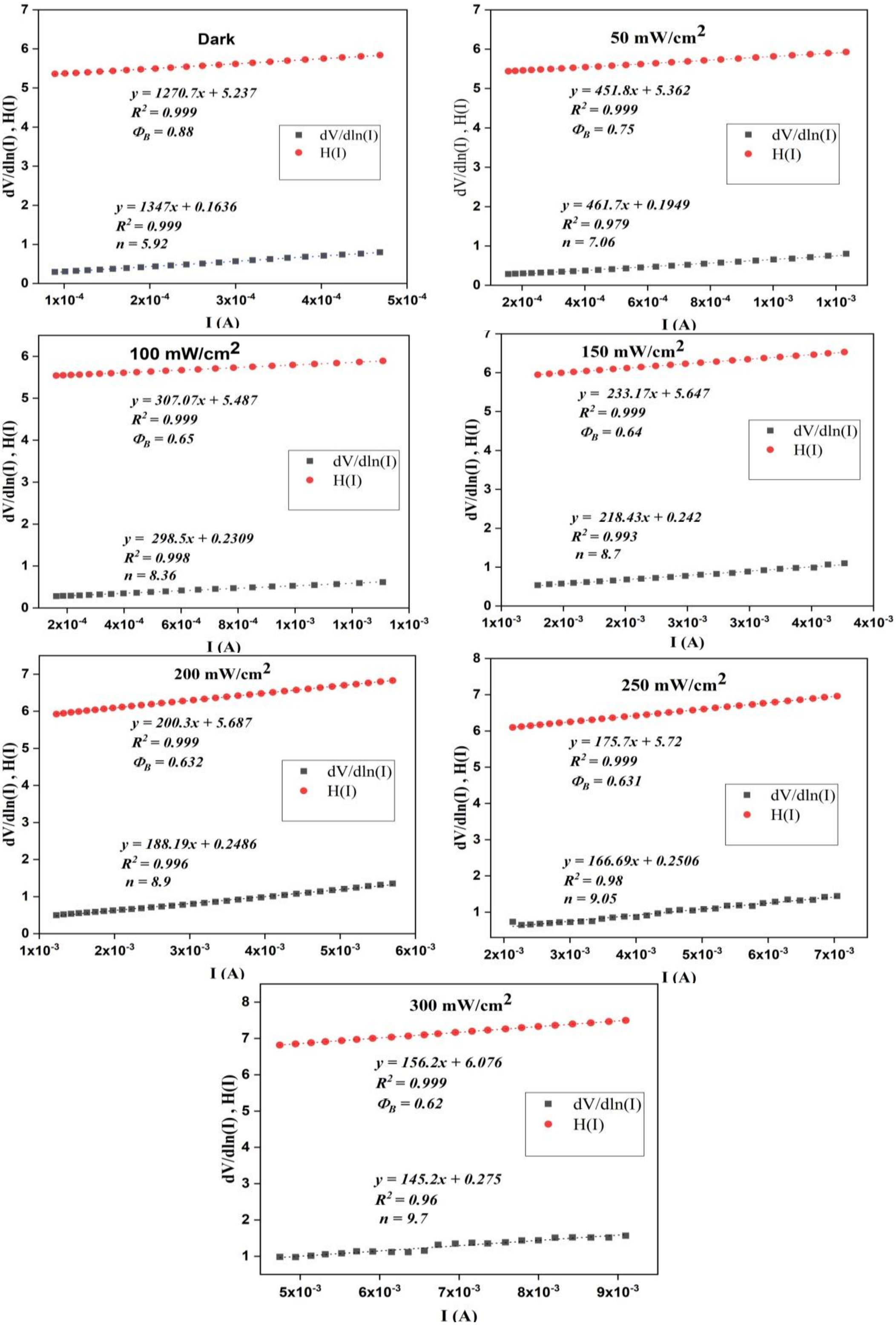

Figure 4.8. The dV/dln(I) and H(I) vs. I characteristics at definite illumination levels

Table 4.2. Basic electrical elements evaluated from the Norde function

P (mW/cm^2)	I_m (μA)	F_{min} (V)	V_m (V)	Φ_B (eV)	R_S (Ω)
Dark	59.3	0.614	0.758	0.661	1527
50	156.0	0.592	0.878	0.642	643
100	310.0	0.582	1.037	0.640	346
150	397.0	0.576	1.117	0.636	283
200	438.0	0.571	1.117	0.628	263
250	480.0	0.568	1.117	0.523	245
300	579.0	0.559	1.157	0.515	208

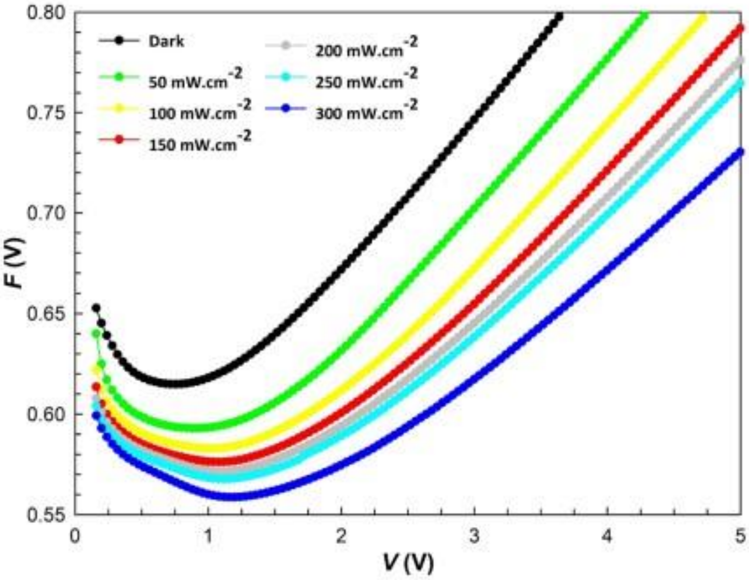

Figure 4.9. The F(V)–V graphs of the device for different illumination intensities

Table 4.2 shows clearly that both R_S and Φ_B values are decreasing with an increase in illumination levels. However, the R_S values obtained from Ohm's law are higher than those evaluated using Cheung's and modified Norde's methods. The discrepancies between the values of Φ_B and R_S on each function are related to defined regions of the *I-V* characteristics for each method. However, the n, R_S, and Φ_B values are influenced by the energy dispersion distribution of N_{SS} and the applied voltage [78, 79]. In general, the density of states at the M/S interface is usually caused by doping bonds, the semiconductor surface defects like oxygen vacancies, rearrangements of metallization-induced structural, doping concentration atoms, and deposited interfacial. The N_{SS} in the semiconductors act as traps or recombination centers and significantly affect the *I–V* characteristics of the produced structure. However, the defects or N_{SS} can be obtained from the relation of n as a function of the voltage applied $n(V)$ and the effective barrier height $\Phi_e(V)$, as expressed in the following equations [80] .

$$n(V)=\frac{q}{kT}\left[\frac{(V-IR_S)}{\ln\left(I/I_O\right)}\right]=1+\frac{\delta}{\varepsilon_i}\left[\frac{\varepsilon_S}{W_D}+qN_{SS}(V)\right] \tag{4.8}$$

$$\Phi_e(V)=\Phi_{B0}+\left[\left(1-\frac{1}{n(V)}\right)V\right] \tag{4.9}$$

Rhoderick and Card have proposed the following relation to evaluating the values of N_{SS} [81].

$$N_{SS}(V)=\frac{\varepsilon_S}{q}\left[\frac{\varepsilon_i}{\delta}\left(n(V)-1\right)-\frac{\varepsilon_S}{W_D}\right] \tag{4.10}$$

Where δ is the thickness of the insulator, ε_S, and ε_i are the semiconductor/insulator permittivity, respectively ($\varepsilon_S = 11.8\varepsilon_0$ and $\varepsilon_0 = 8.85 \times 10^{-14}$ F/cm), and the width of the depletion layer is W_D, which was obtained using C–V measurements at $1 * 10^6$ Hz in the dark as $6.46 \text{x} 10^{-5}$ cm.

$$W_D=\left(2\varepsilon_S\varepsilon_O V_O / qN_D\right)^{0.5} \tag{4.11}$$

Here, the doping atom is N_D. Moreover, the relation between the surface states energy E_{SS} and the conduction band's lower edge (E_C) is represented by.

$$(E_c-E_{ss})=q(\Phi_e-V) \tag{4.12}$$

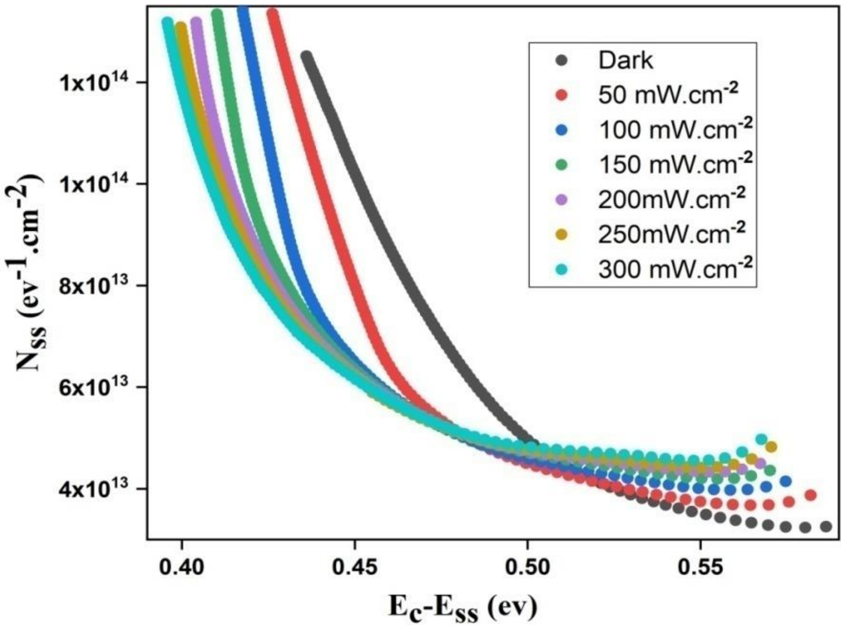

Figure 4.10. The variations of interface states are varied by illumination intensities

Figure 4.10 shows the variation of (E_C - E_{SS}) vs. N_{SS} in the dark and for different illumination intensities. In this graph, while the values of N_{SS} increase by increasing the level of illumination at about under the middle of the energy gap (E_g) for n-type silicon, the values of N_{SS} increment as decreasing the intensity of illumination at about above the middle of E_g. Furthermore, the N_{SS} values exhibit exponential incrementing behavior near the middle of E_g into the bottom of the E_C. Also, the average value obtained of N_{SS} at around (E_C-0.50) eV for each illumination level is close to 5x10^{13} eV^{-1}cm^{-2}. Furthermore, the traps or interface states (N_{SS}) have some locations or discrepancies due to their reordering and restructuring under external influences of electric field and illumination [82].

4.4.2. Photovoltaics Characteristics of The Au/(RuO$_2$:PVC)/n-Si Devices

The values of both I_{SC} and V_{OC} for the produced Au/(RuO$_2$:PVC)/n-Si (MPS) SBDs were found as 6.4μA and 0.118 V at 50 mW/cm^2, respectively. Also, both the fill factor (FF) and efficiency (η) values were obtained from the following relations.

$$FF = (I_m.V_m)/(I_{SC}.V_{OC}) \tag{4.13a}$$

$$\eta = (FF.I_{SC}.V_{OC}) / (A.P_{in}) \tag{4.13b}$$

Where A is the effective contact area, P_{in} is the intensity of the illumination, I_m, and V_m are the values of current and voltage according to the maximum Power Point. These V_m , I_m , η, and FF values were found as 0.079 V, 4.4μA, 0.088 %, and 46% under 50 mW/cm^2, respectively. The low-efficiency obtained value is due to the effect of both the organic interfacial layer and R_S.[83, 84]. However, the obtained quantity is enough for photodiode and photodetector device applications. Also, the low cost of organic materials and ease of production gives a facility for commercial development.

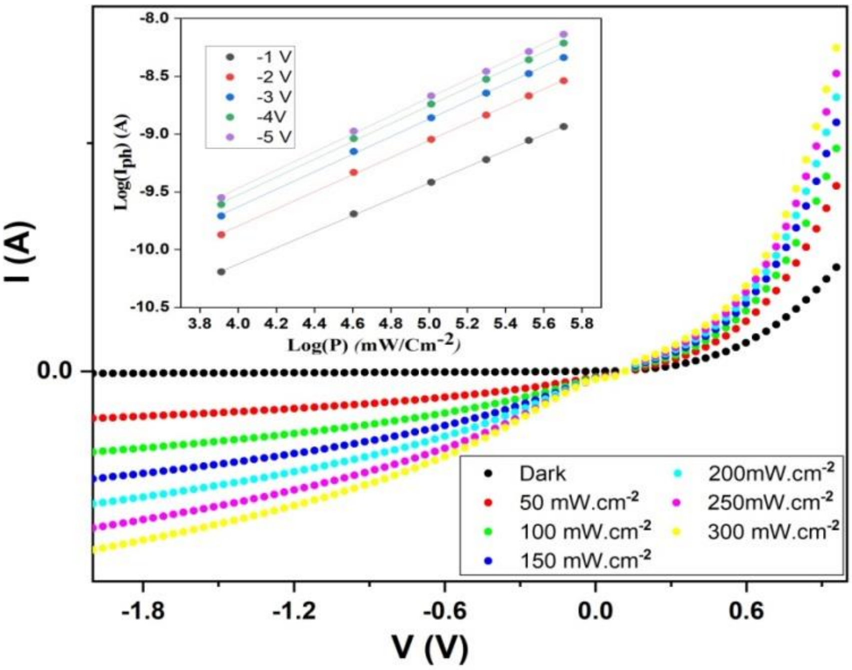

Figure 4.11. The I-V graphs under definite illumination intensities

The solar cell and photodiode conductivity or the photocurrent generated can be investigated from this relation $I_{ph}=AP^m$ [83]. Where P is the illumination intensity, I_{ph} is the photocurrent of the device, and m is an exponent that was evaluated using the graph of double-logarithmic P vs I_{ph}. (Inset in Figure 4.11). This plot exhibits an excellent linear relationship between the P and I_{ph}, which indicates that the produced structure has appropriate photovoltaic performance. Also, the evaluated m values were found as 0.701, 0.740,0.761,0.772, and 0.783 in the range of -1V to -5V (backward bias region), respectively. The obtained values are between 1 and 0.5, which means that The impurity levels control the photo-conduction mechanism, and the photoconduction process exhibits a sub-linear behavior [85, 86]. In addition, both values of photosensitivity (S_{ph}) and photo-response (R) of the produced device were obtained from the next equations.

$$S = I_{ph} / I_{dark} \tag{4.14a}$$

$$R = I_{ph} / (P.A) \tag{4,15b}$$

Where, I_{dark}, I_{ph}, P, and A are the dark current, photocurrent, illumination power, and contact area, respectively. These equations were used to obtain both of them based on the illumination intensity, as shown in Figure 4.12 (a, b). As displayed in Figure 4.12(a), the fabricated device exhibits good photosensitivity because the values of photosensitivity increase as the intensity of illumination increases. While figure 8(b) shows that the structure photoresponse decrement with increased illumination level. This decrement of responsivity may be due to the interlayer (RuO_2:PVC) and N_{SS} [87, 88].

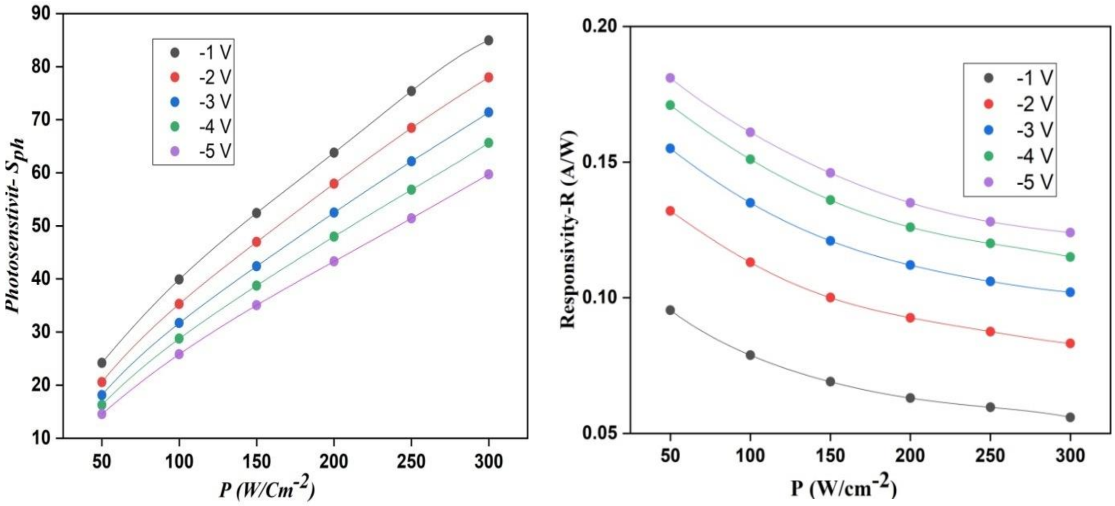

Figure 4.12. (a, b). The Sph vs. P and R vs. P graphs at various illumination.

4.5. IMPEDANCE VOLTAGE CHARACTERISTICS of *Au/(PVC:RuO2)/n-Si* DEVICES

4.5.1. Electric Characteristics of The Au/(RuO_2:PVC)/n-Si Devices

The conductance/capacitance (G/ω and C) data of the fabricated Au/(RuO_2:PVC)/n-Si were analyzed in wide voltage and frequency (±4 V, 5 kHz- 5 MHz) ranges at room temperature, with a small fixed alternating signal (*ac*) of 50 mV as shown in both Figure 4.13 and Figure 4.14. These figures show that both G/ω and C are highly dependent on frequency and voltage. Also, they exhibit three different zones (similar to MOS-type capacitors behavior) based on inversion, depletion, and accumulation regions of (0 V to - 3 V), (0 V to 1.3 V), and ($V \geq 1.29$ V), respectively. Both C and G/ω values decrease as frequency increases, and at low and moderate frequencies, the variations are clearly apparent in both depletion/accumulation regions. This behavior happens because the traps or N_{SS} can easily track the external alternating (*ac*) signal and generate an extra G/ω and C to their actual measured quantities, while at higher frequencies, their life or relaxation time (τ) has not enough time to trace the ac signal. Also, the observed high values G/ω and C at intermediate and low frequencies are due to the polymer layer (RuO_2:PVC), dipole polarization, and special distribution of N_{SS} at the contact of RuO_2:PVC /n-Si and their τ. In contrast, the discrepancies observed at the accumulation region in C and G/ω resulted from both the RuO_2:PVC layer and R_S rather than N_{SS}. Furthermore, Figure 4.13 exhibit a high value for each frequency decrease with increasing frequency in between 0.5 to 1.5 V. These behavior of peaks are because of a specific distribution of N_{SS} at the RuO_2:PVC /n-Si interface. However, the induced energy levels of N_{SS} in the depletion layer are usually caused by discontinuities at the surface of the periodic lattice structure, the impurities of organic in the vacancies, and laboratory conditions. In contrast, the R_S is mainly resulting from the nonuniformity of the doping atoms, back ohmic contact, crystal dislocations and impurities, and rectifier contacts on the interlayer (RuO_2:PVC) [89–92].

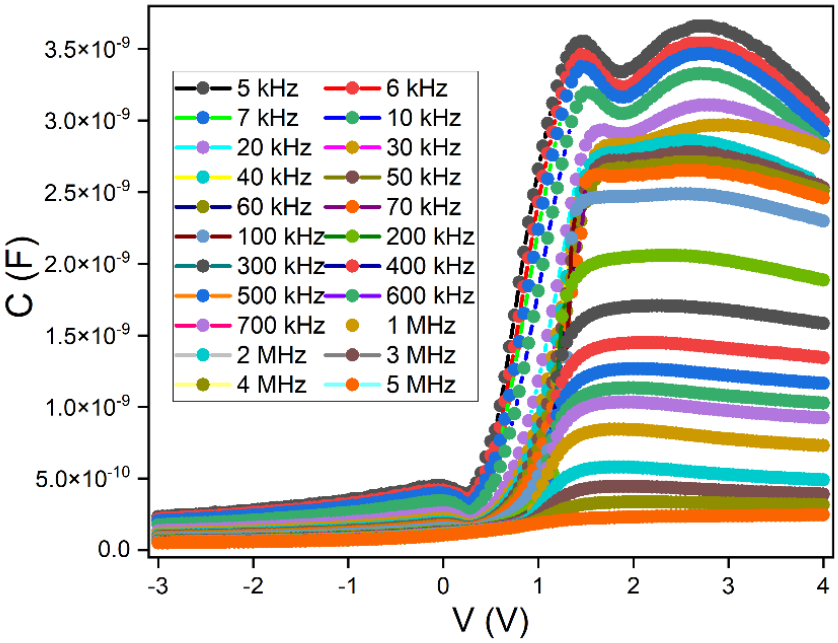

Figure 4.13. The *C–V-f* graph of the Au/ RuO_2:PVC /n-Si device

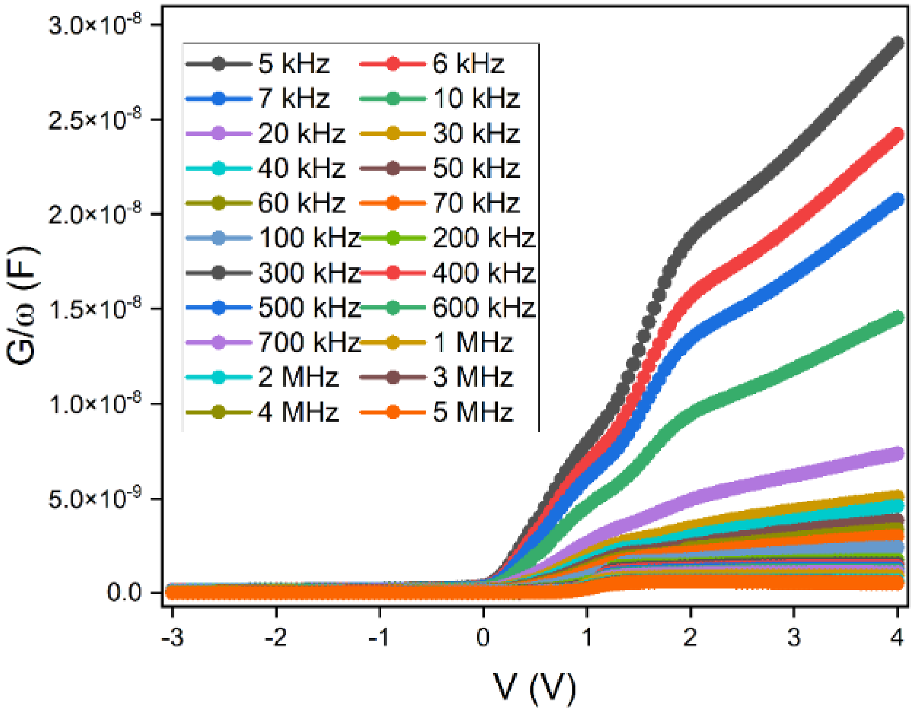

Figure 4.14. The G/ω–V-f graphs of the Au/ RuO2:PVC /n-Si device

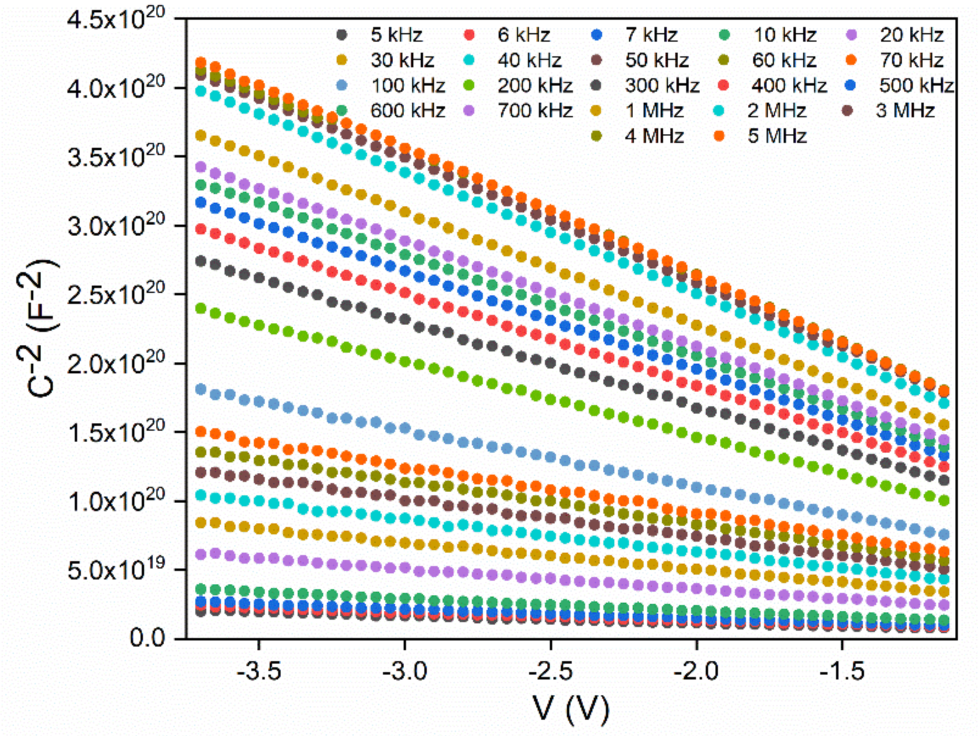

Figure 4.15. The C^{-2} vs V (reverse bias) plot of the Au/ RuO2:PVC /n-Si device

Also, the C^{-2} -V graph in the reverse voltage bias was obtained to extract the basic electrical elements of the fabricated device for each frequency, as shown in Figure 4.15. This plot displays a good linear relation between (-3.7 V to -1.2 V) in the backward voltage range. The following equation illustrates the relation of depletion region capacitance (C) to the reverse bias voltage (V_R) for the SBD structures [3, 93, 94].

$$C^{-2} = \frac{2\left(V_D - (kT/q) - V_R\right)}{q\varepsilon_S\varepsilon_0 N_D A^2} \tag{4.16}$$

Where A is the area of the rectifier-contact, ε_s is the semiconductor permittivity (ε_s = 11.8 ε_o for Si), N_D is the concentration of the donor doping atoms obtained from the slope of the C^{-2} -V plot, ε_o is the vacuum permittivity, V_D is the diffusion potential obtained from this relation $V_D = V_o + kT/q$, where V_o is an intercept-point. Thus, the author basic electric factors of the structure, such as the barrier height (Φ_B), maximum electric field (E_m), diffusion-potential (V_D), energy Fermi level (E_F), and width of depletion layer (W_D) were obtained from the next relations [90, 93, 94].

$$N_D = 2\Big/\left(q\varepsilon_S\varepsilon_O A^2 \tan\theta\right) \tag{4.17a}$$

$$E_F = \frac{kT}{q}.\ln\left(N_C/N_D\right) \quad (4.17b) \qquad E_m = \left(\frac{2qN_D V_O}{\varepsilon_S\varepsilon_0}\right)^{0.5} \quad (4.17c)$$

$$\Phi_B(C-V) = \left(V_0 + kT/q\right) + E_F = V_D + E_F \tag{4.17d}$$

$$W_D = \left(2\varepsilon_S\varepsilon_o V_D/qN_D\right)^{0.5} \tag{4.17e}$$

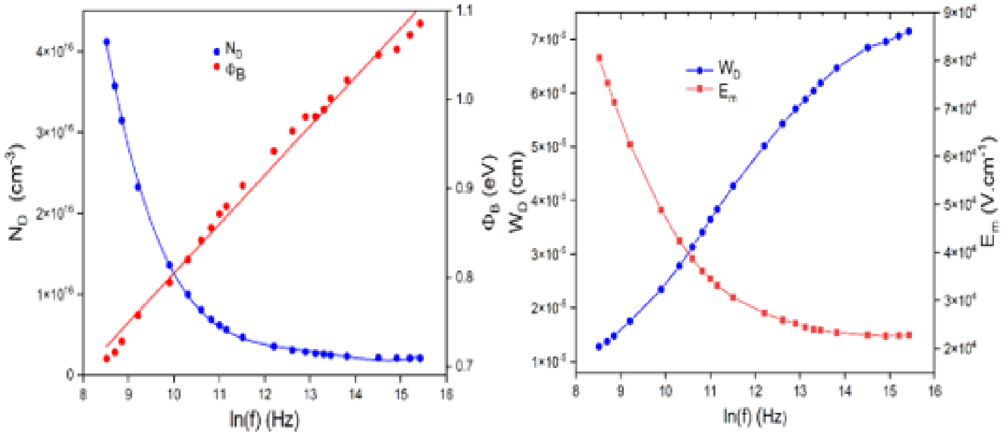

(a) **(b)**

Figure 4.16. (a) *Φ*$_B$ vs. ln(*f*), N_D vs. ln(*f*) plots, (b) *Em* vs. ln(f), W_D vs. ln(*f*) plots at diverse frequencies

Here, N_C represents the conduction band's energy state. The previously evaluated factors are displayed in Table 4.3, and the Φ_B, N_D, W_D, and E_m values were highly dependent on ln(*f*). As shown in both Table 4.3 and related figures, while the values of Φ_B, E_F, and W_D increment as frequency increases, the N_D and E_m values are almost decreasing exponentially. The increasing behavior is because of increased intercept points or diffusion potential as frequency increases. Also, these behaviors were predicted and attributed to that the N_{SS} having a distinct density distribution. The low values obtained for Φ_B (C–V) at low frequencies may be attributed to the presence of the N_{SS} in which the carrier charges can be released or stored. Usually, the *C* value at higher frequencies is mainly independent on frequency and increment as bias voltage increases, but at lower and intermediate frequencies, the value of C depends on the ability of N_{SS} to trace the ac signal. Thus, at low frequency, N_{SS} have the ability to trace the ac signal and creates extra values of C to their measured real quantity, while at high frequencies, the N_{SS} are unable to sufficiently track the *ac* signal and unable to contribute to the values of C [94, 95]. However, the obtained W_D, Φ_B, and E_F parameters were varied from 0.1278 µm, 0.708 eV, and 0.168 eV at 5kHz to 0.714 µm, 1.08 eV, and 0.246 eV at 5 M Hz. In contrast, the values of E_m and N_D are decrement from 8.06 x10^4 V/cm and 41.15x10^{15} cm^{-3} at 5 kHz to 2.28 x10^4 V/cm and 2.08x10^{15} cm^{-3} at 5 MHz.

Table 4.3 The basic evaluated parameters as a function of frequency

f (kHz)	V_D (eV)	N_D x10^{15} (cm^{-3})	E_F (eV)	Em x10^4 (V/cm)	W_D x10^{-5} (cm)	Φ_B (eV)
5	0.539	41.15	0.168	8.06	1.278	0.708
6	0.543	35.71	0.172	7.53	1.377	0.715
7	0.552	31.43	0.175	7.13	1.480	0.728
10	0.574	23.23	0.183	6.25	1.756	0.757
20	0.597	13,58	0.197	4.88	2.345	0.794
30	0.614	9.69	0.205	4.24	2.780	0.820
40	0.630	8.06	0.211	3.87	3.132	0.841
50	0.640	6.91	0.214	3.61	3.410	0.855
60	0.653	6.16	0.217	3.45	3.648	0.871
70	0.659	5.63	0.220	3.31	3.836	0.880
100	0.678	4.68	0.225	3.00	4.268	0.903
200	0.709	3.55	0.232	2.73	5.013	0.942
300	0.729	3.12	0.235	2.60	5.425	0.964
400	0.743	2.88	0.237	2.52	5.703	0.980
500	0.741	2.70	0.239	2.44	5.877	0.981
600	0.748	2.59	0.240	2.40	6.035	0.988
700	0.760	2.51	0.241	2.38	6.184	1.001
1000	0.778	2.35	0.242	2.33	6.465	1.021
2000	0.805	2.17	0.244	2.28	6.844	1.050
3000	0.811	2.12	0.245	2.26	6.956	1.056
4000	0.827	2.10	0.245	2.27	7.061	1.072
5000	0.839	2.08	0.246	2.28	7.147	1.085

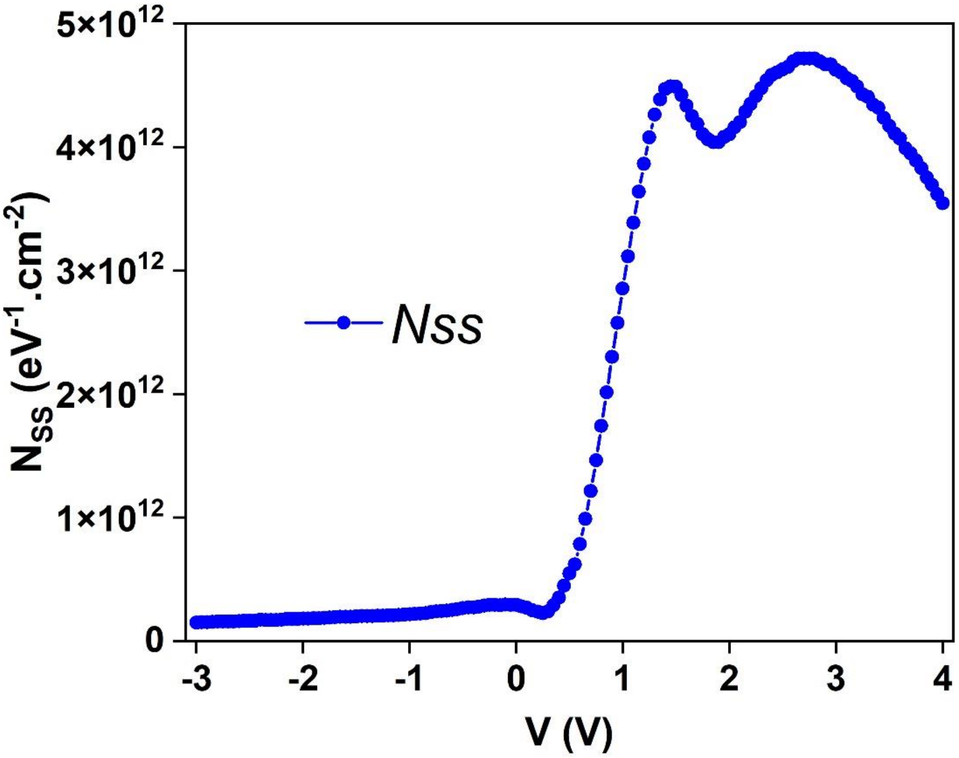

Figure 4.17. The variation of N_{SS} as a function of V.

Usually, the presence of a polymer or an insulator layer in Schottky contacts causes a considerable change in the conduction mechanism at specific voltages and frequencies. Also, the polymer interfacial layer can isolate both the semiconductor and metal but cannot prevent inter-diffusion and reaction. Therefore, the profile of N_{SS} is evaluated based on the energy or voltage from the low/high frequency capacitance method (C_{LH} – C_{HF}) at different frequencies (5 kHz to 5 MHz)[94, 96]. Therefore, the N_{SS} values were evaluated based on this technique by the following equation and illustrated in Figure 4.17.

$$qA.N_{SS} = \left(\frac{1}{C_{LF}} - \frac{1}{C_i}\right)^{-1} - \left(\frac{1}{C_{HF}} - \frac{1}{C_i}\right)^{-1} \tag{4.18}$$

Here, C_i is the interlayer capacitance, which was obtained from the values of C in the accumulation region at enough high frequency. Also, the peak behavior exhibited in this plot is caused by a specific N_{SS} distribution at the contact of the RuO_2:PVC interlayer and the semiconductor. Additionally, in both accumulation and depletion zones, there were clear distinctions between the higher and lower frequencies due to the N_{SS} and polarization at low frequency, while at high frequency is caused by the influence of R_S at the accumulation region [94, 97, 98].Thus, both values of N_{SS} and R_S significantly impact the performance of G/ω-V-f and C-V-f.

4.5.2. Dielectric Characteristics of The Au/(RuO$_2$:PVC)/n-Si Devices

The electrical and dielectric properties of the MPS devices are significantly impacted by the applied signal frequency. The relative permittivity (dielectric permittivity or electric constant) indicates the dielectric substance polarization rate caused by the external electric field and is represented as a complex relative permittivity (ε^*) in various ranges of frequency as presented in the following relation [66, 99, 100].

$$\varepsilon^* = \varepsilon' - j\varepsilon'' \tag{4.19}$$

Where the real (ε') and the imaginary (ε'') elements represent the static permittivity and the loss permittivity, respectively. Both parameter values ε' and ε'' were a function of the frequency and the alternate level of the ac signal ($E = E_0 e^{j\omega t}$). Also, the capacitance and dielectric constant represent the electric charge/energy stored in the structure [66, 89, 101]. Therefore, the values of the dielectric constant were evaluated from the measured capacitances (C_m) using the following relation.

$$\varepsilon' = C_m / C_0 = C_m . \left(d_i / A\varepsilon_0 \right) \tag{4.20}$$

Where C_0 is the capacitance of the Ideal Capacitor, ε_o is the permittivity of free space (8.85 $*10^{-14}$ F/cm), the area of MPS device is A, and d_i is the polymer thickness. In addition, the energy loss under the impact of the polarization of the dielectric substance represents by ε''. Thus, materials having lower dielectric loss are classified as good dielectric substances. The ε'' value was obtained from the measured conductance (G_m) as given in the next relation.

$$\varepsilon'' = \left(G_m / \omega \right) / C_0 = \left(G_m / \omega \right) . \left(di / A\varepsilon_0 \right) \tag{4.21}$$

The dielectric loss was also obtained in relation to the dielectric dissipation factor or dielectric tangent loss (*tan δ*), and given by the next equation.

$$\tan\delta = \varepsilon'' / \varepsilon' \tag{4.22}$$

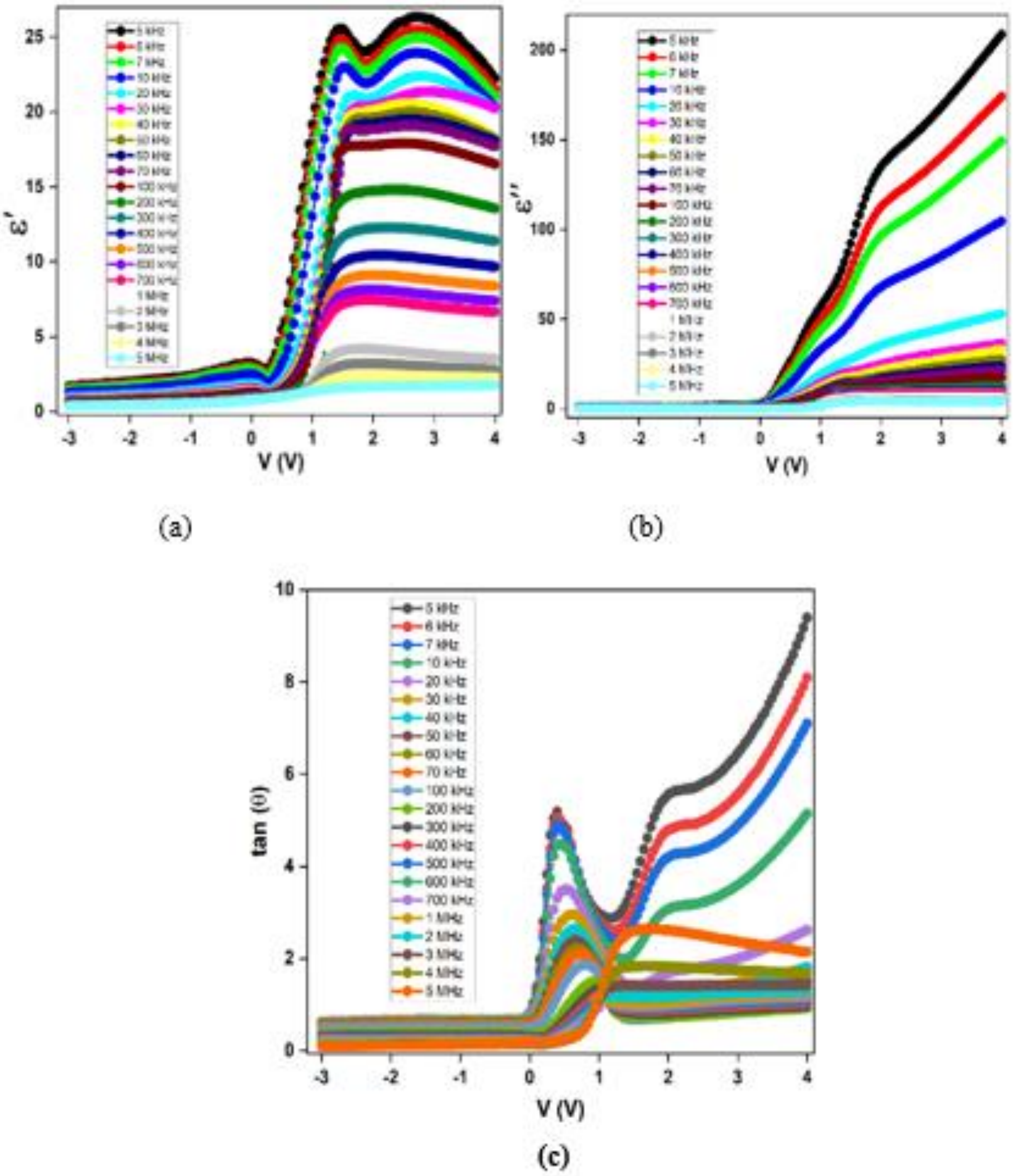

(a) (b)

(c)

Figure 4.18. (a) ε′ vs. V, (b) ε″ vs. V, and (c) tan δ vs. V plots at various frequencies

Figure 4.18 (a) displays the *ε′* variation with respect to the voltage at different frequencies. The highly changed values of *ε′* at low frequencies are due to the space charges or dipoles get sufficient time to reorient to the same external applied electric field direction. Also, the dipoles will accumulate at the *RuO*$_2$*:PVC/n-Si* contact and generate an interface polarization (Maxwell– Wagner-type polarization) and the quantity of ε' is 25 for 5 kHz, and 3 V while, at the strong accumulation zone, this quantity becomes lower than 25. However, it is clear that the evaluated value of ε' for the produced structure, even at 5 kHz for 3 V, is considerably greater than the traditional insulators. Thus, the polymer layer (RuO_2 doped PVC) can be used as an interlayer instead of many conventional insulator materials produced by traditional methods such as thermal and sputtering or wet oxidation. Moreover, as shown in Figure 4.18 (b), the ε'' values almost exhibit the same pattern as the ε' at low frequencies due to the higher movement of carriers charge existing in the interfacial layer. Also, the accumulation and movement of the carrier charges at high frequencies reduce the generated polarization, which reduces the dielectric loss. Furthermore, As displayed in Figure 4.18 (a and b), the values of ε' and ε'' increment as a positive voltage increased, while these quantities decreased as frequency increased. The high values of ε' and ε'' at low and medium frequencies are related to the space-charge polarization. The behaviors of both values of ε' and ε'' are due to the accumulated space charges or dipoles at the interface generating polarization, the barrier's inhomogeneous impacts, and the resistance of electrode contact [102–104].

The other factor that indicates the loss of energy at a specific frequency of the fabricated structure is the tangent dielectric loss ($tan\ \delta$). Figure 4.18 (c) shows the changes of $tan\ \delta$ as a function of the dc applied voltage. As can be clearly seen, at low frequencies, the plot exhibits a peak behavior that moves to the accumulation region with incremented frequency. The behavior of $tan\ \delta$ can be described by the effect of conduction-induced loss as well as interfacial polarization. Also, the peaks observed and their shifted behavior can be explained by the theory of Debye relaxation. Based on this method, higher losses are observed at low frequencies due to electrons hoping with the impact of the ac applied field. Also, the maximum loss observes if ω equals τ^{-1}, whereas, at high frequencies, the capacity of dipoles to change their orientation reduces under the effect of the applied field.

The device's ability to store electric energy is represented by ac electrical conductivity (σ_{ac}), which depends on the semiconductor doping density, bandgap, interfacial layer homogeneity, frequency, temperature, and illumination. The σ_{ac} is a function of both ε'' and frequency. Thus, σ_{ac} was obtained in terms of frequency and ε'' [66, 105].

$$\sigma_{ac} = \omega C.\tan\delta.(d_i / A) = \varepsilon_0 \varepsilon'' \omega \tag{4.23}$$

Figure 4.19 shows the deviation of σ_{ac} at various frequencies as a function of voltage. The larger values of σ_{ac} at high frequencies indicate that the space charges at higher frequencies are probably released. Also, this behavior may be related to a decreased R_S with increased frequency. Which is described via the conduction hopping mechanism or mobile charge carriers [106]. In addition, σ_{ac} is almost independent of the frequency in lower frequencies (5 to 70 kHz). But, at high frequencies (f >70 kHz) is nearly frequency dependent with an increasing behavior due to the R_S effect.

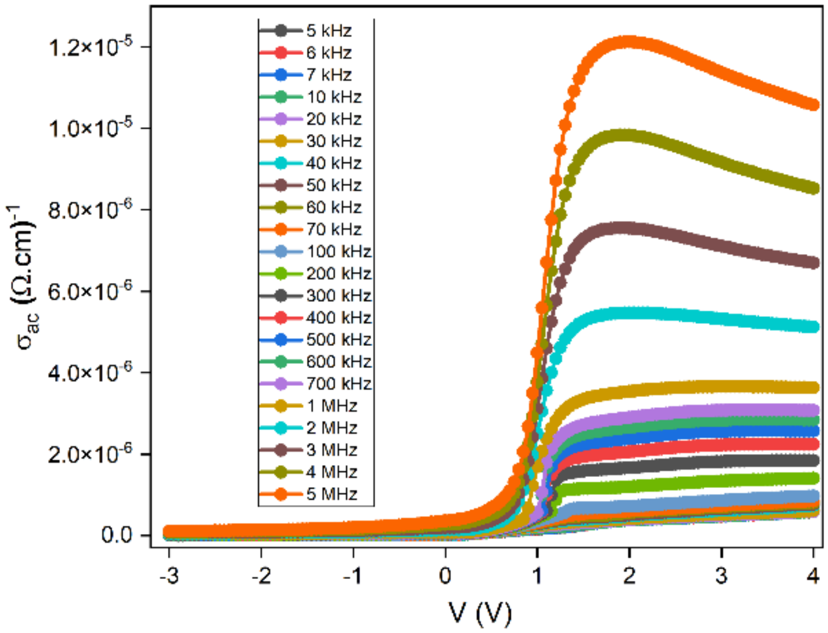

Figure 4.19. The σ_{ac} -V of the structure at various frequencies.

Furthermore, the complex electric modulus (M^*) was extracted to investigate the device's electrical properties, which gives additional details on the conduction phenomena and charge transport process. The M^* physically is used to investigate the dielectric relaxation mechanism and evaluate the relaxation of the electric field in a dielectric material. The values of M^* are obtained from the following equation.

$$M^*(\omega) = M' + jM'' = 1/\varepsilon' = \frac{\varepsilon'}{\varepsilon'^2 + \varepsilon''^2} + j\frac{\varepsilon''}{\varepsilon'^2 + \varepsilon''^2} \tag{4.24}$$

Where both real and imaginary parts of the M^* are M' and M''. As shown in Figure 4.20 (a, b), M' and M'' values are nearly zero at low frequencies due to a decrease in surface and dipole polarization. Also, these values exhibit an incrementing behavior in the depletion and inversion zones with the increased frequency, while it was almost independent of frequency in the accumulation zone. Also, the plot of M'' should exhibit a peak behavior for the process of dielectric relaxation because of a spatial distribution of N_{SS}. which occurs at a maximum dielectric loss ($\omega\tau = 1$)[102–104].

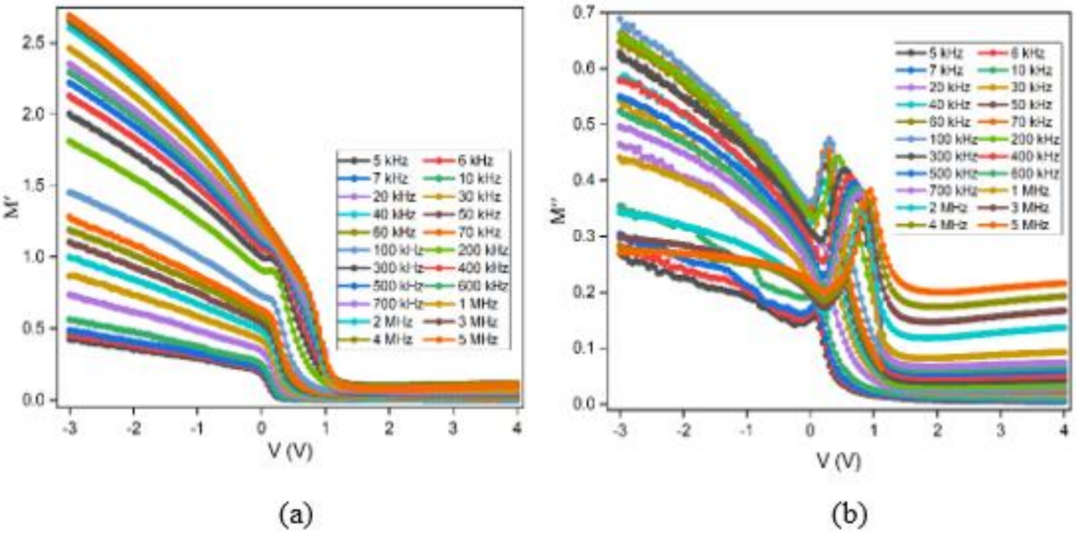

Figure 4.20. (a) M' -V and (b) M'' -V graphs at different frequencies

Also, the structure's dielectric performance can be analyzed from the complex impedance spectroscopy (Z^*) and obtained using the following relation [106, 107].

$$Z^* = Z' - jZ'' = \frac{1}{j\omega C_0\varepsilon^*} = \frac{\varepsilon''}{\omega C_0[\varepsilon'^2 + \varepsilon''^2]} - j\frac{\varepsilon'}{\omega C_0[\varepsilon'^2 + \varepsilon''^2]} \tag{4.25}$$

where Z' and Z'' are the real and imaginary parts. Figure 4.21 (a and b) displays the variation of Z' and Z'' with the applied voltage at various frequencies. As illustrated in these plots, the Z' and Z'' values decrease as frequency and positive voltage increase because of an increment in electron hopping as frequency increases. Additionally, their quantities are almost fixed after a certain high frequency. Figure 4.21 (a) exhibits higher values in the range of 0 to 0.5 V due to the effects of fixed charges and N_{SS}.

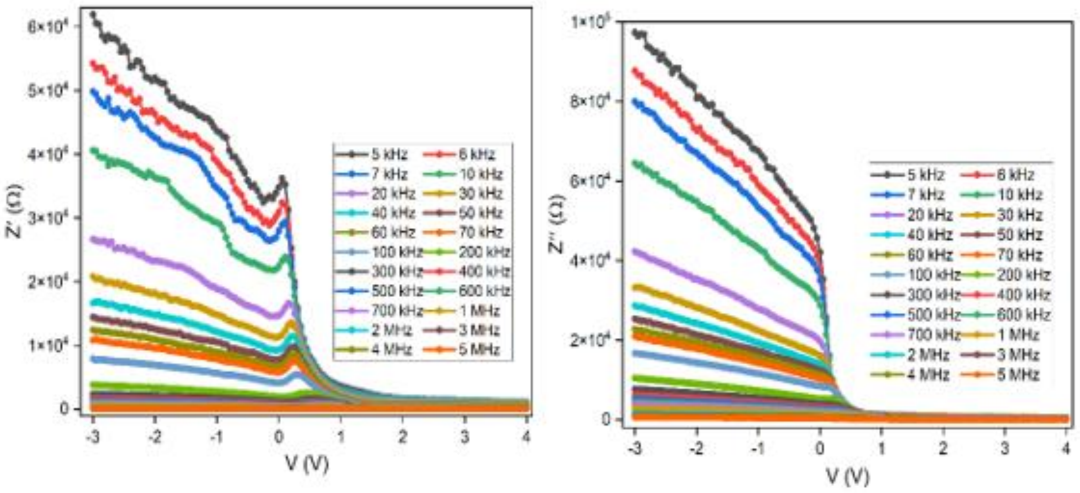

(a) (b)

Figure 4.21. (a) Z' -V and (b) Z'' -V characteristics at different frequencies.

PART 5

CONCLUSION AND RECOMMENDATIONS

5.1.CONCLUSION

In this thesis, firstly, both RuO_2 and RuO_2:PVC nanocrystals were obtained and the effects on their behaviours were investigated. For this purpose, *X*-ray diffraction (XRD), UV-Visible region, and scanning electron microscopy (SEM) were performed. Then the interfacial polymer layer RuO_2:PVC was grown between the metal and semiconductor contact. The SEM images showed that all produced RuO_2:PVC particles were at the nanoscale. The surface morphology variations are attributed to chemical bonding through the interface, the existence of residual oxides, and lattice mismatch. In addition, the XRD results showed that the prepared structures have a nanocrystalline structure.

Insulator materials such as traditional SiO_2, SnO_2, and Si_3N_4 with low dielectric permittivity are used between metal and semiconductors. However, it is seen that these materials have low performance in terms of both diode, photodiode, and capacitor devices. Therefore, in recent years, materials with high dielectric constants or metal-doped polymer materials have been used to optimize the performance of these devices. In this study, Au/(RuO_2:PVC)/n-Si MPS structures are prepared, and their photo response, electrical and dielectric behaviors have been investigated. The RuO_2:PVC interfacial polymer layer, which is grown using the spin-coating technique, separates the semiconductor and metal materials from each other and regulates the charge transitions between them.

The *I-V* measurements in the dark and with definite illumination intensities of the obtained Au/(RuO_2:PVC)/n-Si MPS devices were studied. All measurements were carried out at room temperature. It has been observed that the semilogarithmic *I-V-P* curves of MPS structures obtained at room temperature have a good rectification ratio ($RR=I_F/I_R$) and a linear region at lower bias forward voltages. Also, the observed bending occurs at high forwards bias due to the impact of the series resistance (R_S). The main electronic parameter values of the n, I_o, and Φ_{B0} were calculated from the linear portion of the ln(I)-V curves. Experimental results showed a good linear relationship between Φ_{B0} and n values. Therefore, in the ideal case (n =1), the mean barrier height ($\bar{\Phi}_{B0}$) was found to be 0.92 eV. Additionally, the structure resistance (R_i) values were calculated using Ohm's law. It is clearly seen that R_i values approach the minimum values corresponding to R_S at high forward voltage while reaching maximum values corresponding to R_{Sh} at reverse voltage. Also, n, R_S, and Φ_B values were obtained from both $dV/d(lnI)$-I and $H(I)$-I plots (Cheung functions) of the Au/(RuO_2:PVC)/n-Si MPS structures and their plots were linear. The values of n, BH, and R_S extracted from the ln(I)-V characteristics were different from those obtained with the help of Cheung functions. This is because the values were calculated from two different methods and different voltage regions. Also, Norde functions were used as another method to obtain the R_S and Φ_B values of the structures. It shows that Φ_B values obtained by Cheung functions are higher than those obtained from TE theory/Ohm's law and Norde functions. These differences of Φ_B depend on the applied supply voltage and the nature of the calculation method. However, the *TE* theory, Norde's, and Cheung's methods, display that both values of the R_S and Φ_{B0} decrease as the illumination level and I_o values increase. The higher values observed for n were due to the presence of the interfacial layer RuO_2:PVC, N_{SS}, generation-recombination processes, and barrier inhomogeneity. The energy distribution profile for N_{SS} as a function of (E_C-E_{SS}) also was obtained using the voltage-dependent of BH and $n(V)$ at various illumination intensities. The N_{SS} quantities exponentially increased from the middle of the forbidden band gap to the bottom of the conduction band, and their average value obtained at about (E_C-0.50) eV is nearly at $5\text{x}10^{13}$ $eV^{-1}cm^{-2}$. In addition, the photovoltaic parameters were evaluated, such as the V_{OC}, I_{SC}, FF, and η values. These parameters were found to be 0.118 V, $6.4*10^{-6}$A, 46%, and 0.088 % for 50 mW/cm^2. The evaluated results confirm that the (RuO_2:PVC) interfacial layer with MS structure exhibits a photoconductive behavior and can be used as photodetectors, photodiodes, and solar cells in optoelectronic applications.

Furthermore, the characteristics of both capacitance and conductance (C, G/ω) of the structures were studied at room temperature in wide ranges of voltages and frequencies (±4V, 5 kHz-5MHz). It has been observed that the C and G/ω properties are affected by the changes in frequency and voltage. In typical applications, the value of C and G/ω increases as frequency decreases due to a specific density distribution of the interface states (N_{SS}) or traps between the interface layer and the semiconductor's surface, dipole polarization or polarization processes, and R_S of the structure. Also, the main electrophysical elements Φ_B, N_D, E_m, W_D, V_D, and E_F were evaluated using the interception and slope of the backward bias C^{-2} -V characteristics. The N_D and E_m values are exponentially decreasing, while the Φ_B, E_F, and W_D values are increased with frequency. The density distribution profile of the N_{SS} as a function of voltage was also derived using the low-high frequency capacitance technique (C_{LF}-C_{HF}). The maximum capacitance of MIS/MPS structures in the strong accumulation zone is observed, corresponding to the capacitance of the polymer layer (RuO_2:PVC). The energy distribution profile values of the N_{SS} obtained from both the I-V data and the C_{LF}-C_{HF} methods were found to be in the order of 10^{13} and10^{12} eV^{-1}/cm^2.

In addition, the basic dielectric parameters such as real and imaginary elements of the dielectric constant (ε^*), ac electrical conductivity (σ_{ac}), tangent-loss ($\tan\delta$), complex impedance (Z^*), and complex electric-modulus (M^*) were analyzed. The high quantities observed of ε', ε'' or C, G/ω at lower frequencies and peaks of both ($\tan\delta$)-V and M'' -V graphs were attributed to N_{SS} and polarization process. It was seen that ε', ε'' and $\tan\delta$ values were highly dependent on the voltages applied and frequencies. The influence of the dipoles at the interface on the dielectric performance is very important. In general, there are four types of polarization mechanism which are known as, electronic, ionic, interfacial, and dipole polarizations. Among them electronic polarization can occur at higher frequencies ($f > 10^{15}$Hz). Ionic polarization occurs in the range of 10^{10} to 10^{13} Hz. While dipolar polarization occurs in the mid or high-frequency between 1 kHz–1 MHz because of longer relaxation times. This polarization mechanism has been explained to arise from permanently oriented dipoles, impurities, surface charges, or dislocation. Interface polarization can occur when mobile charge carriers are blocked by a physical barrier and are particularly effective at low frequencies ($f \leq 1$ kHz). Since measurements of the structure took place at frequencies between 5 and 500 kHz, dipolar and interfacial polarizations are likely to predominate in dielectric calculations.

As clearly seen in the ac conductivity (σ_{ac}) curve, the conductivity values were small at the applied reverse voltages, but it increased rapidly in the forward applied voltage. Also, it is increasing behavior with frequency is accompanied by an increase in localized electric current, due to a gradual decrease in series resistance. Furthermore, the real and imaginary component of the electrical module M^* are calculated using the ε' and ε'' values. these values exhibit an incrementing behavior in the depletion and inversion zones with the increased frequency. Also, the plot of M'' have a peak behavior because of a spatial distribution of N_{SS}. In conclusion, it was successfully improved the optical absorption and photoelectrical properties of thin PVC films by adding RuO_2 and the produced Au/(RuO_2:PVC)/n-Si device exhibits a MOS-type behavior. As a result, the fabricated Au/(RuO_2:PVC)/n-Si can be used as a photodiode on account of low- weight/cost and simple production and as a capacitor instead of the typically used oxide/ insulator MOS capacitors.

5.2. RECOMMENDATIONS

It seems that the prepared Au/(RuO_2:PVC)/n-Si MPS structures have good diode properties. However, the series resistors obtained for these structures are slightly high and affect the diode performance negatively. Therefore, in order to minimize the series resistance effect on the structures, more attention should be made to the complete protection of the structures from impurities during the production stage and the good annealing of the ohmic contacts. It is believed that the used of higher dielectric substance between the metal and the semiconductor can reduce the R_S, N_{SS}, leakage current and increase the R_{Sh}, BH, and RR, which positively affects the diode performance.

Some MIS/MPS structured diodes can also feature a solar cell. Especially Si crystals which have a 1,12 eV band gap at room temperature that can benefit from a visible part of the sunlight spectrum. Growing a very thin (~5 nm) interfacial layer on Si using different growth methods can show good solar cell performance.

Different composite materials with high dielectric constants can be used for the prepared Au/(RuO_2:PVC)/n-Si structures to improve the photodiode performance and reach higher capacitance values. In addition, the growth of RuO_2:PVC interfacial layers with different thin-film growth techniques (eg electro-spinning, immersion methods) can positively affect the diode properties or capacitance values of the structures. Thus, the electrical and dielectric performances of the structures can be compared with each other by growing on the same interfacial layer with different techniques. In order to increase the capacitance, it is a correct approach to increase the dielectric constant of the interfacial layer and decrease its thickness.

The measurements in this study were carried out only using the I-V characteristics under various illumination levels and the impedance spectroscopy method, including capacitance/conductance (C-V-f and G/ω-V-f) data at room temperature in dark which cannot give enough information on the conduction mechanism and the nature of BH at M/S interface. Therefore, performing the measurements at various temperatures in a wide frequency range can provide us a more information about the current-conducting mechanism and dielectric properties of the structure.

REFERENCES

1. Streetman, Ben G., and Sanjay Banerjee., “Solid State Electronic Devices.”, ***Prentice Hall,*** New Jersey, (2000).

2. Kittel, C.” Introduction to Solid State Physics”, ***John Wiley & Sons***, Hoboken, NJ, (2005).

3. Sze, S.M. and K.K.N. “Physics of Semiconductor Devices (Third edition).”, ***John Wiley and Sons*** , Canada, (2007).

4. Shah, Mutabar, M. H. Sayyad, and Kh S. Karimov., "Electrical characterization of the organic semiconductor Ag/CuPc/Au Schottky diode.", ***Journal of Semiconductors***, 3(4): 044001 (2011).

5. Zhou, Yi, Changhong Liu, and Shoushan Fan. "Schottky contact of an artificial polymer semiconductor composed of poly (dimethylsiloxane) and multiwall carbon nanotubes." ,***Journal of Materials Chemistry***, *A* 3(38) : 19539-19544 (2015).

6. Reddy, V. Rajagopal. "Electrical properties of Au/polyvinylidene fluoride/n-InP Schottky diode with polymer interlayer.”, ***Thin Solid Films***, 556: 300-306 (2014).

7. Reddy, PR Sekhar, et al. "Modification of Schottky barrier properties of Ti/p-type InP Schottky diode by polyaniline (PANI) organic interlayer." ,***Journal of semiconductor technology and science***, 16(5) : 664-674 (2016).

8. Tozlu, Cem, and Adem Mutlu., "Poly (melamine-co-formaldehyde) methylated effect on the interface states of metal/polymer/p-Si Schottky barrier diode.", ***Synthetic Metals***, 211: 99-106 (2016).

9. Tataroğlu, A. D. E. M., et al., "Single crystal ruthenium (II) complex dye based photodiode." ,***Dyes and Pigments*** ,132: 64-71 (2016).

10. Siva Pratap Reddy, M., et al. "Modified electrical properties and transport mechanism of Ti/p-InP Schottky structure with a polyvinylpyrrolidone (PVP) polymer interlayer. ," ***Journal of Materials Science: Materials in Electronics***, 28: 4847-4855 (2017).

11. Ulusoy, M. U. R. A. T., et al. ,"The electrical characteristic of an MIS structure with biocompatible minerals doped (Brushite+ Monetite: PVC) interface layer.", ***Microelectronic Engineering***, 258: 111768 (2022).

12. Uma, T., T. Mahalingam, and U. Stimming., "Solid polymer electrolytes based on poly (vinylchloride)–lithium sulfate." ,***Materials Chemistry and Physics***, 90.(2-3): 239-244 (2005).

13. Yu, Jie, et al., "Thermal degradation of PVC: A review." ,***Waste management***, 48: 300-314 (2016).

14. Starns, W. H., and D. Edelson., "Mechanistic aspects of the behavior of molybdenum (VI) oxide as a fire-retardant additive for poly (vinyl chloride). An interpretive review.", ***Macromolecules***, 12(5): 797-802 (1979).

15. Iván, Béla. "Thermal stability, degradation, and stabilization mechanisms of poly (vinyl chloride).", 19-32 (1996).

16. Braun, Dietrich. "PVC—origin, growth, and future.", ***Journal of Vinyl and Additive Technology***, 7(4): 168-176 (2001).

17. Meyer, Jens, et al. "Charge generation layers comprising transition metal-oxide/organic interfaces: Electronic structure and charge generation mechanism.", ***Applied Physics Letters***, 96(19) (2010).

18. Meyer, Jens, et al. "Transition metal oxides for organic electronics: energetics, device physics and applications.", ***Advanced materials***, 24(40) : 5408-5427 (2012).

19. Batzill, Matthias. "Fundamental aspects of surface engineering of transition metal oxide photocatalysts.", ***Energy & Environmental Science***, 4(9) :3275-3286 (2011).

20. Marschall, Roland, and Lianzhou Wang. "Non-metal doping of transition metal oxides for visible-light photocatalysis." ,***Catalysis Today***, 225: 111-135 (2014).

21. Haque, Farjana, et al. "Two-dimensional transition metal oxide and chalcogenide-based photocatalysts." ,***Nano-micro letters***, 10(2) : 1-27 (2018).

22. De Almeida, J. S., and R. Ahuja. "Electronic and optical properties of Ru O 2 and Ir O 2." ,***Physical Review B***, 7(16) : 165102 (2006).

23. Devadas, Abirami, et al. "Tailoring of RuO2 nanoparticles by microwave assisted "Instant method" for energy storage applications.", ***Journal of Power Sources***, 196(8):4044-4053 (2011).

24. Dai, Baoying, et al. "Piezo-phototronic effect on photocatalysis, solar cells, photodetectors and light-emitting diodes.", ***Chemical Society Reviews***, 50(24): 13646-13691 (2021).

25. Mehtougui, N., et al. "Structural, electronic and mechanical properties of RuO2 from first-principles calculations.", ***Materials science in semiconductor processing***, 15(4) : 331-339 (2012).

26. Zhang, Rumin, et al. "Thermionic emission theory and diffusion theory applied to CdTe PV devices.", ***Journal of Semiconductors***, 36(1) : 012002 (2015).

27. Sharma, B.L., “Metal-Semiconductor Schottky Barrier Junctions and Their Applications (First edition).”, ***Plenum Press***, New York and London, (1984).

28. Cowley, A. M., and S. M. Sze. "Surface states and barrier height of metal-semiconductor systems.", ***Journal of Applied Physics***, 36(10): 3212-3220 (1965).

29. Card, H. C., and E. H. Rhoderick. "Studies of tunnel MOS diodes I. Interface effects in silicon Schottky diodes.", ***Journal of Physics D: Applied Physics***, 4(10): 1589 (1971).

30. Altındal, Ş., et al. "The role of interface states and series resistance on the I–V and C–V characteristics in Al/SnO2/p-Si Schottky diodes.", ***Solid-State Electronics,*** 47(10): 1847-1854 (2003).

31. Campbell, Ian H., et al. "Controlling Schottky energy barriers in organic electronic devices using self-assembled monolayers.", ***Physical Review B***, 54(20): R14321 (1996).

32. Yakuphanoglu, F., M. Kandaz, and B. F. Senkal. "Current–voltage and capacitance–voltage characteristics of Al/p-type silicon/organic semiconductor based on phthalocyanine rectifier contact.", ***Thin Solid Films***, 516(23): 8793-8796 (2008).

33. Vural, Ö., et al. "Current–voltage characteristics of Al/Rhodamine-101/n-GaAs structures in the wide temperature range.", ***Current Applied Physics***, 10(3): 761-765n (2010).

34. Kanbur, H. A. T. İ. C. E., et al. "Effects of illumination on IV, CV and G/wV characteristics of Au/n-CdTe Schottky barrier diodes.", ***Journal of Optoelectronics and Advanced Materials***, 13(5): 713 (2011).

35. Çetinkaya, H. G., et al. "Photovoltaic characteristics of Au/PVA (Bi-doped)/n-Si Schottky barrier diodes (SBDs) at various temperatures.", ***Current Applied Physics***, 13(6): 1150-1156 (2013).

36. Demirezen, S., Ş. Altındal, and I. Uslu. "Two diodes model and illumination effect on the forward and reverse bias I–V and C–V characteristics of Au/PVA (Bi-doped)/n-Si photodiode at room temperature.", ***Current Applied Physics***, 13(1): 53-59 (2013).

37. Soylu, Murat, et al. "Photoelectrical characterization of a new generation diode having GaFeO3 interlayer.", ***Solar Energy Materials and Solar Cells***, 124: 180-185 (2014).

38. Mekki, A., et al. "Graphene controlled organic photodetectors.", ***Synthetic Metals***, 217: 43-56 (2016).

39. Ersöz, Gülçin, et al. "Investigation of photo-induced effect on electrical properties of Au/PPy/n-Si (MPS) type schottky barrier diodes.", ***Journal of Materials Science: Materials in Electronics***, 28: 6413-6420 (2017).

40. Lapa, Havva Elif, et al. "Effect of illumination on electrical parameters of Au/(P3DMTFT)/n-GaAs Schottky barrier diodes.", ***Indian Journal of Physics***, 94: 1901-1908 (2020).

41. Alptekin, Sebahaddin, and Şemsettin Altındal. "Electrical characteristics of Au/PVP/n-Si structures using admittance measurements between 1 and 500 kHz.", ***Journal of Materials Science: Materials in Electronics***, 31: 13337-13343 (2020).

42. Tataroğlu, A., Ş. Altındal, and Y. A. S. H. A. R. Azizian-Kalandaragh. "CVf and G/ω-Vf characteristics of Au/(In2O3-PVP)/n-Si (MPS) structure.", ***Physica B: Condensed Matter***, 582: 411996 (2020).

43. Tezcan, Ali Osman, et al. "Investigation of electrical and photovoltaic properties of Au/n-Si Schottky diode with BOD-Z-EN interlayer.", ***Journal of Materials Science: Materials in Electronics***, 32: 12513-12520 (2021).

44. Ongun, Onur, et al. "Fabrication, illumination dependent electrical and photovoltaic properties of Au/BOD-Pyr/n-Si/In schottky diode.", ***Journal of Materials Science: Materials in Electronics***, 32(12): 15707-15717 (2021).

45. Altındal, Şemsettin, et al. "The illumination effects on the current conduction mechanisms of the Au/(Er2O3: PVC)/n-Si (MPS) Schottky diodes.", ***Journal of Applied Polymer Science***, 139(27) : e52497 (2022).

46. Elamen, Hasan, et al. "The photoresponse behavior of a Schottky structure with a transition metal oxide-doped organic polymer (RuO2: PVC) interface.", ***Polymer Bulletin***, : 1-20 (2023).

47. Altındal, Şemsettin, et al. "The illumination effects on the current conduction mechanisms of the Au/(Er2O3: PVC)/n-Si (MPS) Schottky diodes.", ***Journal of Applied Polymer Science***, 139(27) :e52497 (2022).

48. Mekki, A., et al. "Graphene controlled organic photodetectors." ,***Synthetic Metals***, 217: 43-56 (2016).

49. Soylu, Murat, et al. "Photoelectrical characterization of a new generation diode having GaFeO3 interlayer.", ***Solar Energy Materials and Solar Cells***, 124: 180-185 (2014).

50. Demirezen, S., et al. "Synthesis, electrical and photo-sensing characteristics of the Al/(PCBM/NiO: ZnO)/p-Si nanocomposite structures.", ***Sensors and Actuators A: Physical***, 317: 112449 (2021).

51. Ashcroft, N.W. and M.N.D." Solid State Physics (Second edition).", ***Cengage Learning***, Boston(1976).

52. Tang, Ching W., and Steven A. VanSlyke. "Organic electroluminescent diodes.", ***Applied physics letters***, 51(12): 913-915 (1987).

53. Guo, Chang. "Synthesis and Performance Characterization of Polymer Semiconductors for Organic Thin Film Transistors." (2015).

54. Koehler, M. and Hümmelgen, I., "A scanning tunneling microscope with subangstrom resolution,", ***Applied Physics Letters***, 70(25):3254-3256, (1979).

55. Gilliot, Mickaël, Aomar Hadjadj, and Jérôme Martin. "Investigation of the correlation between dielectric function, thickness and morphology of nano-granular ZnO very thin films.", ***Thin Solid Films***, 597: 65-69 (2015).

56. Taşçıoğlu, İlke, et al. "Analysis of the forward and reverse bias IV characteristics on Au/PVA: Zn/n-Si Schottky barrier diodes in the wide temperature range.", ***Journal of Applied Physics***, 109(5) (2011).

57. Nicollian, E. H. and Brews, J. R., "MOS (metal oxide semiconductor) physics and technology," ,***Wiley***, IEEE Press, 2002.

58. Chiang, Chwan K., et al. "Electrical conductivity in doped polyacetylene.", ***Physical review letters***, 39(17): 1098 (1977).

59. Yun, Minseong. "*Fabrication and characterization of polymer based metal-oxide-semiconductor and non-volatile memory devices*.", ***University of Missouri***, Columbia, (2009).

60. Özden, Şadan, Cem Tozlu, and Osman Pakma. "Temperature dependent electrical transport in Al/Poly (4-vinyl phenol)/p-GaAs metal-oxide-semiconductor by sol-gel spin coating method.", ***International Journal of Photoenergy***, 2016 (2016).

61. Rhoderick, E. H., "Metal-semiconductor contacts," , ***Solid State and Electron Devices***, 129(1):1-14 (1982).

62. Yosef BADALI., "Farkli X Materyaller Kullanilarak Au/(Bi2O3-x:PVA)/4HSiC Yapilarin Hazirlanmasi Ve Elektriksel Ve Dielektrik Özelliklerin Incelenmesi", Doktora Tezi, ***Gazi University Ileri Teknolojiler Anabilim Dali***, (2019).

63. Reichman, J. "The current-voltage characteristics of semiconductor-electrolyte junction photovoltaic cells.", ***Applied Physics Letters***, 36(7): 574-577 (1980).

64. McVay, Elaine, et al. "Impact of Al2O3 passivation on the photovoltaic performance of vertical WSe2 Schottky junction solar cells.", ***ACS Applied Materials & Interfaces***, 12(52): 57987-57995 (2020).

65. Nicollian, E.H., and Brews, J.R., "MOS (Metal Oxide Semiconductor) Physics and Technology," ,***John Wiley & Sons, Inc***., (2002).

66. Bunget, I. and P.M., "Physics of Solid Dielectrics,", ***Elsevier***, Amsterdam, (1984).

67. Bunget, I., and Popescu, M., "Physics of Solid Dielectrics (Materials Science Monographs)," ,***Martinus Nijhoff*** ,(1984).

68. Liu, Hongbo, and Brahim Dkhil. "Effect of resistivity ratio on energy storage and dielectric relaxation properties of 0–3 dielectric composites.", ***Journal of materials science***, 52: 6074-6080 (2017).

69. Rani, Neha, et al. "X-ray analysis of MgO nanoparticles by modified Scherer's Williamson-Hall and size-strain method.", ***Materials Today***, 12: 543-548 (2019).

70. Demirezen, Selçuk. "The role of interface traps, series resistance and (Ni-doped PVA) interlayer effects on electrical characteristics in Al/p-Si (MS) structures.", ***Journal of Materials Science: Materials in Electronics***, 30: 19854-19861 (2019).

71. Nawar, Ahmed M., et al. "Analyzed electrical performance and induced interface passivation of fabricated Al/NTCDA/p-Si MIS–Schottky heterojunction.", ***Applied Physics A***, 126: 1-18 (2020).

72. Zhou, Qin, et al. "Barrier inhomogeneity of Schottky diode on nonpolar AlN grown by physical vapor transport.", ***IEEE Journal of the Electron Devices Society***, 7: 662-667 (2019).

73. Buyukbas Ulusan, A., and A. Tataroglu. "Analysis of barrier inhomogeneities in AuGe/n-Ge Schottky diode.", ***Indian Journal of Physics***, 92: 1397-1402 (2018).

74. Tataroğlu, A., Ş. Altındal, and Y. A. S. H. A. R. Azizian-Kalandaragh. "Electrical and photoresponse properties of CoSO 4-PVP interlayer based MPS diodes.", ***Journal of Materials Science: Materials in Electronics***, 31: 11665-11672 (2020).

75. Cheung, S. K., and N. W. Cheung. "Extraction of Schottky diode parameters from forward current-voltage characteristics.", ***Applied physics letters***, 49(2) : 85-87 (1986).

76. Norde, Herman. "A modified forward I-V plot for Schottky diodes with high series resistance.", ***Journal of applied physics***, 50(7) : 5052-5053 (1979).

77. Bohlin, K. E. "Generalized Norde plot including determination of the ideality factor.", ***Journal of Applied Physics***, 60(3) : 1223-1224 (1986).

78. Tecimer, Habibe Uslu, et al. "Integration of Zn-doped organic polymer nanocomposites between metal semiconductor structure to reveal the electrical qualifications of the diodes.", ***Polymer Bulletin***, 75: 4257-4271 (2018).

79. Sharma, Mamta, and S. K. Tripathi. "Analysis of interface states and series resistance for Al/PVA: n-CdS nanocomposite metal–semiconductor and metal–insulator–semiconductor diode structures.", ***Applied Physics A***, 113: 491-499 (2013).

80. Card, H. C., and E. H. Rhoderick. "Studies of tunnel MOS diodes I. Interface effects in silicon Schottky diodes.", ***Journal of Physics D: Applied Physics***, 4(10): 1589 (1971).

81. Werner, Jürgen H., and Herbert H. Güttler. "Barrier inhomogeneities at Schottky contacts.", ***Journal of applied physics***, 69(3): 1522-1533 (1991).

82. Demirezen, Selçuk, and Seçkin Altındal Yerişkin. "A detailed comparative study on electrical and photovoltaic characteristics of Al/p-Si photodiodes with coumarin-doped PVA interfacial layer: the effect of doping concentration.", ***Polymer Bulletin***, 77(1) : 49-71 (2020).

83. Gupta, R. K., and F. Yakuphanoglu. "Photoconductive Schottky diode based on Al/p-Si/SnS2/Ag for optical sensor applications.", ***Solar Energy***, 86(5): 1539-1545 (2012).

84. Mc McGlynn, S. P. "Concepts in Photoconductivity and Allied Problems.", ***Journal of the American Chemical Society***, 86(24): 5707-5707 (1964).

85. Yakuphanoglu, Fahrettin, and W. Aslam Farooq. "Photoresponse and electrical characterization of photodiode based nanofibers ZnO and Si.", ***Materials science in semiconductor processing***, 14(4): 207-211 (2011).

86. Grimmeiss, H. G. "Photoelectronic properties of semiconductors. " ,***By Richard H. Bube***, Cambridge University Press, Cambridge 1992.

87. Kaya, Fikriye Şeyma, et al. "Effect of illumination on the electrical characteristics of Au/n-GaP/Al and Au/Chlorophyll-a/n-GaP/Al structures.", ***Materials Science and Engineering: B***, 265: 114980 (2021).

88. Ulusan, A. Buyukbas, et al. "Photoresponse characteristics of Au/(CoFe2O4-PVP)/n-Si/Au (MPS) diode.", ***Journal of Materials Science: Materials in Electronics***, 32(12): 15732-15739 (2021).

89. Alsmael, Jaafar Abdulkareem Mustafa, et al. "The Impact of Dopant on the Dielectric Properties of Metal-Semiconductor With ZnFe 2 O 4 Doped Organic Polymer Nanocomposites Interlayer.", ***IEEE Transactions on Nanotechnology***, 21: 528-533 (2022).

90. Barkhordari, Ali, et al. "The influence of PVC and (PVC: SnS) interfacial polymer layers on the electric and dielectric properties of Au/n-Si structure.", ***Silicon***, 15(2): 855-865 (2023).

91. Reddy, V. Rajagopal, et al. "Microstructural, electrical and frequency-dependent properties of Au/p-Cu2ZnSnS4/n-GaN heterojunction.", ***Journal of colloid and interface science***, 499: 180-188 (2017).

92. Acar, F. Z., A. Buyukbas-Ulusan, and A. Tataroglu. "Analysis of interface states in Au/ZnO/p-InP (MOS) structure.", ***Journal of Materials Science: Materials in Electronics***, 29: 12553-12560 (2018).

93. Akbaş, Ahmet Muhammed, et al. "Frequency response of C–V and G/ω-V characteristics of Au/(nanographite-doped PVP)/n-Si structures.", ***Journal of Materials Science: Materials in Electronics***, 32: 993-1006 (2021).

94. Alptekin, Sebahaddin, and Şemsettin Altındal. "Electrical characteristics of Au/PVP/n-Si structures using admittance measurements between 1 and 500 kHz.", ***Journal of Materials Science: Materials in Electronics***, 31: 13337-13343 (2020).

95. Sevgili, Ömer, Yashar Azizian-Kalandaragh, and Şemsettin Altındal. "Frequency and voltage dependence of electrical and dielectric properties in metal-interfacial layer-semiconductor (MIS) type structures.", ***Physica B: Condensed Matter***, 587: 412122 (2020).

96. Taşçıoğlu, İlke, et al. "Frequency dependent electrical and dielectric properties of Au/P3HT: PCBM: F4-TCNQ/n-Si Schottky Barrier Diode.", ***Journal of Electronic materials***, 46: 2379-2386 (2017).

97. Taşçıoğlu, İlke, et al. "Effects of interface states and series resistance on electrical properties of Al/nanostructure CdO/p-GaAs diode.", ***Journal of alloys and compounds***, 541: 462-467 (2012).

98. Hill, W. A., and C. C. Coleman. "A single-frequency approximation for interface-state density determination.", ***Solid-State Electronics***, 23(9): 987-993 (1980).

99. Raju, Gorur Govinda.,” *Dielectrics in electric fields: Tables, Atoms, and Molecules*.” ,***CRC press***, (2017).

100. Demkov, Alexander A., and Alexandra Navrotsky, eds. "*Materials fundamentals of gate dielectrics*.", ***Springer***, Dordrecht, (2005).

101. Daniel, V.V. "Dielectric Relaxation.", ***Academic Press***, London, (1967).

102. Barkhordari, Ali, et al. "Dielectric properties of PVP: BaTiO3 interlayer in the Al/PVP: BaTiO3/P-Si structure.", ***Silicon***, 14(10): 5437-5443 (2022).

103. Altındal Yerişkin, Seçkin, Muzaffer Balbaşı, and Adem Tataroğlu. "Frequency and voltage dependence of dielectric properties, complex electric modulus, and electrical conductivity in Au/7% graphene doped-PVA/n-Si (MPS) structures.", ***Journal of Applied Polymer Science***, 133(33) (2016).

104. Tripathi, Ramna, et al. "Dielectric relaxation of ZnO nanostructure synthesized by soft chemical method.", ***Current Applied Physics***, 10(2): 676-681 (2010).

105. Pottel, R. "August Chelkowski: Dielectric Physics." , ***Elsevier***, Amsterdam, (1980).

106. Akbaş, Ahmet Muhammed, et al. "Frequency dependence of the dielectric properties of Au/(NG: PVP)/n-Si structures.", ***Journal of Materials Science: Materials in Electronics***, 32: 7657-7670 (2021).

107. Mc Badapanda, Tanmaya, et al. "Frequency and temperature dependence behaviour of impedance, modulus and conductivity of BaBi4Ti4O15 Aurivillius ceramic.", ***Processing and application of ceramics***, 8(3): 145-153 (2014).

RESUME

Hasan Meloud M ELAMEN he graduated first and elementary education in this city. He completed high school education in Souq Aljomaa High School, after that, he started undergraduate program in Tripoli University Department of Electric and Electronic Engineering in 1990. Then in 1999, he started assignment as a Research Assistant in the center for solar energy researches and studies. He completed M. Sc. Education in Huddersfield University in 2010 in Embedded System Engineering. He started his Ph.D. education program at Karabuk University in Department of Electrical-Electronics Engineering in 2018.